Tuan-Anh Nguyen

Polyhederal Oligomeric Silsesquioxanes: Effects on Adhesion, Water Resistance and Water Vapour Barrier Properties of Paperboard

Thesis for the degree of Philosophiae Doctor

Trondheim, November 2013

Norwegian University of Science and Technology
Faculty of Natural Sciences and Technology
Department of Chemical Engineering

NTNU – Trondheim
Norwegian University of
Science and Technology

NTNU
Norwegian University of Science and Technology

Thesis for the degree of Philosophiae Doctor

Faculty of Natural Sciences and Technology
Department of Chemical Engineering

ISBN 978-82-471-4683-5 (printed ver.)
ISBN 978-82-471-4684-2 (electronic ver.)
ISSN 1503-8181

Doctoral theses at NTNU, 2013:277

Printed by NTNU-trykk

PREFACE

This thesis is submitted for fulfilment of the PhD degree at the Norwegian University of Science and Technology (NTNU). It is based on the experimental work performed partly at the Paper and Fiber Research Institute (PFI) and the Department of Chemical Engineering, NTNU from August 2009 to January 2010, and mainly at SINTEF Materials and Chemistry from February 2010 to January 2013. The research work was supervised by Professor Øyvind Weiby Gregersen (NTNU) and Senior Scientist, Dr. Ferdinand Männle (SINTEF Materials and Chemistry).

I received my BSc. in the field of Polymer and Composite Materials from the Faculty of Chemical Technology, Hanoi University of Technology (HUT), in June 2003. I then continued the research in same field in HUT in 2004. I pursued master degree in Industrial Chemistry from Chung-nam National University (CNU), South Korea, from March 2005 to February 2007. After that, I worked as researcher at IMS laboratory, Pohang University of Science and Technology (POSTECH), South Korea from March 2007 to March 2009.

This PhD study has been performed within the scope of the joint project "Fiber based packaging materials: Development of innovative and sustainable barrier concepts (SustainBarrier)" initiated from NTNU and PFI in cooperation with SINTEF. Marianne Lenes (PFI) has been the project manager. This study was financially supported by the Research Council of Norway and the industrial partners Dynea AS, Elopak AS, Forestia AS, Korsnäs AB, Peterson Linerboard AS, and Södra Cell AB in the KMB project (Sustain-Barrier 182619).

ACKNOWLEDGEMENTS

First of all I would like to acknowledge my supervisors, Professor Øyvind Weiby Gregersen at Norwegian University of Science and technology (NTNU) and Dr. Ferdinand Männle at SINTEF Materials and Chemistry for their helpful supervision and guidance during my PhD work.

I would like to thank Marianne Lenes at the Pulp and Paper Research Institute (PFI) for her support throughout this work. I also thank Lisbeth Blekkan Roel, the secretary of the Department of Chemical Engineering (NTNU) for her help.

My colleagues at SINTEF Materials and Chemistry are acknowledged for their good cooperation and instruction in using instruments (ATR-FTIR, DSC, MFI, NMR, SEM, mini-extruder, T-peel test, liquid coating, and optical microscope).

The financial support for this work from the Norwegian Research Council and the industrial partners Dynea AS, Elopak AS, Forestia AS, Korsnäs AB, Peterson AS, and Södra AB is greatly acknowledged.

My warmest thanks my parents for their great support and encouragement throughout my studies abroad.

CONTENTS

ABSTRACT

Polyhedral oligomeric silsesquioxanes (POSS) is a special class of silicon compounds with the possibility of attaching different types of chemical groups to its central core cage which is composed of silicon and oxygen. POSS is immensely tunable, from non-reactive to multiple reactive, and from hydrophobic to hydrophilic and biodegradable types. Among them, POSS compounds with fatty acid moieties having a bio-based content of more than 90% have been a topic of current interest. These POSS compounds can be produced from renewable sources and are called bio-POSS.

This work has focused on the use of bio-POSS as additives for polyethylene (PE) containing layer of food packaging PE coated paperboard. The bio-POSS was added to PE to improve interlayer adhesion, or used as a coating constituent to improve water and water vapour barrier properties of paperboard. The results of this work are achieved within the scope of the research and development project cooperated between the Paper and Fiber Research Institute (PFI), Norwegian University of Science and Technology (NTNU) and SINTEF Materials and Chemistry: "Fibre-based packaging materials: development of innovative and sustainable barrier concepts" (SustainBarrier).

It has been shown that when using bio-POSS octa-(ethyl octadeca-*10,13* dienoamide) silsesquioxane at ratio of 3-5 wt% with polyethylene (PE), the adhesion of bio-POSS/PE coating layer to paperboard can be improved. However, addition of 10 wt% or more bio-POSS to PE lead to a decrease in adhesion strength. The melt flow index (MFI test) shows that the melt flow properties of PE/bio-POSS blends was slightly decreased with increasing bio-POSS content up to 5 wt%, but significantly decreased when bio-POSS content was increased above 5 wt%. Hydroxyl bonding interaction between amide group in bio-POSS and hydroxyl groups at the paperboard surface and an increased extent of mechanical interlocking were probably responsible for the adhesion improvement. ATR-FTIR analysis of the interaction at the interface between the blends and the paperboard showed the presence of amide-hydroxyl bonds.

Bio-POSS octa-(ethyl erucamide) silsesquioxane was coated on a paperboard substrate via liquid coating using a bar coater. The water resistance and the water vapour barrier properties of the coated paperboard were improved. When the bio-POSS coating layer was dried at 80^{o}C, the water resistance and water vapour barrier properties were further improved, while UV treating

the coating layer had little effect. Dried and UV treated coatings were characterized by solid state proton nuclear magnetic resonance (^{1}H-NMR) and the result demonstrated that no reaction of the double bonds occurred in the bio-POSS coating layer. Multiple coating considerably enhanced the water resistance and water vapour barrier properties of the paperboard, due to an increase in the coating thickness and a reduction in number of pores in the coating layer.

The introduction of ferric stearate ($FeSt_3$) at 0.5 wt% as pro-oxidant led to a limited oxidative degradation of polyethylene (PE). [3-(11-aminoundecanoyl) amino) propane-1-] silsesquioxane or amino-POSS was used as an accelerator at different concentrations. The PE/amino-POSS/ $FeSt_3$ compounds were converted to film samples and exposed to thermal ageing at 70°C in a circulation oven. The surface of the aged compound films contains carbonyl groups, as characterized by ATR-FTIR. The melt flow index (MFI) test showed that the melt flow of the thermally treated compounds increased due to an oxidation and a chain scission. The tensile yield strength of the compound films was slightly decreased with increasing amino-POSS content and thermal aging time, while elongation at break was moderately decreased when compared to reference PE film containing no pro-oxidant. When the films were laminated with paperboard, the adhesion decreased with increasing amino-POSS content. However, the adhesion increased when the films were thermally aged prior to coating. The improvement in adhesion can be explained as the result of an interaction between C=O of the compounds and OH of paperboard, and mechanical adhesion at the interface, as identified by ATR-FTIR, the CI and the MFI. The films are not brittle after thermal aging which makes their use in industrial packaging feasible.

LIST OF PUBLICATIONS

This thesis contains a summary of the following appended papers:

Paper 1: "Polyethylene/octa-(ethyl octadeca-*10,13* dienoamide) silsesquioxane and the adhesion strength to paperboard"
Published in the International Journal of Adhesion and Adhesives (2012) 38: p. 117–124.

Paper 2: "Effects of hydrophobic polyhedral oligomeric silsesquioxane coating on water vapour barrier and water resistance properties of paperboard"
Paper has been accepted for publication in the Journal of Sol-Gel Science and Technology (JSST), DOI: 10.1007/s10971-013-3208-1.

Paper 3: "Effects of a pro-oxidant additive on the adhesion of polyethylene/amino-functionalized POSS compounds to paperboard"

Submitted to Journal of Applied Polymer Science, Ref. APP-2013-07-2568.

CONFERENCE CONTRIBUTION

Tuan-Anh Nguyen, Ferdinand Männle, Øyvind Weiby Gregersen

"Polyethylene/octa (ethyl octadeca-*10,13* dienoamide) silsesquioxanes and the adhesion to paperboard"

Poster presented at *35th Annual Meeting of the Adhesion Society*, Feb 26-29th 2012, Astor Crown Plaza, New Orleans, Louisiana, USA

Link: http://as.omnibooksonline.com/index.html

ABBREVIATIONS

LDPE: Low density polyethylene

POSS : Polyhedral oligomeric silsesquioxanes

Bio-POSS (Paper 1): Octa-(ethyl octadeca-10,13 dienoamide) silsesquioxane;

Bio-POSS (Paper 2): Octa-(ethyl erucamide) silsesquioxane

Amino-POSS (Paper 3): [3-(11-aminoundecanoyl) amino) propane-1-] silsesquioxane

$FeSt_3$: Ferric stearate

CTMP : Chemithermomechanical pulping

ATR-FTIR: Attenuated total reflectance Fourier transform infrared spectroscopy

SEM: Scanning electron microscopy

^{1}H NMR: Proton nuclear magnetic resonance spectroscopy

^{29}Si NMR: 29-Silicon magnetic resonance spectroscopy

XPS: X-ray photon spectroscopy

I_{aI}, I_{aII}: Peak intensity of amide I, II

T_m: Melting temperature

MFI: Melt flow index

CI: Carbonyl index

WTR: Water transmission rate

WVTR: Water vapour transmission rate

WVP: Water vapour permeability

σ_M Ultimate tensile strength

$\boldsymbol{\varepsilon_B}$: Elongation at break

Chapter 1
INTRODUCTION

1.1. Introduction

The food industry always demands packaging materials with improved barrier properties and reduced weight as well as improved environmental profile. Progress in barrier properties can cause improved shelf life of food and reduced loss of food in the chain from producer to consumer. Cellulose based materials such as paper and paperboard are widely used in food packaging applications due to its advantages such as low cost, low weight, good stiffness, easy processing, renewability and recyclability. Two of the most critical required characteristics of packages for food packaging is its strength and its barrier properties especially against water and oxygen [1,2]. The application of coating is commonly used to modify the surface of paper, for instance, mineral pigments are coated on paper surface to improve print quality, gloss, brightness and opacity of the paper product. Barrier coating polymers like polyethylene (PE), ethyl vinyl acetate (EVA), ethyl vinyl alcohol (EVOH), polyamide (PA) are frequently laminated with paper to provide good water and water vapour barrier. A good adhesion between the polymer containing layers and the paper in such laminates is a requirement. However, the polymer containing layer has a disadvantage that is its non-recyclability. Coatings based on natural polymers such as chitosan, whey protein and wheat gluten has been used. However, use of paper coated with biodegradable material is still not common.

Inorganic-organic hybrid polymers represent a new kind of material which has the potential to give high barrier properties with respect to permeation rates of oxygen, water vapour and volatile organic compounds [3,4]. Recently, there has been much interest in inorganic-organic hybrid materials based on several types of polyhedral oligomeric silsesquioxane (POSS) compounds. In fact, POSS is a special class of three-dimensional inorganic/organic hybrids with a molecular structure composed of an inorganic silica core cage and organic groups surrounding the core cage. The combination of POSS and organic polymers may create novel materials that exhibit properties intermediate and superior to those of traditional polymers and inorganic materials. Furthermore, the organic groups of POSS can be further modified to obtain tailored properties. The use of POSS compounds as primary coating components or as coating additives is believed to increase the environmental friendliness and the recyclability of new fibre-based packaging solutions.

1.2. The scope of this study

A principal goal of the project "Fibre-based packaging materials: Development of innovative and sustainable barrier concepts" (SustainBarrier, BIA-328) is to develop and utilise wood-fibre based cellulose structures and inorganic-organic hybrid polymers in new innovative industrial applications. Therefore, the objective of this PhD work was to examine the possibility of combining polyhedral oligomeric silsesquioxanes (POSS) with the polymer containing coating layer, or using POSS compounds as coating materials. The adhesion concepts, the chemical and physical interaction giving adhesion between coating constituents and paperboard, and barrier properties were studied.

1.3. Outline of the thesis

This thesis contains a review of the results from the paper 1-3 and is composed of five chapters as follows:

Chapter 1 contains the introduction and the scope of this study.

Chapter 2 gives an overview on polyhedral oligomeric silsesquioxanes (POSS), pro-oxidant compound. The adhesion concept and the barrier properties are discussed.

Chapter 3 gives an outline of the instrumental techniques applied in this work to determine the adhesion strength, mechanical and melt flow properties of polymers, the film morphology, surface characteristics and barrier properties.

Chapter 4 presents a summary of three appended papers.

Chapter 5 is the overall discussion.

Chapter 6 summarizes the overall conclusions, and suggestion for future works

Chapter 2

LITERATURE OVERVIEW

2.1. Polyhedral oligomeric silsesquioxane (POSS)

2.1.1. Introduction

Polyhedral oligomeric silsesquioxanes (often abbreviated as an acronym POSS) is a class of silicon compounds that have the general formula of $(RSiO_{1.5})_n$, where n is the number of silicon atoms (n=8, 10 or 12), R can be hydrogen or an organic group (halogens, alkyl, alkenyl, aryl, arylene, or other derivatives). The POSS molecule has a special structure composed of an inorganic core cage $(SiO_{1.5})_n$ and organic groups peripherally attached at each Si vertex. This class of silicon compounds is well-defined, highly symmetric molecules [5-9]. The term "polyhedral" originates from its caged structure, and "silsesquioxane" can be understood as follows: *sil*–silicon, *sesqui*–each Si atom is bound to an average of one and a half oxygen, *ane*–Si atom bonds to one hydrocarbon group [5].

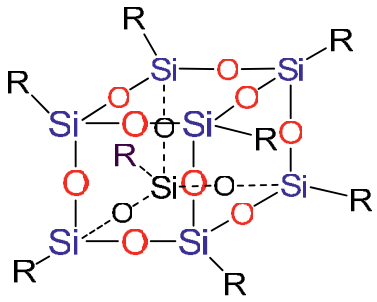

Fig. 1. Typical structures of T8-POSS [5-9]

The most common type is the octahedral oligomeric silsesquioxane (T_8POSS or POSS) with a molecular structure consisting of a silicon-oxygen cubic cage and eight organic groups peripherally attached to eight Si vertexes (see Fig. 1). Here, the symbol "T" refers to conventional nomenclature from silicon nuclear magnetic resonance (^{29}Si NMR) literature, which represents three oxygen atoms bonded to one silicon atom.

Depending on the reactivity of the organic groups, POSS can be classified into non-reactive (non-functional) and reactive POSS (mono-functional or multi-functional). The POSS molecule has a well-defined structure with a nanoscale size, approximately 1-5 nm in diameter when

organic groups R are included. Typical physical properties of POSS compounds are listed in Table 1.

Table 1. Typical physical properties of POSS [5]

Property	**Value or typical behaviour**
Density range	0.9–1.3 g/cm^3 typical (up to 1.82 g/cm^3)
Refractive index range	1.40–1.65
Molecular size	1–5nm
Form	Colourless, odourless crystalline solids, some waxes and liquids
Polarity	Very low (fluoroalkyl), low (alkyl), phenyl (medium) to polyionic (high)
Thermal stability	250–350°C typical (some types > 400°C)
Purity	Standard purity > 97%

2.1.2. Preparation and characterization of POSS

POSS compounds are commonly synthesized by a sol-gel process through hydrolytic condensation of trifunctional organosilicon monomers $RSiX_3$. The overall reaction is described in Figure 2:

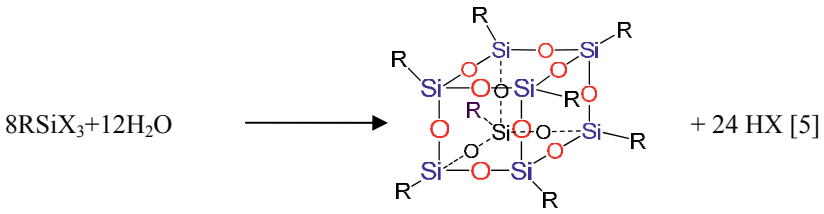

Fig. 2. Overall reaction of POSS synthesis

where X is a highly reactive group, such as Cl, OH or alkoxy, R is organic groups.

The organic R groups of POSS can be further modified through substitution reactions, reactions involving acid derivatives and reactions of unsaturated systems.

Several methods have been used for investigating the structure of different POSS types, in particular the solution ^{29}Si NMR, solid state ^{29}Si NMR, FTIR spectroscopy, and X-ray photon spectroscopy (XPS) [10].

2.1.3. Application of POSS

POSS materials have nano-dimension, inorganic cores and functional peripheral organic groups which are ideal for incorporation into organic polymers. Depending on the organic groups, POSS molecules can be attached to polymer backbones by copolymerization or chemical grafting to form POSS/polymer nanocomposites (reactive POSS), or be physically dispersed in polymer matrices by physical blending to form POSS/polymer blends (un-reactive POSS). In the recent years, a considerable number of applications of POSS compounds in thermoplastic polymers [11-18], thermosets [19-23], coatings [24-27], porous materials [28,29] and medicine [9, 30-32] have been investigated. For new applications in the future, POSS has been suggested for cosmetic formulations, where it could act as a dispersant, emollient or viscosity modifier. POSS has recently been copolymerized to create new, colourless and transparent polyimide. POSS are ideally suited as calibration standards for mass spectroscopy and gel permeation chromatography (GPC or SEC) [33].

Fina *et al.* [11] investigated the influence of POSS functionalization on polypropylene (PP)-based nanocomposites. By increasing the alkyl chain length of organic groups (from octamethyl to octaisobutyl), the compatibility between POSS compounds and PP is increased. This was directly observed as a more even dispersion as determined by SEM. The thermoxidative behaviour of the PP matrix is improved at high POSS loadings.

Joshi *et al.* [12] fabricated nanocomposites from high density polyethylene (HDPE) and octamethyl-POSS by a melt mixing method. The products with a homogeneous dispersion (at nano/molecular level) of octamethyl-POSS (up to 1 wt%) in HDPE under shear conditions are obtained. At concentration higher than 1 wt %, octamethyl-POSS crystallizes into nanocrystals, and at 10 wt % loading, octamethyl-POSS agglomerates are formed. They showed that octamethyl-POSS are miscible in HDPE at low concentrations (up to 2 wt %) and immiscible at higher concentrations (>5 wt %) and higher temperature (>180 °C).

The s of methyl-, vinyl-, phenyl-POSS and polypropylene (PP) were successfully prepared by Fina *et al.* [18]. Submicron dispersions are obtained in vinyl-POSS/PP and phenyl-POSS/PP while methyl-POSS aggregates are formed within methyl-POSS/PP. The PP/polysilsesquioxane showed an increased thermoxidative stability and combustion resistance, in terms of lower rate of heat release. Better mechanical performances (higher elastic modulus as well as higher elongation at break) were also achieved.

Mirchandani *et al.* [25] used silanol functional oligomeric silsesquioxane in modification of hydroxyl functional acrylic polyol (AP) resin. The process was carried out by physical ing and also by chemical reaction using tetrakis 2-ethylhexyl titanate as a catalyst. The pre-products including ed (b-APS) and reacted (r-APS) were then cured with hexamethylene diisocyanate to obtain silsesquioxane modified polyurethane (PU). The higher glass transition temperature and storage modulus from dynamic mechanical analysis (DMA) indicates the superior mechanical properties of "silsesquioxane-modified" PU over the conventional unmodified PU. Silsesquioxane modified PU was used as a coating material with remarkable improvement in the performance properties of the coatings such as hardness, tensile strength, heat resistance and gloss.

Above are recent applications of POSS in thermoplastics and coatings. In general, when POSS compounds are used in blends with thermoplastics, improvements in several polymer properties (such as mechanical, thermoxidative, hardness and viscosity) can be achieved.

2.2. Pro-oxidant

Conventional plastic packaging films and carrier bags will be discarded after use and may remain in the environment for many years, leading to a pollution problem. One approach is to incorporate a pro-oxidant additive into plastic materials which will accelerate the degradation of the plastic in the environment. Common pro-oxidants presently being used for the preparation of "oxo-biodegradable" thermoplastics are based on stearate salt of a transition metal such as cobalt (Co), iron (Fe), manganese (Mn) or nickel (Ni). Such stearates can drive the oxidation process which, under the action of heat or light, will reduce the molecular weight of the polymer to a low molecular level where bacteria and fungi in the soil or disposal environment can further reduce the material into water, carbon dioxide and biomass [34-38].

2.3. Adhesion

Adhesion is the inter-atomic and intermolecular interaction at the interface of two surfaces in contact. It is a multi-disciplinary topic that includes surface chemistry, physics, rheology, stress analysis, and fracture analysis. The adhesion strength can be measured as the mechanical force that is needed to separate two surfaces. The surface characteristics of the two materials will affect the adhesion.

2.3.1. Surface roughness and adhesion

Generally, surface roughness is a very important feature of the substrate, particularly for coating and printing. In case of a smooth surface (Fig. 3a), the substrate and the coating are held together only by interfacial attractive forces per unit of geometric area. In case of rough surface (Fig. 3b), the actual contact area is larger than the geometric area. The rough surface contains pores, holes and crevices. When a resin is coated on a rough surface, the adhesion of the coating layer to the substrate is normally better than for a smooth surface. However, a rough surface may be a drawback if the resin does not sufficiently penetrate into the microscopic pores and crevices. The actual contact area can be smaller than the geometric area and thus adhesion reduced.

High surface roughness may also cause imperfect coverage of the substrate. Holes and pores in the coating will allow liquid or gas to easily permeate through such defects and come in direct contact with the uncovered part, causing major problems such as wetting and reduction the mechanical properties (Fig. 3c) [39].

The scale of the roughness can vary from macroscopic to microscopic to sub-microscopic (from hundreds of microns to nanometres). The surface roughness is adequately expressed by a simple Wenzel roughness factor $r = A/A_o$, where A is the 'true' surface area, A_o the nominal area. For an ideal smooth surface, r can be calculated from elementary geometric formulae. For a simple real surface, r can be calculated from straight forward measurements, such as profilometry [40].

(a) (b) (c)

Fig. 3. Geometries of surface interactions between a coating and a substrate, adapted from [39]:
a) Smooth interface
b) Rough surface on a microscopic scale
c) Rough surface with incomplete penetration of coating.

In order to get better adhesion, the surface of the substrate is some times roughened prior to the coating process. Roughening the substrate's surface gives an increase in the surface area and also in the surface free energy. Furthermore, roughened surface may be able to redistribute the stress when stressed, so as to increase energy dissipation during failure of the joint. The strengthening of an interface resulting from increasing roughness may change the mechanism of fracture from a less to more energetic mode [41,42].

2.3.2. Relationship between wetting, spreading and adhesion

When a drop of liquid is placed on a surface it may spread completely or it may have a limited spreading tendency and remain as a drop having a definite angle θ with the surface (see Fig. 4). The relationship between contact angle θ, the surface free energy of the substrate (γ_S), the surface tension of the liquid (γ_L), and the interfacial tension (γ_{SL}) between solid and liquid can be expressed by Young's equation [39,43]:

$$\cos\theta = \frac{\gamma_S - \gamma_{SL}}{\gamma_L}, \text{ (Eq. 1),}$$

If γ_L is lower than γ_S, the liquid drop will spread spontaneously on the substrate's surface. The contact angle θ is reduced during spreading until the system has reached equilibrium. When $\gamma_L + \gamma_{SL} < \gamma_S$, the liquid will spread throughout to form a thin wide circle on the substrate with the contact angle 0^o, and the adhesion reach maximum. In order to obtain good adhesion, the surface tension of the liquid should be lower than the surface free energy of the substrate ($\gamma_L < \gamma_S$). For example, the adhesion of polyethylene when coated on paperboard can be increased if $\gamma_{paperboard}$ is higher than $\gamma_{molten\ PE}$ (31 mJ/m^2) [44].

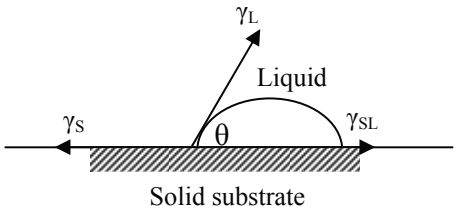

Fig. 4. Contact angle of liquid drop on a solid substrate, adapted from [39]

When a liquid is coated on a substrate with a rough surface and $\gamma_L < \gamma_S$, the liquid can spontaneously spread, leading to its penetration into pores, holes and crevices of the substrate. Such penetration is analogous to penetration of a liquid into a capillary on the micro scale. The penetration length into a capillary as a function of time can be estimated as follows:

$$L = 2.24\left[\frac{\gamma}{\eta}(r\cos\theta)t\right]^{\frac{1}{2}} \quad \text{(Eq. 2)}$$

where L is distance of penetration (m), r: radius of capillary (m), t is time of penetration (s), θ is contact angle, γ is surface tension (mNm^{-1}) and η is viscosity (Pa.s) of the liquid [39].

From this equation, the rate of penetration (L/t) increases with increasing surface tension of the liquid. Especially, the rate is strongly affected by the viscosity of the liquid. The lower the viscosity of the liquid, the more rapid penetration into pores of the substrate. It is important to keep the viscosity low for a long enough time for penetration to fill into the pores. Beside, the rate is also affected by contact angle. When the contact angle is zero, the rate is highest.

2.3.3. Work of adhesion

The work of adhesion between the solid substrate and the liquid (the negative of the Gibbs energy of adhesion) is the work to separately split two surfaces and may be calculated through the Dupré equation [45]: $W_a = \gamma_S + \gamma_L - \gamma_{SL}$ (Eq. 3)

Combining Young's equation (Eq. 2) and Eq. 3, obtaining the Young-Dupre equation:

$$W_a = \gamma_L(1 + \cos\theta) \text{ (Eq.4)}$$

Eq. 4 implies that the work of adhesion between the solid and the liquid can be determined from surface tension of the liquid and contact angle measurements.

2.3.4. Adhesion theory

Adhesion mechanisms are known to be dependent on the surface characteristics of the materials. The most important mechanisms of adhesion are mechanical interlocking, physical adsorption, chemical bonding, electrostatic attraction, diffusion, weak boundary layer and acid-base interaction.

i) The mechanical interlocking mechanism

The mechanical interlocking mechanism is the simplest. It is based on the factor that at the microscopic level all surfaces are very rough consisting of voids, holes, crevices and other irregularities. The adhesive penetrates into micro-cavities, resulting in a formation of mechanical interlocks at the interface. The adhesive must not only wet the substrate, but also have the right rheological properties to penetrate pores and openings in a reasonable time [46,47].

ii) The physical adsorption mechanism

When an adhesive is applied to a substrate, the adhesive spreads spontaneously on the surface of adherent when the join is formed. This has resulted in adhesive materials being developed which have a lower surface tension than the adherent surfaces. According to this theory, in the

event of intimate contact between the adhesive and the adherent, the adhesive strength arises as a result of secondary intermolecular forces at the interface. These may include Van-der-Waals forces (dipole-dipole, dipole-induced dipole interactions) and hydrogen bonds [46,47].

iii) The chemical bonding mechanism

This mechanism is relatively similar to the physical adsorption mechanism in which the strong chemical bonds (ionic, covalent metallic) are formed at the interface between the adhesive and the adherent. The introduction of molecular bonding between the adhesive and the adherent will obviously improve the adhesive bond strength. By using surface treatments, or additional coupling agents to perform reactions at the surfaces, chemical bonds between the adhesive and the substrate can be obtained [46,47].

iv) Electrostatic interaction

The mechanism of electrostatic interaction is that electrostatically charged bonds are formed at the interface by the interaction between the adhesive and adherent which contributes significantly to the bond strength. This is a controversial theory [46] as many have doubted the actual significance of the forces involved. While this concept may be useful to explain some specific examples of adhesion, significant doubts have been cast regarding its overall value. These include improved adhesion strengths with lowering of temperature for a large number of adhesive systems (lower temperatures should result in poorer electrostatic forces). Also it has been identified that virtually no changes in adhesion performance result with gross variations in the electronic character of the adhesives [46,47].

v) The diffusion mechanism

The diffusion theory predicts that adhesion is increased by intermolecular diffusion and entanglement across the interface. This mechanism is particularly relevant for polymers where a movement and entanglement of long molecules can occur. This can be viewed as a molecular interlock enabled adhesion. Parameters affecting the diffusion process are contact time, temperature, molecular weight of polymers, chemical interaction between polymers, polymer structure and physical form (liquid, solid). While the diffusion theory applies well for cases of self-adhesion or auto-adhesion, it has found limited application where two polymers are not soluble or the chain movement of the polymer is constrained by its highly cross-linked, crystalline structure, or when it is below its glass transition temperature (T_g). Such inter-

diffusion will occur only if the polymer chains are mobile (i.e. the temperature is above T_g) and compatible [46,47].

For the diffusion mechanism to be relevant for paper materials, it is necessary to break the hydrogen bonds of the carbohydrate polymers in the papers surface. This may happen to some extent for adhesives which are dissolved or dispersed in water but should not be relevant for other adhesive systems. The crystalline portion of cellulose is not likely to be involved [44].

vi) Weak boundary layer (WBL) theory

The weak boundary theory is a theory of de-bonding rather than bonding or adhesion. According to the WBL theory, bond failure seems to occur at the interface, usually a cohesive rupture of a weak boundary layer is the real event. This theory suggests that true interfacial failure rarely occurs. In most cases joint failure results from a cohesive failure of a weak boundary layer. Weak boundary layers can originate from the adhesive, the adherend, the environment, or combination of any of the three. Weak boundary layers can occur on the adhesive or adherent side if an impurity concentrates near the bonding surface and forms a weak attachment to the substrate [47].

vii) Acid-base interaction

The acid-base interaction mechanism is based on the Bronsted acid-base concept to predict the relative magnitude of hydrogen bonding between polymers and oxide surface in the presence of moisture. Donor-acceptor interactions, defined as the formation of acid-base interactions between adhesive and substrate, have also been proposed as a major type of intrinsic adhesion force operating across the interface [46,47].

2.4. Permeability and plastics packaging

2.4.1. Introduction

The food packaging industry always demands good barrier properties of the packaging materials. The package must protect the product against physical hazards and atmospheric environmental influences, such as rain, water vapour, gases and odours. Packaging materials are therefore required to act as barriers between the outside environment and the interior atmosphere of the package in order to maintain food quality. The selection of packaging material will depend on their resistance to gases, water vapour and odours. In terms of gas barrier, oxygen, carbon dioxide, nitrogen and sulphur dioxide are the main ones of interest in

packaging. In addition barrier against both liquid water and water vapour is often important [48].

A consideration of the overall structure of a pack includes the combination of materials for the body of the container.

The selection of packaging materials will be governed by consideration of the following factors:

(i) Physical properties: strength, rigidity.

(ii) Processability (compatibility with the process of preservation, machine handling during filling, heat sealing, storage conditions, and after purchase handling

(iii) Barrier properties

(iv) Cost of the materials and conversion processes relative to the cost of the product.

2.4.2. Rate of transmission

At what rate a gas, vapour or liquid will pass through a polymeric material depends on the properties of the permeating molecules, the properties of the polymer, and the degree of interaction between polymer and permeating molecules. In addition environmental conditions like temperature and gas pressure on both sides of the barrier are important.

Crystalline structures have a greater degree of molecular packing and the individual crystalline regions may be considered as almost impermeable to a diffusing molecule. Thus, diffusion can only occur in the amorphous zones or at regions of imperfection in the crystal structure. Semi-crystalline polymers tend to be less permeable compared to amorphous ones.

Permeation of a gas or vapour through a polymeric material is generally of the activated diffusion type. The presence of cracks, pinholes and voids will lead to rather catastrophic loss of barrier properties.

Generally, the permeation of a gas, vapour or liquid through a polymer film includes four stages, as follows:

(i) Absorption of the permeating species on to the surface of the polymer

(ii) Solution of the gas or vapour into the polymer matrix;

(iii) Diffusion through the wall along a concentration gradient;

(iv) Desorption from the other surface.

The permeability coefficient (P) is calculated as: $P = D * S$, in which D is the diffusion coefficient and S is solubility coefficient.

This equation assumes that both D and S are independent of concentration. It is true for oxygen, hydrogen, nitrogen and other gases, and in case of carbon dioxide the theory is also reasonably accurate. However, the theory breaks down where considerable reaction between the polymer and diffusing molecules takes place (*e.g.* water and cellulose film or many solvent vapours diffusing through plastic films)

There are three assumptions in the simple treatment of permeation which are:

(i) diffusion is in a steady state condition,

(ii) the concentration-distance relationship through the polymer is linear,

(iii) diffusion takes places in one direction only (that is, through the film with no net diffusion along or across it)

For example, polyethylene will be more permeable to liquids of similar solubility parameter, e.g. hydrocarbons, than to liquids of differing solubility parameter but of similar molecular size and shape.

The permeability coefficient of a polymer can be expressed by $P = F * G$, where a factor F is determined by the nature of the polymer, and a function G is determined by the nature of the gas and an interaction function H.

The permeability data of polyethylene: LDPE (low density and crystallinity), HDPE (high density and crystallinity) to H_2O (at 90% RH and 25^oC) is 800 and 130 (cm^3 mm)/(s cm^2 cm Hg), respectively.

2.4.2.1. Variables affecting permeability of polymers

In many polymer systems, the permeation rate is inversely proportional to the thickness of the polymer film or the permeability coefficient is independent of thickness. However, there are some exceptional cases where the permeability coefficient increases or decreases with thickness. In case of coated films with an irregular surface *e.g.* containing pinholes will lead to a high transmission rate. Therefore, it is common to use multilayer structure coating structures, multiple coating or laminating to interrupt gas transmission for packaging materials.

Molecular structure can lead to good barrier properties of polymers. In fact, a structure that leads to a good gas barrier, but a poor water vapour barrier. Polymers with a high polarity, such as polyvinyl alcohol or cellulose, have high gas barriers, but poor water barriers. Contrarily, non-polar hydrocarbon polymer, such as polyethylene (PE) or polypropylene (PP) have excellent water barrier but poor gas barrier properties.

The polymer with good all-round barrier properties must posses the following properties:

(i) Some degree of polarity (having the nitrile, chloride, fluoride, acrylic or ester groups);
(ii) High chain stiffness;
(iii) Inert to the permeating species;
(iv) Close chain-to-chain packing ability brought about by molecular symmetry or order, crystallinity or orientation;
(v) Some bonding or attraction between chains;
(vi) High glass transition temperature.

In general, linear polymers with a simple molecular structure have good chain packing and lower gas permeability (*e.g.* HDPE) than those containing side groups (*e.g.* polypropylene PP).

2.4.2.2. Effect of permeating species

The composition and molecular structure of the polymer play an important role in determining the permeability of a barrier material. Likewise, the molecular structure of the permeating gas or liquid is of importance in the following manner. Small molecules diffuse faster than larger ones. Non-polar molecules diffuse more rapidly than polar ones.

2.4.2.3. Thickness of polymer films

The permeability coefficient is normally independent of the thickness. There is however an inverse relationship between thickness and the number of pinholes. Many packaging materials consist of coated polymer layers, laminated films or multi-layers.

The permeability P of a simple case of a laminate consisting of two layers can be determined as: $\frac{1}{P} = \frac{l_1}{lP_1} + \frac{l_2}{lP_2}$, where l is total thickness, $l = l_1 + l_2$, and the permeability of two layers are P_1 and P_2.

If a barrier polymer is used as a thin coating in a multilayer structure, normal layer materials will have different characteristics which depend on the grade and thickness of the material and the number of pinholes. The permeability rate of a multilayer material can be expressed as follows:

$$\frac{1}{P_t} = \frac{1}{P_x} + \frac{1}{P_y} + \frac{1}{P_z} \ldots$$

where P_t is total permeability, $P_{x,y,z}$ are the permeabilities of the separate layers.

Chapter 3
MATERIALS AND METHODS

3.1. Materials

3.1.1. Polyhedral oligomeric silsesquioxanes (POSS) compound

The POSS compound used in Paper 1 was bio-POSS octa-(ethyl octadeca-*10,13* dienoamide) silsesquioxane which is a derivative of unsaturated fatty acid (octadeca-*10,13* dienoic acid) with a typical structure as shown in Figure 5:

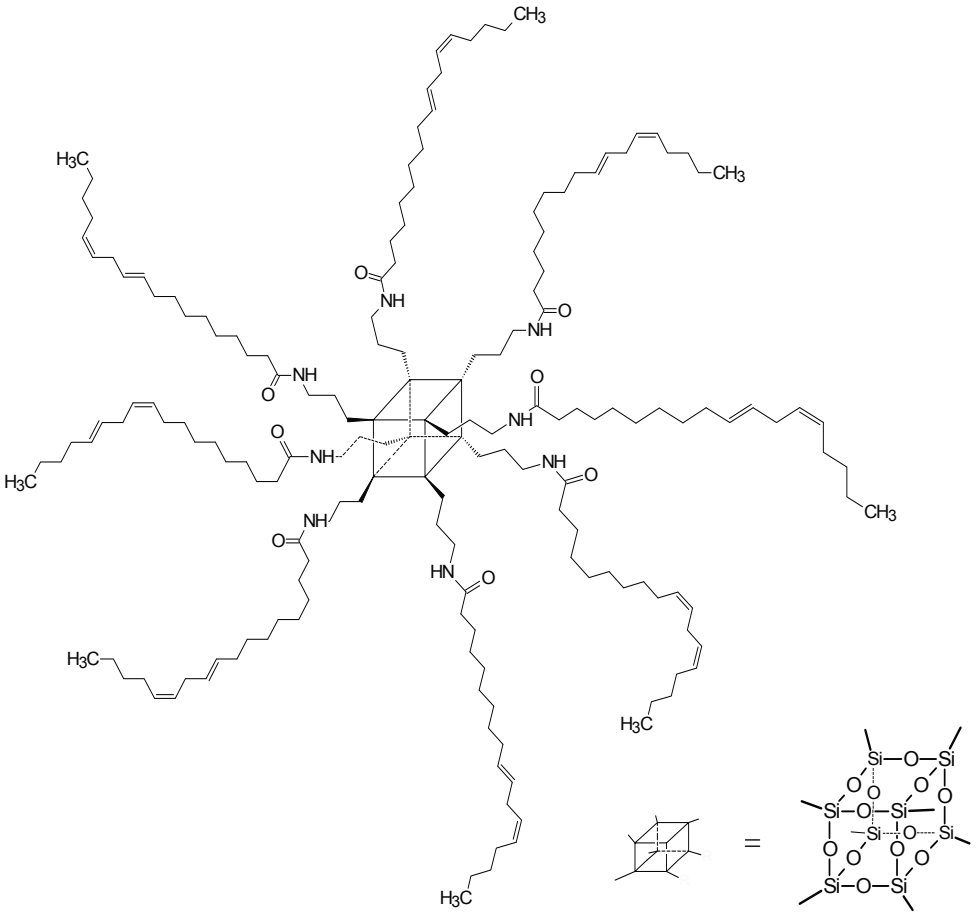

Fig. 5. Typical structure of octa-(ethyl octadeca-10,13 dienoamide) silsesquioxane

The POSS compound used in Paper 2 was octa-(ethyl eruciamide) silsesquioxane (Figure 6). This is a derivative of unsaturated fatty acid (erucic acid).

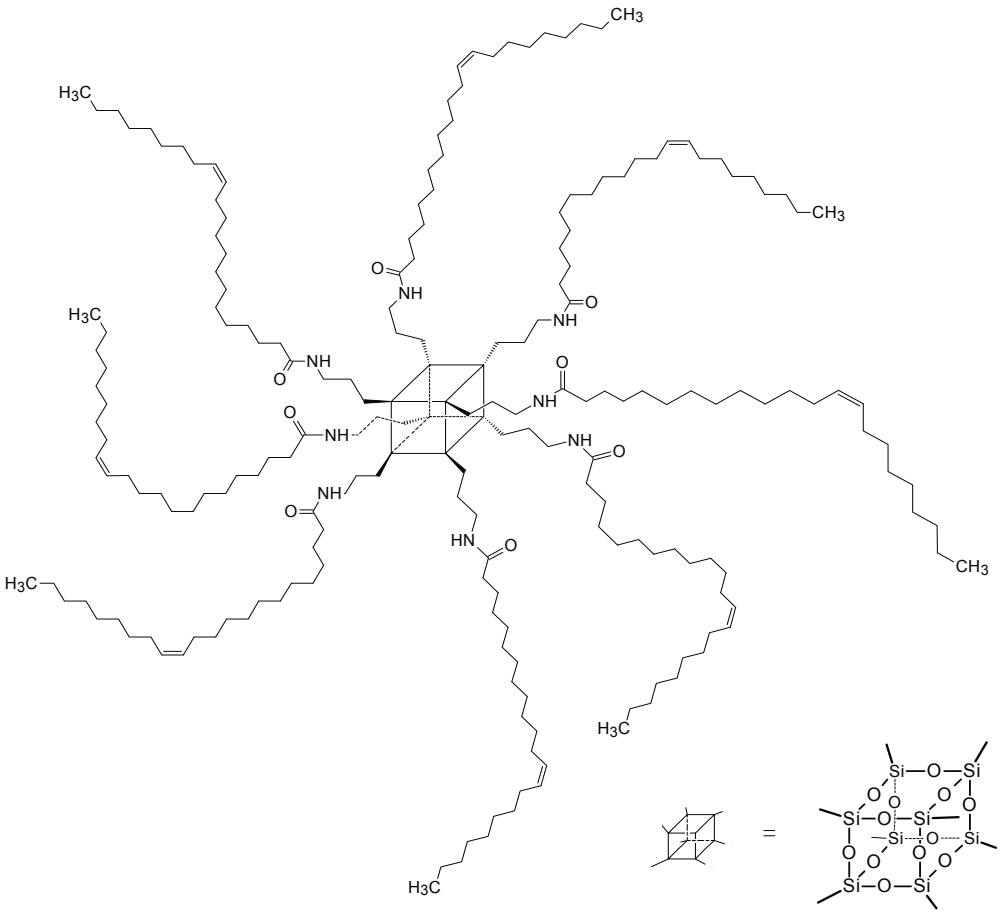

Fig. 6. Typical structure of octa-(ethyl erucamide) silsesquioxane (bio-POSS)

The POSS compound used in Paper 3 was [3-(11-aminoundecanoyl) amino) propane-1-] silsesquioxane (Figure 7).

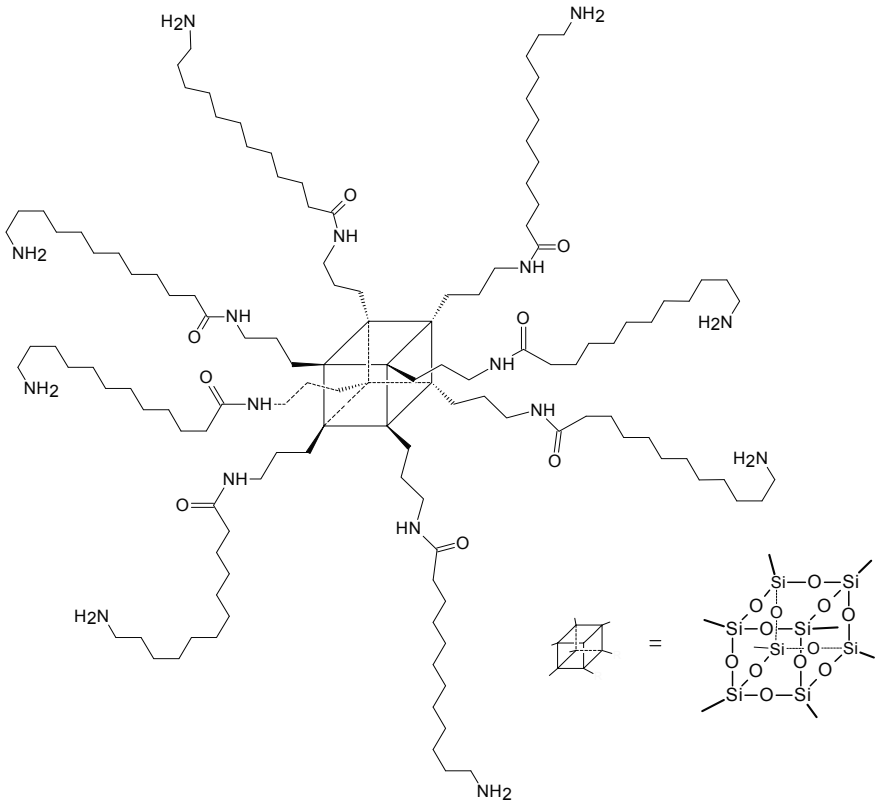

Fig. 7. Typical structure of [3-(11-aminoundecanoyl) amino) propane-1-] silsesquioxane (amino-POSS)

The POSS compound in Paper 1 was supplied by Jotun AS, Norway.

The POSS compounds in Paper 2 and Paper 3 were synthesized in our laboratory by a two-step procedure [49]. 3-aminopropyltriethoxy silane was converted to amine functionalized POSS by a sol-gel process. In the second step, the amine groups were modified by a fatty acid (erucic acid in Paper 2)/ by an amino acid (11-aminoundecanoic acid in Paper 3).

The POSS compounds in Paper 1 and Paper 2 are derivatives of unsaturated fatty acids that are biological and renewable, and therefore called bio-POSS. The POSS compound in Paper 3 is a derivative of amino acid (11-aminoundecanoic acid), therefore called amino-POSS.

3.1.2. Low density polyethylene (LDPE)

The low density polyethylene LDPE used in Paper 1 (pellet) was supported by Ineos Polyolefins & Polymers Europe with melting point (T_m) of 120°C and melt flow index (MFI) of 0.5 g/10 min (190°C/ 2.16 kg).

The LDPE in Paper 3 (powder state) was provided by Normatch AS, Norway, and has a T_m of 120°C, MFI of 20 g/10 min at 190°C/ 2.16 kg).

3.1.3. Pro-oxidant additives

The pro-oxidant additive used in Paper 3 was a masterbatch of ferric stearate ($FeSt_3$) in polyethylene with an iron content of 0.4 wt% which was provided by Nor-X Industry AS, Norway. The pro-oxidant additive contains stearic acid in addition to ferric stearate, about 0.1 wt%.

3.1.4. Paperboard

Single side coated, three-ply paperboard was supplied by Korsnäs AB, Sweden. The two sides of the paperboard are different. One side is pigment coated, the other side is uncoated, and thus the two sides have different chemical composition, structure and colour (brown and white), respectively (Fig. 8). The paperboard is composed of four different layers, as shown in Fig. 9:

(i) the top layer which is coated by white pigments and binders (pre-coated side).

(ii) the dense layer is bleached kraft pulp

(iii) the middle layer is a mixture of unbleached kraft pulp and chemithermomechanical pulp (CTMP),

(iv) the bottom layer is unbleached kraft pulp of a pine and spruce softwood mix.

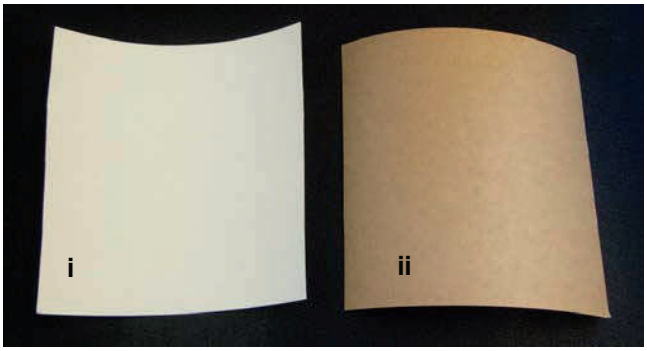

Fig. 8. Two side of paperboard: (i) pre-coated side; (ii) uncoated side

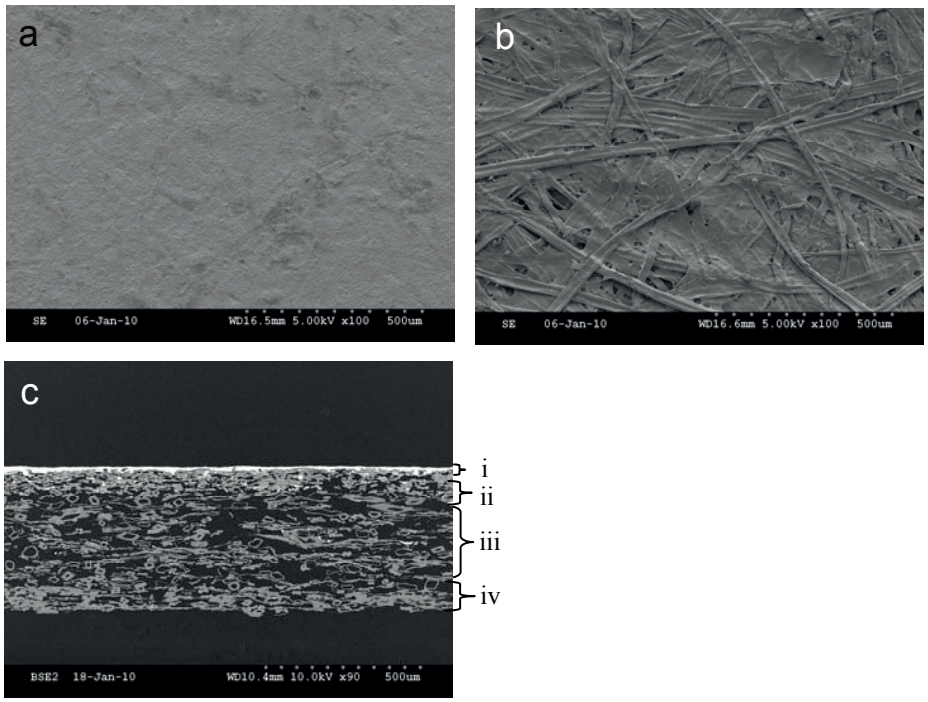

Fig. 9. SEM images of paperboard:
a) Pre-coated side; b) Uncoated side; c) Cross-section

Figure 9 shows scanning electron microscope (SEM) images of paperboard:

(a) is the pre-coated side (side coated with mineral pigments (white colour);

(b) is uncoated side (brown),

(c) is the cross-section of the paperboard which illustrates four different layers (i, ii, iii and iv).

As can be observed, the pre-coated side of the paperboard is quite smooth; the uncoated side of the paperboard is very rough, containing large fibres. A rough surface is advantageous for the mechanical adhesion of a polymer coating. If the porous structure of the paperboard is not barrier coated, it will be permeable for gases and liquids.

3.2. Sample preparation

3.2.1. Preparation of polyethylene/ octa-(ethyl octadeca-10,13 dienoamide) silsesquioxane (Paper 1)

Bio-POSS octa-(ethyl octadeca-*10,13* dienoamide) silsesquioxane was first dried at 150^{o}C to fully remove the hydrocarbon solvent. Polyethylene and dried bio-POSS were then melt mixed at different ratio (99/1, 97/3, 95/5, 90/10, 80/20 and 60/40) in a twin screw 15cc micro extruder DSM MIDI2000 (Fig. 10). The product was cut into 2 mm length pellets.

Fig. 10. A twin screw 15cc micro extruder, DSM MIDI2000

3.2.2. Preparation of polyethylene/[(3-(11-aminoundecanoyl) amino) propane-1-] silsesquioxane / ferric stearate compounds (Paper 3)

The pro-oxidant masterbatch containing ferric stearate ($FeSt_3$) was called masterbatch A and used as received. [3-(11-aminoundecanoyl) amino) propane-1-] silsesquioxane (amino-POSS) was dried at 120^{o}C to fully remove 2-butoxy ethanol solvent. Masterbatch B including 90 wt% PE powder and 10 wt% dried amino-POSS was prepared in a twin screw 15cc micro extruder (DSM MIDI2000). After that, the mixture of PE, A and B was melt mixed at different weight ratio (see Table 2). The final product was cut into 2 mm length pellets.

Table 2. Compositions of PE/amino-POSS/ $FeSt_3$ compounds.

Sample code	PE (pellet) wt%	mb A wt%	mb B wt%	Composition (wt%) PE	$FeSt_3$	amino-POSS
PE	100	0	0	100	0	0
90505	90	5	5	99	0.5	0.5
85510	85	5	10	98.5	0.5	1
80515	80	5	15	98	0.5	1.5

3.2.3. Preparation of thin film (Paper 1 and Paper 3)

Thin film was prepared by compression moulding on a hydraulic compressor Fontijne TH200 (Fig. 11). The condition was set at: the temperature of up/down plate was 180°C/180°C and the pressure was kept at 10 MPa. The mould dimension was 10×10×0.1 (mm)

Fig. 11. Hydraulic compressor Fontijne TH200

3.2.4. Compression moulding coating (Paper 1 and Paper 3)

The films were coated on paperboard by compression moulding coating using a hydraulic compressor. The temperature of the up/down plate was 200°C/20°C and 300°C/20°C, and the pressure was kept at 10 MPa. Fig. 12 illustrates the compression moulding coating process.

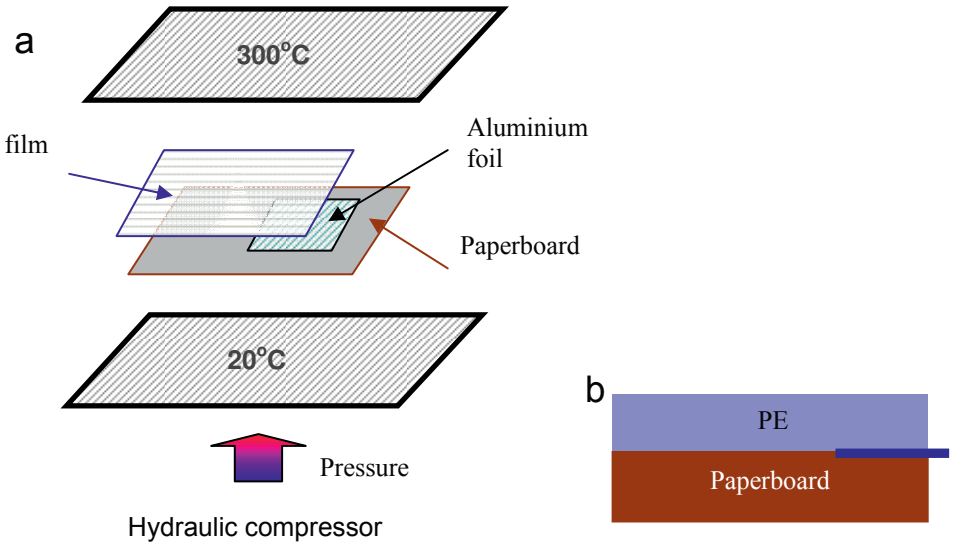

Fig. 12. a) Schematic drawing of compression moulding coating;
b) Cross-section of sample

3.2.5. Preparation of solvent based coating (Paper 2)

The coating solution was prepared by dissolving bio-POSS into toluene solvent at a weight ratio of 90:10 on a microwave synthesizer Biotage Initiator 2.0 (figure 13). The paperboard was mounted on a flat steel plate by clamping the edges of the paperboard to inhibit wrinkling of the paperboard during the coating process, as illustrated in figure 14. The coating solution was coated on the paperboard using a TQC Baker film applicator VF2146**,** 60mm in width, 30µm in gap.

Fig. 13. Microwave synthesizer Biotage Initiator 2.0

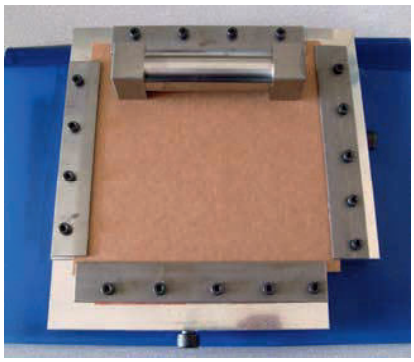

Fig. 14. TQC Baker film applicator and flat steel plate

3.2.6. Preparation for water and water barrier test (Paper 3)

The specimens for water and water barrier test were similar. An aluminium cup (38.0 mm in inner diameter and 12.0 cm in depth with an exposure coating area of 1133.54 mm^2) was mounted on the paperboard and bio-POSS coated ones. Polyurethane adhesive was used to seal an aluminium cup to the paperboard, see Figure 15a. A small hole was carved in the top of the cup to fill water in. After fully filling about 11g distilled water into the cup, the hole was tightly sealed by polyurethane adhesive. At least three specimens were prepared for each test. The specimens were then placed in a climate chamber (KB 8400 F, 400 litres, Termaks AS), set at 50 % of relative humidity (RH) and 23^oC. A fan was used to keep uniform conditions for all test specimens. The arrangement of specimens for each test is illustrated in Fig. 15b: (i) for the water barrier test: the water stays in direct contact with the paperboard, (ii) for the water vapour barrier test, liquid water stay in the bottom of the tray and only water vapour is in contact with the paperboard. The weight of each specimen was measured at 24h intervals for 30 days.

A reference sample was made by substituting the paperboard by using a milk carton (from Tina AS) which is 30µm-polyethylene coated paperboard.

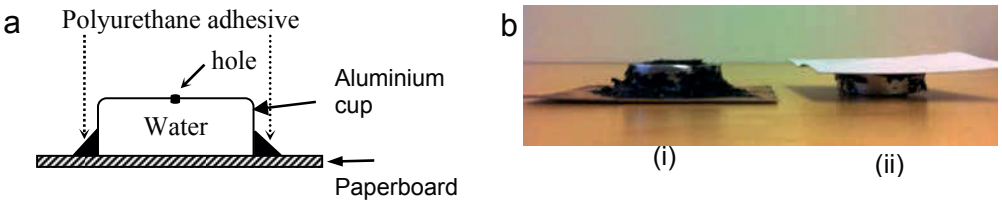

Fig. 15. Sample preparation
(a) A schematic drawing of the specimen test for water permeability and water vapour permeability;
(b) Specimen arrangement in climate chamber: (i) for water barrier test; (ii) for water vapour barrier test

3.3. Characterization methods

3.3.1. Scanning Electron Microscopy (SEM)

Scanning electron microscopy (SEM) is an analytical technique that produces high magnification images using electrons instead of light. A beam of electrons having energy within the range 0.1-30 keV is produced at the top of the microscope by an electron gun. The electron beam follows a vertical path at high vacuum through the microscope. The beam travels through electromagnetic fields and lenses, which focus the beam down toward the sample. Once the beam hits the sample, electrons and X-rays are emitted from the sample. Detectors collect these X-rays, backscattered electrons, and secondary electrons and convert them into signals that can be sent to a screen similar to a television screen and/or a digital picture recording unit. This produces the final image.

In Paper 1 and Paper 2, SEM was performed using a JEOL JSM-5900LV instrument (see Fig. 16b) to study the morphology of PE/bio-POSS films and the cross-section of the paperboard respectively.

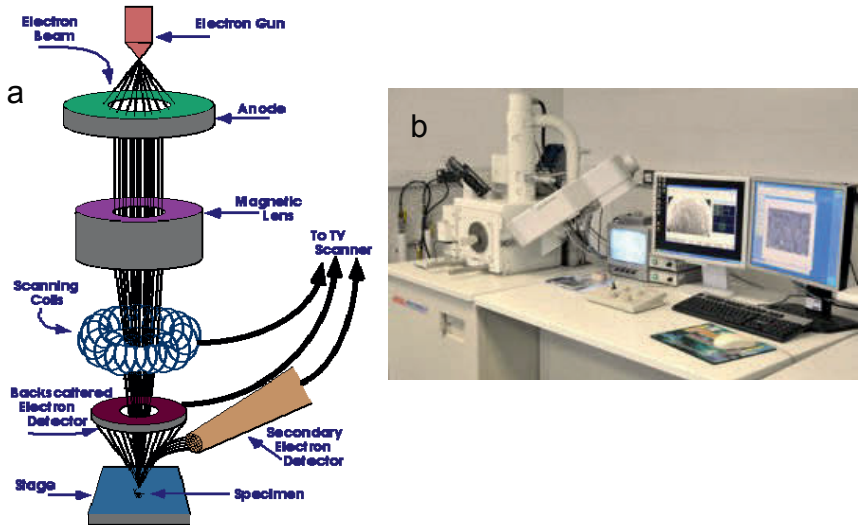

Fig. 16. a) Schematic diagram of a scanning electron microscope; adapted from [51]
b) SEM instrument JEOL JSM-5900LV

3.3.2. Optical microscopy

The optical light microscope is another important tool for the studies of microstructure. It uses visible light and a system of lenses to magnify images of small samples. The image from an

optical microscope can be captured by normal light-sensitive cameras to generate a micrograph. Originally images were captured by photographic film but developments in CMOS and charge-coupled device (CCD) cameras allow the capture of digital images [52].

Fig. 17. The optical microscope Leica M420 fitted with digital microscope colour camera Image Leica DFC295.

Optical microscopy (Figure 17) was used to examine the top surface of the PE/bio-POSS blend films, fracture surface of the de-bonded films after T-peel test in Paper 1, top surface and cross-section of the bio-POSS coated paperboards in Paper 2.

3.3.3. Attenuated Total Reflection Fourier Transform Infrared (ATR-FTIR) spectroscopy

Attenuated total reflectance (ATR) is an analytical technique used in conjunction with infrared spectroscopy which enables samples to be directly examined in the solid or liquid state without further preparation.

An ATR instrument operates by measuring the changes that occur in a totally internally reflected infrared beam when the beam comes into contact with a sample (as illustrated in Fig. 18). The crystal materials for ATR are Zinc Selenide (ZnSe), Gemanium (Ge), or diamond. The refractive index of the ATR crystal is typically in the range of 2.38–4.01 at 2000 cm^{-1}. The ATR crystal must be cleaned before inserting a sample.

In this study, ATR-FTIR was used to characterize the surface characteristics of polyethylene/bio-POSS blends in Paper 1, top surface of the bio-POSS coated paperboard in Paper 2, and polyethylene/amino-POSS/$FeSt_3$ compounds in Paper 3.

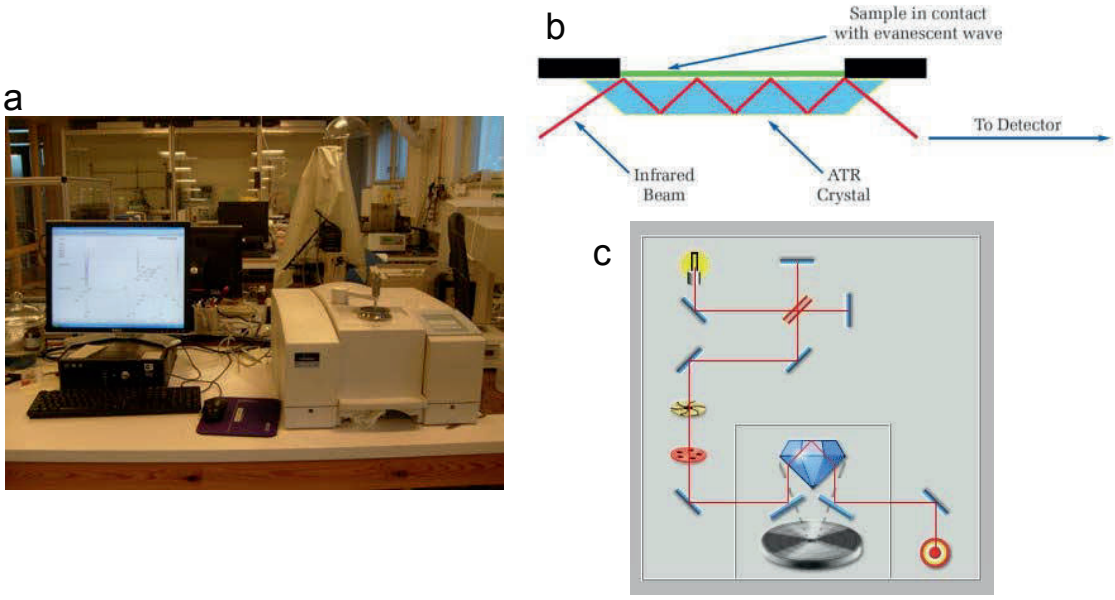

Fig. 18. a) PerkinElmer FT-IR (Spectrum One) with ATR plate;
b) A multiple reflection ATR system, and c) light path in the ATR technique, adapted from [53]

3.3.4. Nuclear magnetic resonance (^{1}H NMR) spectroscopy

Nuclear magnetic resonance (NMR) spectroscopy is a research technique that exploits the magnetic properties of certain atomic nuclei to determine the structure of unknown organic compounds. When placed in a magnetic field, NMR active nuclei absorb electromagnetic radiation at a frequency characteristic of the isotope. The most commonly studied nucleus is ^{1}H corresponding with ^{1}H NMR. ^{1}H NMR spectra of most organic compounds are characterized by chemical shifts in the range +14 to –4 ppm and by spin-spin coupling between protons. The integration which builds up the NMR-spectrum reflects the number of protons that has the same chemical environment in the molecules [54,55].

Solid and liquid state NMR is two kinds of NMR spectroscopy. Solid state NMR is characterized by the presence of anisotropic (directionally dependent) interactions. Liquid state NMR requires that the material is soluble into a solvent (such as $CDCl_3$). The liquid state NMR spectra consist of a series of very sharp transitions, due to averaging of anisotropic NMR interactions by rapid random tumbling. Whereas, solid state NMR spectra are very broad, as the full effects of anisotropic or orientation-dependent interactions are observed in the spectrum. High-resolution NMR spectra can provide the same type of information that is available from corresponding liquid state NMR spectra, but a number of special techniques/equipment are

needed, including magic-angle spinning, cross polarization, special 2D experiments, enhanced probe electronics, etc [56,57].

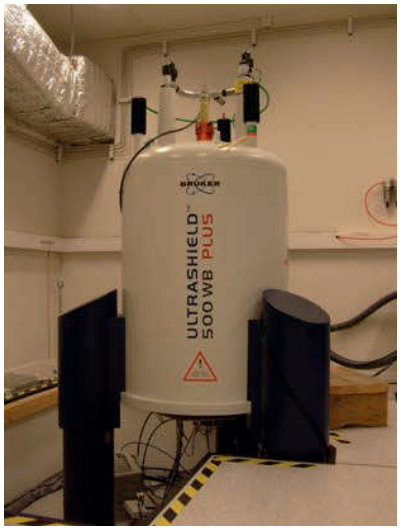

Fig. 19. Bruker Avance III spectrometer

In Paper 2, solid state and high resolution liquid ^{1}H NMR spectroscopy were performed on a Bruker Avance III spectrometer (see Fig. 19) to characterize the bio-POSS coating layer.

3.3.5. Adhesion testing

Adhesion testing or peel testing is a method to characterize the adhesion between layers. It is used extensively to evaluate the bonding strength of tape, adhesives and flexible substrates, including rubber, films, biomaterials, dental materials, medical packaging and consumables. It is performed by applying a peeling tension load to the specimen at various angles (90° and 180° being the most common). The specimen is pulled at a constant speed until either the sample is split or fails. Parameters such as peak peel load, average peel strength and statistical measures of peel strength variability are typically used to characterize behaviour under peel loading. Types of failure are noted as cohesive, adhesive, or substrate failure [58,59].

In Paper 1 and Paper 3, the adhesion between PE-containing film and the paperboard was evaluated by the T-peel test at 180^{o} and a peel rate of 30 mm/min. on a testing device Zwich Z250 (see Fig. 20). The testing was done at 23^{o}C and 30 % RH.

3.3.6. Tensile testing

A tensile test is used to determine the modulus of elasticity, elastic limit, elongation, proportional limit, tensile strength, and yield strength. The result of a tensile test is a load versus elongation curve which is then converted into a stress versus strain curve (see Fig. 21). The tensile testing is followed the ISO 527-1 standard [60].

In this study, the tensile test was performed on a Zwich Z250 testing device (see Fig. 20) to determine the effect of POSS compounds on the mechanical properties of the PE/POSS films (PE/bio-POSS films in Paper 1, and PE/amino-POSS films in Paper 3).

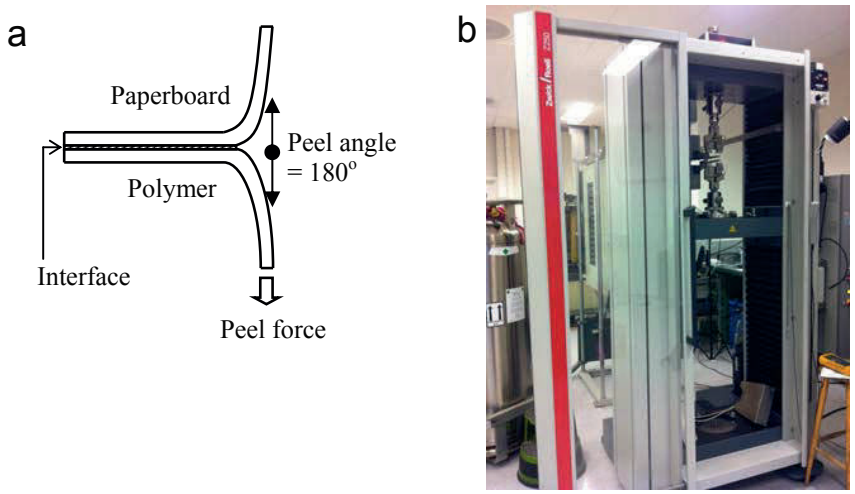

Fig. 20. a) Schematic drawing of T-peel test; b) Testing device Zwich-Z250

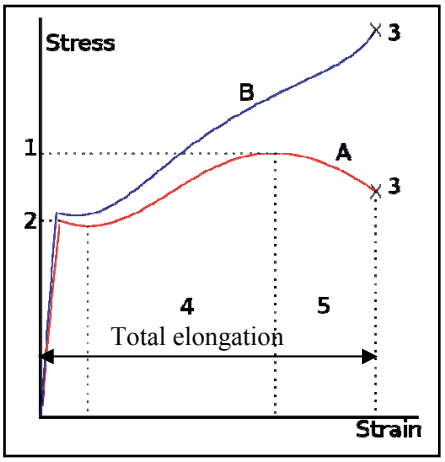

Fig. 21. A typical stress–strain curve, adapted from [61]
1) Ultimate strength; 2) Yield strength; 3) Rupture; 4) Strain hardening region; 5) Necking region; A) Engineering stress; B) Actual stress

3.3.7. Carbonyl index

A carbonyl index (CI) can be used to determine the amount of each of the carbonyl groups formed during the oxidation of a polymer. This is done by analyzing the ATR-FTIR spectra of the polymeric film. CI is calculated as the ratio of the absorbance (A) of the carbonyl absorption band in the 1700–1780cm^{-1} region and C-H scissoring at 1464 cm^{-1} in the spectrum:

$$C.I. = \frac{A_{1700-1780cm^{-1}}}{A_{1464cm^{-1}}} \text{ (Eq. 5) [62-64].}$$

The peaks at 1740, 1715 and 1705 cm^{-1} in the carbonyl range are attributed to ester, ketone and acid group, respectively.

In Paper 3, CI was used to assess the formation of carbonyl groups at 1736 cm^{-1} during the thermal oxidation of PE/amino-POSS/$FeSt_3$ films.

3.3.8. Melt flow index (MFI)

Melt flow index (MFI) is an assessment of average molecular mass and is an inverse measure of the melt viscosity. The higher a MFI, the easier the polymer flows under the test conditions. Knowing the MFI of a polymer is vital to anticipating and controlling its processing. The factors that can affect flow properties of a polymer include molecular weight distribution, the presence of co-monomers, the degree of chain branching and crystallinity [65].

The MFI is calculated as the amount (in grammes) of a polymer that is extruded out during 10 minutes through a standard die of 2.09 mm in diameter and 8.00mm in length when a fixed pressure is applied to the melt via a piston and a load of total mass of 2.16 kg at a temperature of 190°C (some polymers are measured at a higher temperature, at different weights and at different orifice sizes):

$$\text{MFI} = \frac{\text{Average extrudate weight}}{\text{Time}} \text{ (g/10 min.) (Eq. 6)}$$

In this study, the effect of adding bio-POSS (in Paper 1) and amino-POSS (in Paper 3) on the melt flow property of PE was investigated by using the MFI method on a test device Davenport 3/80 (see Fig. 22).

Fig. 22. Test device Davenport 3/80

3.3.9. Barrier properties

a) Water transmission rate (WTR)

The pure water transmission rate is defined as the amount of water that passes through a membrane per unit time and per unit area. The WTR is calculated as:

$$WTR = (W_1 - W_2)/tA \text{ , } (\text{g/m}^2 \text{ day}), \text{ (Eq. 7)},$$

where WTR is the rate of water passed through the substrate, W_1 and W_2 are the weights (in grams) of the sample holder which is sealed by the tested sample and contain liquid water before and after water permeability test during the time period t (days), and A is tested area (m^2).

b) Water vapour transmission rate (WVTR)

Water vapour transmission rate (WVTR) measure the ability of moisture transport through a sheet material of specific thickness and steady state conditions. According to the ASTM E96/E96M-10 [67], WVTR is measured at 23^{o}C with a surrounding atmosphere of 50% relative humidity (RH), and an atmosphere of 0% RH and 23^{o}C inside the test cup. The result is reported as grams per square meter over a 24 hrs. Calculation of the WVTR is expressed as follows:

$$WVTR = G/tA \ (\text{g/m}^2\text{day}), \text{ (Eq. 8)}$$

where WVTR is rate of water vapour transmission, G is weight change in grams for the time period t; A is test area, m^2.

c) Water vapour permeability (WVP)

The water vapour permeability (WVP, gm/m^{2}dayPa) was calculated as:

$$WVP = \frac{WVTR.L}{\Delta p} = \frac{WVTR.L}{S.(R_1 - R_2)}, \text{ (Eq. 9)}$$

where WVTR is the measured water vapour transmission rate (g/m^{2}day) through the paperboard, L is the mean thickness (m) of the paperboard and Δp is vapour pressure difference across two sides of the paperboard, S is saturation vapour pressure at the test temperature and calculated as $S = \exp(20.836 - 5132/T)$, where T is Kelvin temperature; R_1 and R_2 is relative humidity outside and inside the test cup [66].

In Paper 2, WTR, WVTR and WVP of paperboard and bio-POSS coated paperboards were respectively measured.

Chapter 4
SUMMARIES OF THE APPENDED PAPERS

4.1. Polyethylene/octa-(ethyl octadeca-10,13 dienoamide) silsesquioxane blends and the adhesion strength to paperboard (Paper 1)

Adhesion between polyethylene (PE) and paperboard is an important property of PE coated paperboard for food packaging. The adhesion can be affected by surface treatment of the paperboard or modifying the PE containing layer prior to coating. In Paper 1, the adhesion property of PE coated paperboard was examined and the effect of modifying the PE containing layer using bio-POSS octa-(ethyl octadeca-*10,13* dienoamide) silsesquioxane was investigated.

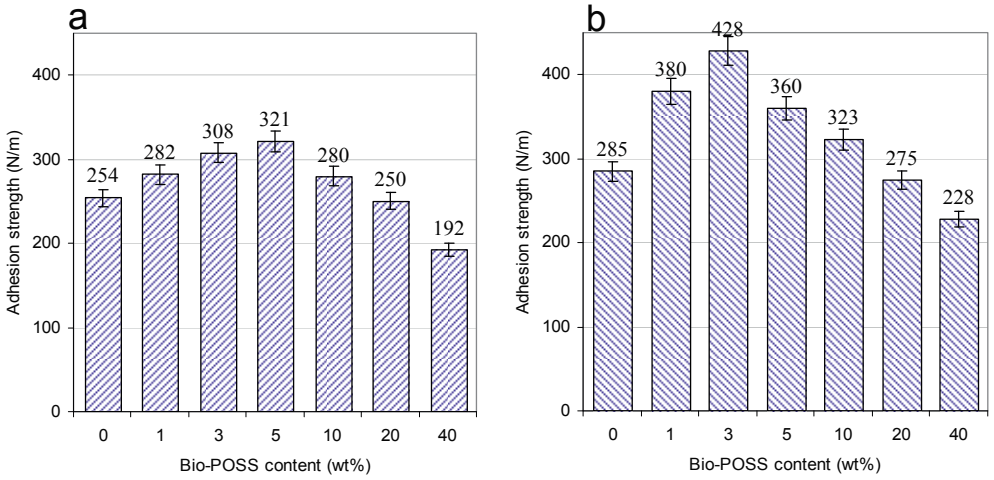

Fig. 23. Adhesion strength of PE/bio-POSS blends to paperboard when coated at: a) 200°C/20°C, and b) 300°C/20°C

After drying at 150°C for 24 hrs, bio-POSS was mixed with polyethylene at different ratios. The PE/bio-POSS products were coated on the paperboard by compression moulding coating. The T-peel test showed that low content of bio-POSS significantly improved the adhesion strength between PE and the paperboard: at 5 wt% and 3 wt% bio-POSS when coating temperature was 200°C/20°C and 300°C/20°C, respectively. However, loading bio-POSS content above 5 wt% dramatically decreased the adhesion of the blends to paperboard (see Figure 23).

Optical microscopy of the fracture surfaces showed that the failure of the adhesive joint was located at the interface between the films and the paperboard (apparently interfacial failure, as can be seen in Figure 24).

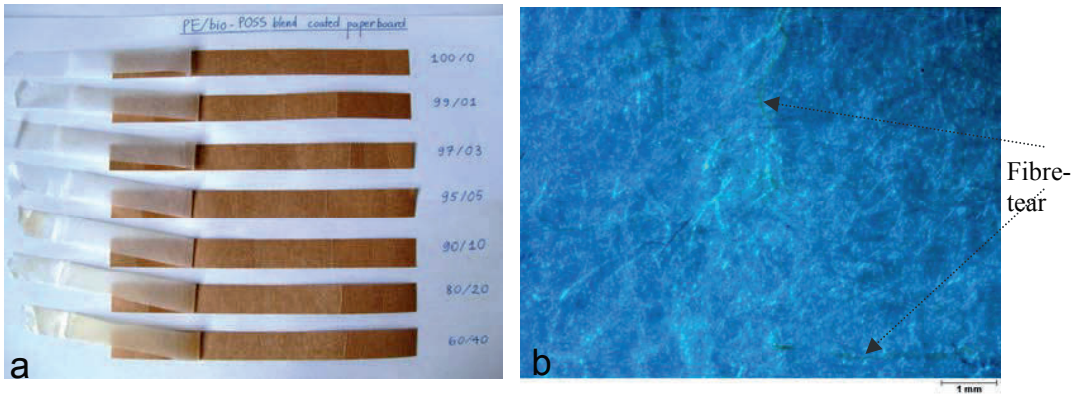

Fig. 24. Sample of PE/bio-POSS blends coated paperboard after peeling (a), and typical fracture surface of blend side with fibre-tear effect (b)

The interaction at the interface between the blends (amide group) and the paperboard (hydroxyl group) and mechanical interlocks were the probable reasons for adhesion improvement. Such interfacial interaction leads to an alteration in the band shapes in the ATR-FTIR spectra of amide groups of the blends and hydroxyl groups of the paperboard: in Figure 25a, the intensity ratio I_{aI}/I_{aII} between amide I (near 1713 cm^{-1}) and amide II (near 1645 cm^{-1}), is always higher than 1 (the blends before coating); on the fracture surface (Figure 25b), such ratio varies on bio-POSS contents: $I_{aI}/I_{aII}<1$ (1,3,5 wt%), $I_{aI}/I_{aII}>1$ (10,20,40 wt%); the spectra of the top surfaces (Figure 25c) are relatively similar to those before coating (Fig. a): I_{aI} is always higher than I_{aII}.

The interfacial interaction between amide groups of the blends and hydroxyl groups of the paperboard could also alter the hydroxyl band. As can be seen in Figure 26, the spectrum a, b, c shows a little change in the band shape of OH, as an unsmooth curve of OH band. Whereas, the band shapes of OH group in the spectrum d, e, and f are relatively similar to that of OH in the reference paperboard, reflecting an inconsiderable interaction.

In conclusion, bio-POSS octa-(ethyl octadeca-*10,13* dienoamide) silsesquioxane can be an effective additive in improving the adhesion property of food packaging material PE-coated paperboard.

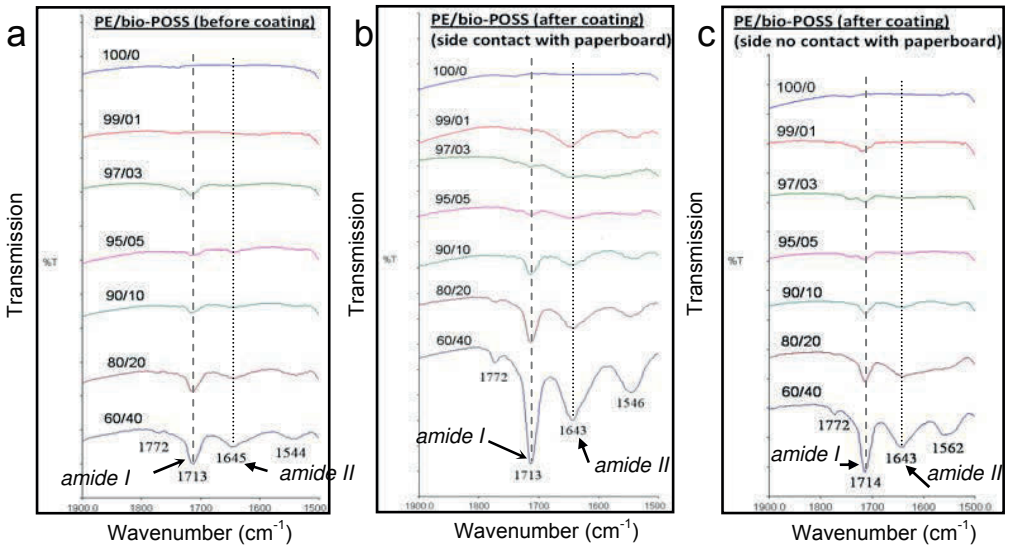

Fig. 25. ATR-FTIR spectra of PE/bio-POSS blends in the region 1900-1500 cm^{-1}: (a) before coating, and after coating: (b) side contact with paperboard, (c) side contact with mould

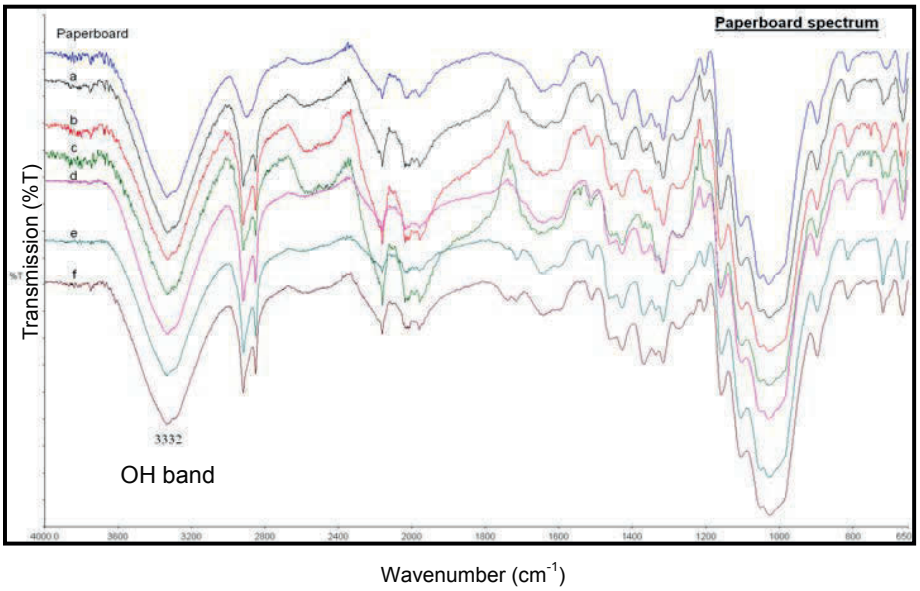

Fig. 26. ATR-FTIR spectrum of reference paperboard and fracture surface paperboard side after peeling blend films with bio-POSS content:
(a): 1%; (b) 3%; (c): 5%; (d): 10%; (e): 20%; (f): 40%

4.2. Effects of hydrophobic polyhedral oligomeric silsesquioxane coating on water vapour barrier and water resistance properties of paperboard (Paper 2)

The substitution of fossil based packaging materials with materials from renewable sources is a topic of current interest. Polyhedral oligomeric silsesquioxanes with fatty acid moieties can have a renewable raw material content of more than 90% and are therefore called bio-POSS. The objective of Paper 2 was to examine how bio-POSS octa-(ethyl erucamide) silsesquioxane coating influences the water resistance and water vapour barrier properties of paperboard.

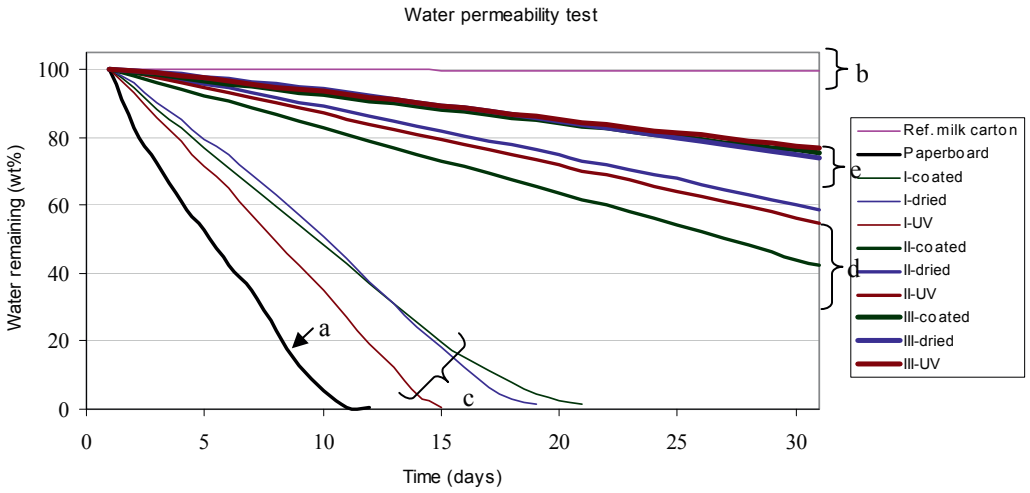

Fig. 27. Water permeability of bio-POSS coated paperboard: a) Un-coated paperboard; b) Reference sample; c) Single coated (I—); d) Double coated (II─); e) Triple coated (III▬)

By liquid coating bio-POSS on paperboard (approx. 30µm in coating thickness), an increase in the water resistance and the water vapour barrier properties of the paperboard were obtained. Further improvement was achieved by drying the bio-POSS coating layer at 80°C. Especially, the water resistance and the water vapour barrier properties of paperboard were considerably enhanced by multiple coating (see Figure 27 and 28).

Table 3 shows the water transmission rate (WTR) and water vapour transmission rate (WVTR) of paperboard before and after bio-POSS coating. High WTR and WVTR of the uncoated paperboard reflect that the uncoated paperboard has an inhomogeneous porous structure. It leads to a high standard deviation of WTR and WVTR of the uncoated paperboard. The standard deviations are decreased when bio-POSS was coated on the paperboard, especially by

multiple coating. The structure of the paperboard became more homogeneous with bio-POSS coating.

Significant enhancement in the water resistance and water vapour barrier properties by multiple coating was due to the increase in the coating layer thickness. The thicker coating layer contains less pores and depressions on its top coated surface, as seen using the pinhole test.

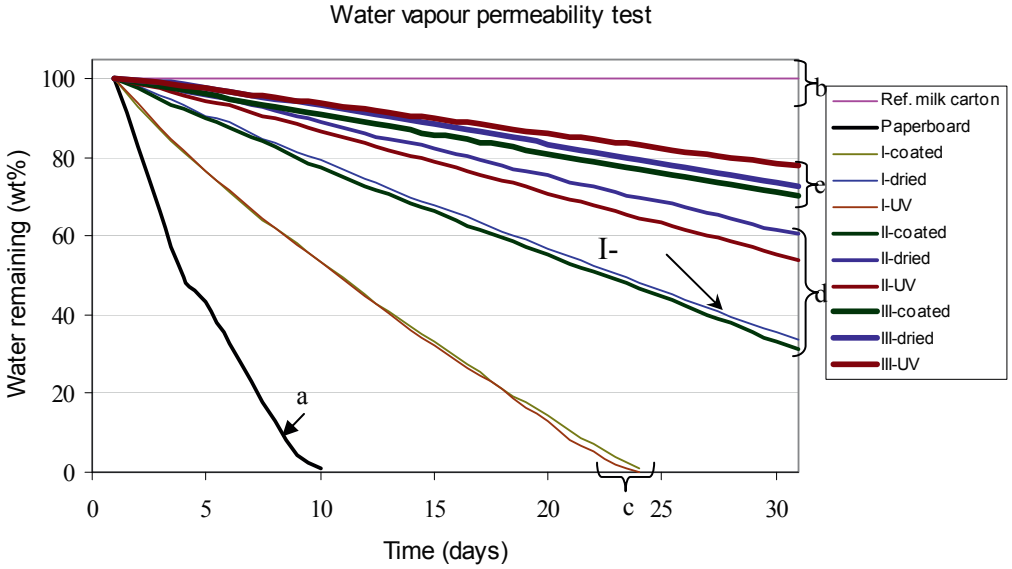

Fig. 28. Water vapour permeability of bio-POSS coated paperboard: a) Un-coated paperboard; b) Reference sample; c) Single coated (I—); d) Double coated (II─); e) Triple coated (III▬)

Table 3. Water transmission rate (WTR) and water vapour transmission rate (WVTR) of bio-POSS coated paperboard

Substrate	WTR (g/m^2day)	WVTR (g/m^2day)
Paperboard	999±333	1011± 447
Single coating (I—)		
I-coated	579±88	477±129
I-dried	506±133	209±28
I-UV-treated	595±193	450±78
Double coating (II─)		
II-coated	194±18	229±19
II-dried	142±23	128±16
II-UV-treated	152±17	163±18
Triple coating (III▬)		
III-coated	83±8	105±11
III-dried	74±15	80±21
III-UV treated	71±12	72±12

A crosslinking reaction between the double bond of bio-POSS's organic groups could not be found by using solid state ^{1}H-NMR of the post treated coating layer. In figure 29, the peak at 5.8 ppm was attributed to hydrogen (H) attached to double bond (C=C) that was similar in the spectra of 3 samples.

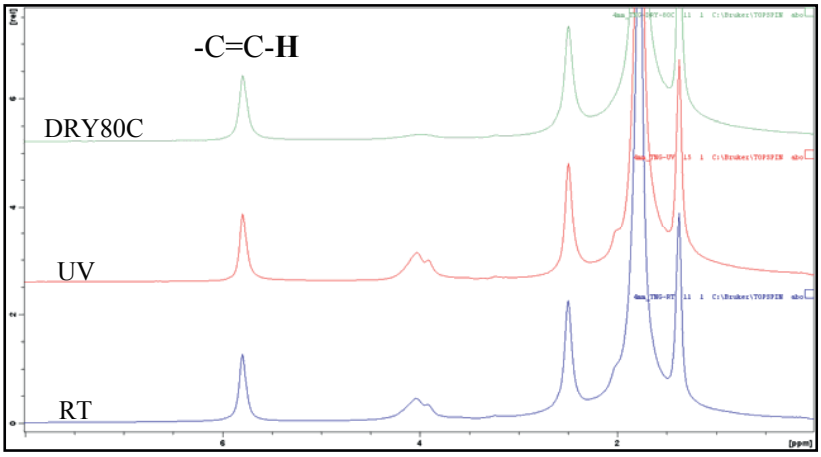

Fig. 29. Solid state 1H NMR spectrum of bio-POSS layer: (RT): dry at room temperature; (DRY80C): dried at 80^{o}C; (UV): UV-treated

In addition, bio-POSS octa-(ethyl erucamide) silsesquioxane coating successfully improves the water resistance and water vapour barrier properties of paperboard.

4.3. Effects of a pro-oxidant additive on the adhesion of polyethylene/amino-functionalized POSS compounds to paperboard (Paper 3)

The introduction of a pro-oxidant additive such as a transition metal salt can promote the degradation of polyethylene, resulting in a formation of carbonyl groups (C=O) on the PE's surface. The surface polarity of PE increases, leading to an improvement in adhesion when PE is coated on board. The objective of Paper 3 was to investigate the effect of ferric stearate ($FeSt_3$) on the degradation of polyethylene in compound with amino functionalized POSS (PE/amino-POSS). The effect on the adhesion of the films to paperboard was also investigated.

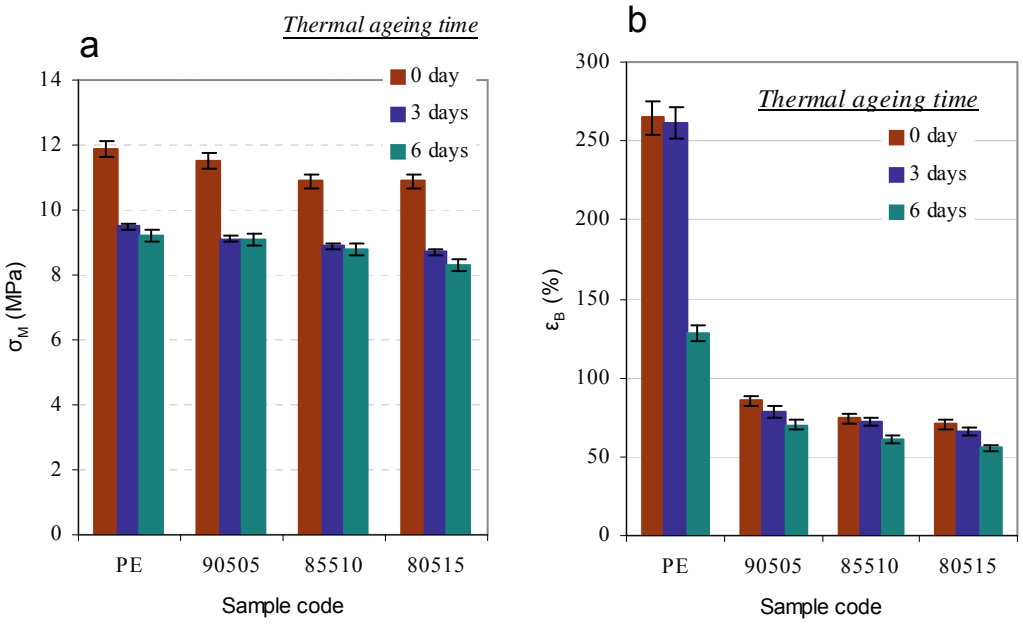

Fig. 30. Effect of thermal aging on the ultimate tensile strength (a), and elongation at break (b) of PE/amino-POSS/$FeSt_3$ films

PE/amino-POSS/$FeSt_3$ compounds were prepared by melt mixing the mixture of PE, masterbatch amino-POSS/PE, masterbatch $FeSt_3$/PE in different weight ratios on micro-extruder. The PE/amino-POSS/$FeSt_3$ compounds were converted to thin films and thermally aged at 70°C in an air circulation oven. The mechanical testing showed that tensile yield strength of the films was slightly decreased with increasing amino-POSS content and the thermal aging time. Elongation at break was moderately decreased but still kept above 50% as shown in figure 30: sample code 90505, 85510 and 80515 corresponds with the sample containing 5 wt% $FeSt_3$ and 5, 10 and 15 wt% amino-POSS, respectively.

The compounds were coated on paperboard by compression moulding. The adhesion strength (determined by T-peel testing) was decreased with increasing amino-POSS content. When the compounds were thermally aged at 70°C in air circulation oven prior to coating, the adhesion was increased with the thermal ageing time. The improvement in adhesion was up to approx. 30% in the sample of the aged compounds (99% PE/0.5 wt% amino-POSS/0.5 wt% $FeSt_3$) coated paperboard, as illustrated in figure 31:

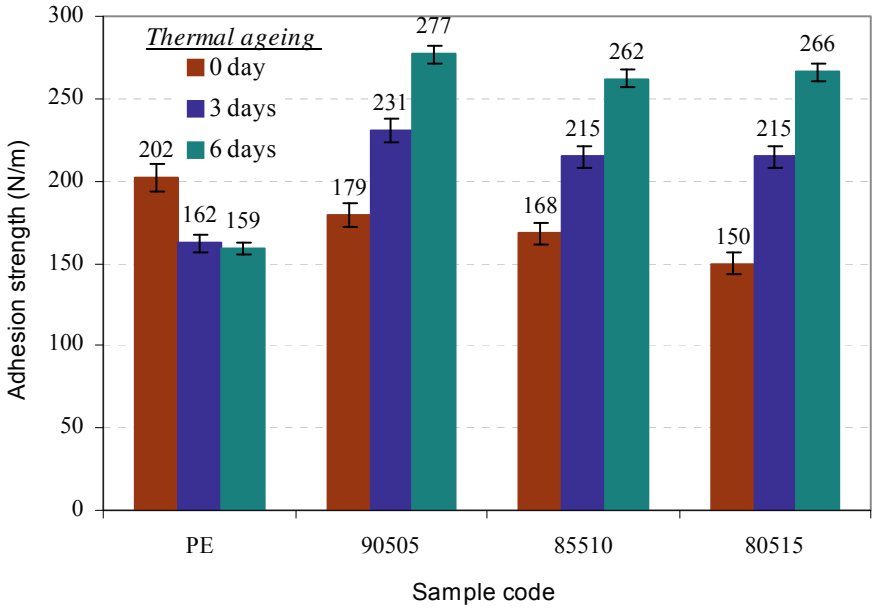

Fig. 31. Adhesion strength of PE/$FeSt_3$/amino-POSS compounds to paperboard

During thermal ageing, the polymer chain scission occurred, leading to an increase in the MFI of the compounds (figure 32). Carbonyl group was formed on the surface of the film due to an oxidative degradation, as identified by ATR-FTIR (Fig. 33). The calculation of the CI shows that the carbonyl group was increased with the thermal aging time and the oxidative degradation of PE was limited by amino-POSS, see figure 34.

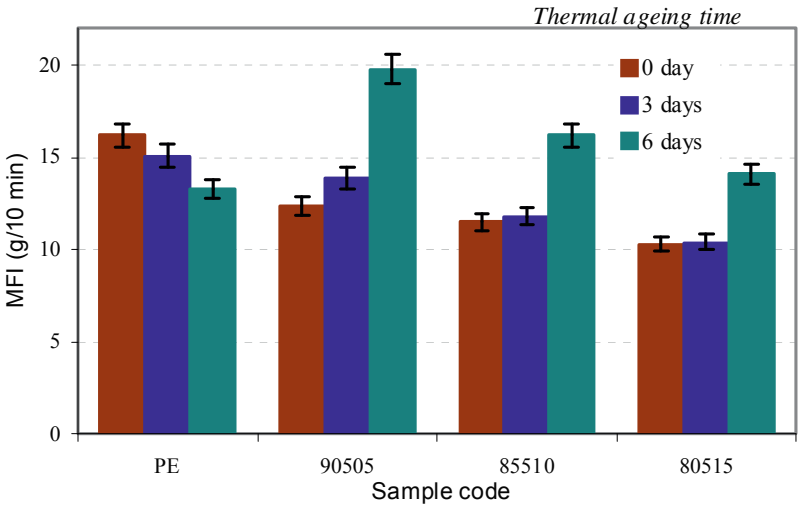

Fig. 32. Melt flow index of PE and PE/amino-POSS/$FeSt_3$ compounds

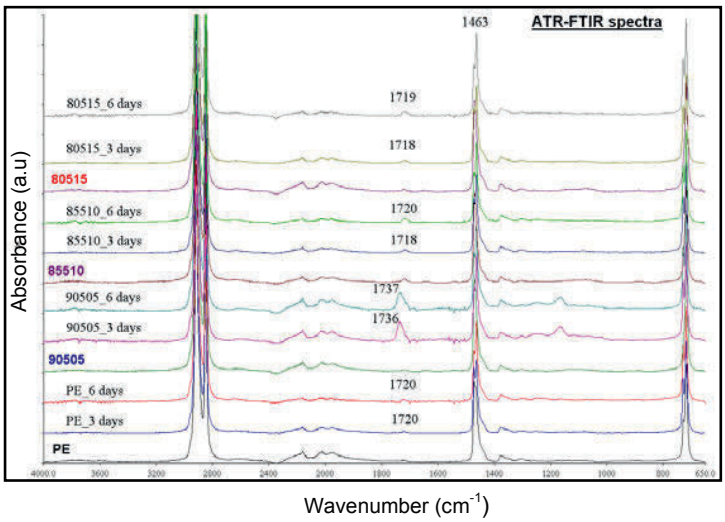

Fig. 33. ATR-FTIR spectra of the compounds before and after thermal ageing

The formation of carbonyl groups can lead to an increase in the surface polarity of the PE/amino-POSS/$FeSt_3$. When the compounds were coated on paperboard, interfacial interaction between C=O of the compounds and OH of paperboard may occur, thereby improving the adhesion. Furthermore, improved mechanical adhesion by improved mechanical interlocking could be a reason for the adhesion improvement.

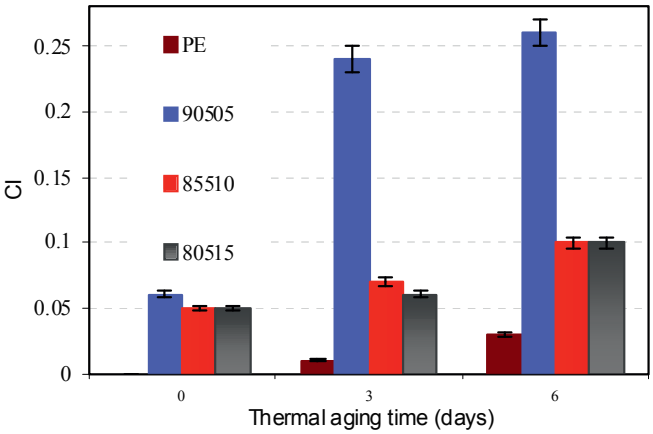

Fig. 34. Carbonyl index (CI) of PE and PE/amino-POSS/$FeSt_3$ film

Chapter 5
OVERALL DISCUSSION

This thesis addresses the adhesive and barrier properties of coatings on paper materials which contain different POSS materials. In this chapter the mechanisms behind the observed behaviour will be discussed for the different experiments seen in connection.

In chapter three the different possible mechanisms for adhesion between a surface and an adhesive were presented. The surfaces of paper materials are characterized by being rough on a micro scale as the wood fibres themselves typically have a cross sectional thickness off 4-30 microns depending on fibre wall thickness and degree of collapse of the lumen. Further paper materials have a high porosity (20-75%) with a network of interconnected pores penetrating the entire sheet of paper. The surface of paper fibres is hydrophilic and has a rather high surface energy in its natural state. However hydrofobation chemicals such as resin acids are often used to make the paper somewhat more water repellent and then also reduce the papers surface energy.

This rough and porous surface of paper means that adhesives that have a sufficiently low surface energy and sufficiently low viscosity will to a certain extent penetrate the structure. It is therefore reasonable to assume that changing the coating material so that the viscosity is reduced tends to improve adhesion due to improved mechanical interlocking. Therefore this is suggested as one possible explanation for the enhanced adhesion when a few percent bio-POSS was mixed with PE in Paper 1. Mechanical interlocking affects the adhesion of polyethylene (PE)/bio-POSS blends to paperboard through reduced viscosity as measured by the melt flow index of the blends. At high temperature and pressure of the coating process, PE/bio-POSS blends are melted. Molten blends can act as a highly viscous liquid. The melt spreads over the paperboard surface and penetrate into holes, pores and depressions, leading to formation of mechanical interlocks at the interface. The same behaviour may have been important in paper three where the addition of iron stearate increased melt flow index, probably by polymer chain cutting and thereby reduced viscosity of the mixture. It is likely that this have made the coating penetrate further into the paper and thereby increased the adhesion by mechanical interlocking. Another phenomenon that is connected with mechanical interlocking may also have played a role for adhesion. When the chemical composition of a coating changes, so will the mechanical

properties of that coating. This means that the strength of the mechanical interlocking will increase if the strength properties of the film material increase. Unfortunately it is difficult to measure the strength of the films on the paper surface directly and this was outside the scope of this thesis. However it is recommended that this is studied in future work.

For surface coatings that are mixtures of different materials, e.g. PE and bio-POSS as in paper one, there is always a risk that non-perfect mixing or a separation after lamination but before the material solidifies can cause the layer facing the paper to have a different chemical composition than the bulk of the coating. If such a separation happens it would be normal for a material that may reduce the interfacial energy to be concentrated at the interface. In this case the amino-groups in bio-POSS and their interaction with hydroxyl groups in the paper carbohydrates could have had such an effect. Such separation was not measured directly, but the mixing of bio-POSS and PE was observed not to be perfect (by microscopy) and the adhesion was falling when 10% or more bio-POSS was added. If such a layer is formed at the interface, there is a risk that either the bond between the paper and the interface layer or between the interface layer and the bulk of the coating material may be a weak boundary layer and explain the reduced strength of the adhesion joint with increasing amounts of bio-POSS of the PE/bio-POSS coated paperboards.

Chapter 6

CONCLUSIONS AND FUTURE WORK

It has been shown that the adhesion of polyethylene (PE) to paperboard was successfully improved (approx. 50%) by introducing 3-5 wt% bio-POSS octa-(ethyl octadeca-*10,13* dienoamide) silsesquioxane into PE layer. It is probable that the improvement in adhesion strength is due to mechanical adhesion and interface interaction between the amide of bio-POSS and the hydroxyl groups of paperboard. An examination of the fracture surface showed that the adhesion failure occurred at interface between the PE/bio-POSS film and the paperboard. The measured adhesion was then the adhesion strength between PE/bio-POSS blends and paperboard, not cohesion of PE/bio-POSS films or the strength of the paperboard. The miscibility between bio-POSS and PE, as well as its effect on the adhesion of PE/bio-POSS to paperboard were not studied in this study, and should be studied in future work.

The extremely low water resistance and water vapour barrier properties of paperboard were improved by liquid coating bio-POSS octa-(ethyl erucamide) silsesquioxane. Approx. 60% reduction in water transmission rate (WTR) and water vapour transmission rate (WVTR) were obtained. Heat drying further increased water and water vapour barrier, but UV-treatment of the bio-POSS coating layer did not have a significant effect. Multiple coating induced a significant improvement in the water resistance as well as the water vapour barrier properties of paperboard. This study demonstrated that bio-POSS coating can give a reasonable water barrier to substitute the fossil based material for the water and water vapour barrier of food packaging coated paperboard.

The oxidative degradation of polyethylene (PE) was promoted by introducing ferric stearate ($FeSt_3$) at 0.5 wt% as a pro-oxidant. The oxidation was limited by the presence of octa-(ethyl 11-aminoundecanoamide) silsesquioxane (amino-POSS). Because of oxidative degradation, carbonyl groups were formed on the surface of PE/amino-POSS/$FeSt_3$ compounds, especially when they were thermally aged at 70^{o}C in a circulation oven. When the compounds were coated on paperboard, the adhesion strength was increased up to 30%. The interaction between C=O of the compounds and OH of paperboard and mechanical adhesion could explain the adhesion improvement. Although the tensile yield strength and elongation at break of the PE/amino-POSS/$FeSt_3$ film were decreased. Elongation at break was still over than 50% after 6 days thermal aging which is acceptable for a coating material on paperboard for packaging.

This work confirmed that POSS compounds with fatty acid moieties (bio-POSS) can be used as additives in the polyethylene layer in food packaging PE-coated paperboard. As for continuation of this work, studying the miscibility between bio-POSS and PE is needed. An investigation of the effect of miscibility on the adhesion strength to paperboard would give a better understanding of the adhesion mechanism.

Bio-POSS compounds are potentially interesting for liquid barrier coating. This work showed that liquid coating bio-POSS on paperboard by using bar coater can create a smooth surface with wear resistant properties. Even though no complete water and water vapour barrier properties of paperboard can be obtained by 30μm bio-POSS coating layer, the change in concentration of bio-POSS coating solution and coating thickness can make the barrier more effective.

This work has presented the effective effect of ferric stearate ($FeSt_3$) on the oxidative degradation of polyethylene/POSS blends. The use of $FeSt_3$ can combine the recyclability of plastic films with the improvement in adhesion. It may lead to an industrial application to produce food packaging PE coated paperboard with improved adhesion, in which thermal treatment of PE containing pro-oxidant before the coating process is required.

References

1. Rhim JW, Lee JH, Hong SI. Water resistance and mechanical properties of biopolymer (alginate and soy protein) coated paperboards. LWT- Food Sci Technol 2006; 39: 806–13.
2. Suchada T, Tunyarut J, Ampron S, Pornchai R, Dheerawan B. The improvement of water resistance property of paperboard by SF_6 plasma. Jnl Metal, Mater Minerals 2008; 18(2): 153–6.
3. Amberg-Schwab S, Hoffmann M, Bader H, Gessler M. Inorganic-organic polymers with barrier properties for water vapour, oxygen and flavours. Jnl Sol-Gel Sci Technol 1998; 13: 141–6.
4. Amberg-Schwab S, Katschorek H, Weber U, Hoffmann M, Burger A. Barrier properties of inorganic-organic polymers: Influence of starting compounds, curing conditions and storage. Scaling-up to industrial application. Jnl. Sol-Gel Sci Technol 2000; 19: 125–9.
5. Markovic E, Constantopolous K, Matisons JG. Polyhedral oligomeric silsesquioxanes: from early and strategic development through to materials application. Application of Polyhedral Oligomeric Silsequioxanes: Chap. 1. C. Hartmann-Thompson (ed.) Advances in Silicon Science, 2011; 3: 1–46.
6. Schwab JJ, Lichtenhan JD. Polyhedral oligomeric silsesquioxane (POSS)-based polymers. Appl Organometal Chem 1998; 12: 707–13.
7. Li GZ, Wang LC, Ni H, Pittman CU. Polyhedral oligomeric silsesquioxane (POSS) polymers and copolymers: a review. Jnl Inorg Organomet Polym 2001; 11(3): 123–54.
8. Pan G. Polyhedral oligomeric silsesquioxane (POSS). Physical properties of polymers handbook, Chap.34. Mark JE (ed.), Springer 2007; 6: 577–84.
9. Wu J, Mather PT. POSS polymers-physical properties and biomaterials applications. Jnl Macromol Sci: Part C: Polymer Reviews 2009; 49: 26–30.
10. Cordes DB, Lickiss PD. Preparation and characterization of polyhedral oligosilsesquioxanes. Application of Polyhedral Ologomeric Silsequioxanes: Chap. 2. C. Hartmann-Thompson (ed.) Advances in Silicon Science 3 (2011) 47–133.
11. Fina A, Tabuani D, Frache A, Camino G. Polypropylene-polyhedral oligomeric silsesquioxanes (POSS) nanocomposites. Polym 2005; 46: 7855–66.

12. Joshi M, Butola BS, Simon G, Kukaleva N. Rheological and viscoelastic behavior of HDPE/octamethyl-POSS Nanocomposites. Macromol 2006; 39: 1839–49. Joshi M, Butola BS. 13. Isothermalcrystallization of HDPE/octamethyl polyhedral oligomeric silsesquioxane nanocomposites: role of POSS as a nanofiller. Jnl Appl Polym Sci 2007; 105: 978–85.

14. Misra R, Fu BX, Morgan SE. Surface energetics, dispersion and nanotribomechanical behavior of POSS/PP hybrid nanocomposites. Jnl Polym Sci, part B: Polym Phys 2007; 45: 2441-55.

15. Zhou Z, Zhang Y, Zhang Y, Yin N. Rheological behavior of polypropylene/ octavinyl polyhedral oligomeric silsesquioxane composites. Jnl Polym Sci Part B: Polym Phys 2008; 46: 526–33.

16. Sánchez-Soto M, Schiraldi DA, Illescas S. Study of the morphology and properties of melt-mixed polycarbonate–POSS nanocomposites. Euro Polym Jnl 2009; 45: 341–52.

17. Lim SK, Hong EP, Choi HJ, Chin IJ. Polyhedral oligomeric silsesquioxane and polyethylene nanocomposites and their physical characteristics. Jour Indus Eng Chem 2010; 16: 189–92.

18. Fina A, Tabuani D, Frache A, Camino G. Polypropylene-polysilsesquioxane blend. Euro Polym Jnl 2010; 46: 14–23.

19. Zhang Z, Liang G, Wang X. The effect of POSS on the thermal properties of epoxy. Polymer Bulletin, 2007; 58: 1013–20.

20. Zhang Z, Gu A, Liang G, Ren P, Xie J, Wang X. Thermo-oxygen degradation mechanisms of POSS/epoxy nanocomposites. Polym Degrad Stab, 2007; 92: 1986–93.

21. Ramírez C, Rico M, Torres A, Barral L, López J, Montero B. Epoxy/POSS organic–inorganic hybrids: ATR-FTIR and DSC studies. Euro Polym Jnl, 2008; 44: 3035–45.

22. Li Q, Hutcheson SA, McKenna GB, Simon SL. Viscoelastic properties and residual stresses in polyhedral olygomeric silsesquixanes-reinforced epoxy matrices. Jnl Polym Sci, part B: Polym Phys 2008; 46: 2719–32.

23. Matějka L, Murias P, Pleštil J. Effect of POSS on thermomechanical properties of epoxy–POSS nanocomposites. Euro Polym Jnl, 2012; 48, 260–74.

24. Amerio E, Sangermano M, Colucci G, Malucelli G, Messori M, Taurino R, Fabbri P. UV Curing of organic-inorganic hybrid coatings containing polyhedral oligomeric silsesquioxane blocks. Macromol Mater Eng 2008; 293, 700–7.

25. Mirchandani G, Waghoo G, Parmar R, Haseebuddin S, Ghosh SK. Oligomeric silsesquioxane reinforced polyurethane with enhanced coating performance. Progress in Organic Coatings 2009; 65(4): 444–9.

26. Jerman I, Koželj M, Orel B. The effect of polyhedral oligomeric silsesquioxane dispersant and low surface energy additives on spectrally selective paint coatings with self-cleaning properties. Solar Energy Materials and Solar Cells, 2010; 94: 232–45.

27. Männle F, Tofteberg TR, Skaugen M, Bu H, Peters T, Pascal D. C. Dietzel, Pilz M. Polymer nanocomposite coatings based on polyhedral oligosilsesquioxanes: route for industrial manufacturing and barrier properties. Jnl Nanopart Res 2011; 13: 4691–701.

28. Su HW, Chen WC. Preparation of nanoporous poly (methyl silsesquixane) films using core-shell silsesquioxane as porogen. Mater Chem Phys 2009; 114(2-3): 736–41.

29. Zhang L, Abbenhuis HCL, Yang Q, Wang YM, Magusin PCMM, Mezari B, van Santen RA, Li C. Mesoporous organic-inorganic hybrid materials built using polyhedral oligomeric silsesquioxane blocks. Angew Chem Int Ed 2007; 46(26): 5003-6.

30. Kannan RY, Salacinski HJ, Butler PE, Seifalian AM. Polyhedral oligomeric silsesquioxane nanocomposites: the next generation material for biomedical applications. Acc Chem Res 2005; 38(11): 879–84.

31. Kidane AG, Edirisinghe MJ, Bonhoeffer P, Seifalian AM. Flow behaviour of a POSS biopolymer solution. Biorheology 2007; 44: 265–72.

32. Wheeler PA, Fu BX, Lichtenhan JD, Weitao J, Mathias LJ. Incorporation of metallic POSS, POSS copolymers, and new functionalized POSS compounds into commercial dental resins. Jnl Appl Polym Sci 2006; 102(3): 2856–62.

33. DeArmitt C. Polyhedral Oligomeric Silsesquioxanes in Plastics. Application of Polyhedral Oligomeric Silsequioxanes: Chapter 5. C. Hartmann-Thompson (ed.) Advances in Silicon Science 2011; 3: p. 209–28.

34. Scott G. Photo-biodegradable plastics. Their role in the protection of the environment. Polym Degrad Stab 1990; 29: 135–54.

35. Roy PK, Surekha P, Raman R, Rajagopal C. Investigating the role of metal oxidation state on the degradation behaviour of LDPE. Polym Degrad Stab 2009; 94(7): 1033–9.

36. Männle F, Rodseth KR, Kleppe EA, Hauge R, Tanem BS. Combination of additives for use in preparation of themoplastics. US Patent Application Publication US 2009/0226749 A1, p1.

37. Männle F, Jørgensen JK, Tanem BS. Increased performance of thermoplastic packaging materials by using a mild oxidizing biobased additive. Int Jnl Polym Sci 2012, doi:10.1155/2012/297923.

38. http://en.wikipedia.org/wiki/Oxo_Biodegradable

39. Wicks ZW, Jones FN, Pappas SP, Wicks DA. Organic Coating: Science and Technology: Chapter 6, 3rd (ed.) John Wiley & Sons, Inc, 2007; 121–5.

40. Wenzel RN. Industrial and Engineering Chemistry 28, 1936; 988–94.

41. Dillard DA, Pocius AV (Editor). Adhesion Science and Engineering II, Elsevier (2002) Ch2. 74-138, Ch7. 317–49.

42. Holmberg K, Jönsson B, Kronberg B and Lindman B. Surfactants and Polymers in Aqueous Solution. Ch 18.John Wiley & Sons, Ltd. (2002) 389–402.

43. Young T. Miscellaneous works of the late Thomas Young. London: John Murray; 1855.

44. Kemppi A. Studies on the adhesion between paper and low density polyethylene. Laboratory of Paper Chemistry. Åbo Akademi University. Åbo, 1997; 7–39.

45. Dupré A. Theorié mécanique de la chaleour. Paris: Gauthier-Villars; 1869.

46. http://www.slideshare.net/ashrikant58/05adhesion-and-adhesives-theory

47. http://www.specialchem4adhesives.com/home/editorial.aspx?id=1449

48. Ashley RJ. Permeability and Plastic Packaging. Polymer Permeability. Chap. 7, Comyn J. (Ed.) Elsevier Applied Science Publishers, p. 269–91.

49. http://www.sintef.no/Projectweb/FunzioNano/Synthesis-of-FunzioNano-/

50. http://www1.chm.colostate.edu/Files/CIFDSC/dsc2000.pdf

51. http://www.purdue.edu/rem/rs/sem.htm

52. http://en.wikipedia.org/wiki/Optical_microscope

53. FT-IR spectroscopy, Attenuated Total Reflectance (ATR). www.perkinelmer.com

54. http://en.wikipedia.org/wiki/Proton_NMR

55.http://www2.chemistry.msu.edu/faculty/reusch/VirtTxtJml/Spectrpy/nmr/nmr1.htm

56. http://en.wikipedia.org/wiki/Solid-state_nuclear_magnetic_resonance

57. http://mutuslab.cs.uwindsor.ca/schurko/ssnmr/ssnmr_schurko.pdf

58. http://www.mecmesin.com/knowledge-centre/test-types/peeladhesion-testing

59. http://www.mts.com/en/products/application/materials-testing/adhesives-coatings/peel/index.htm

60. ISO 527-1: Standard test method for plastics -determination of tensile properties

61. http://en.wikipedia.org/wiki/Ultimate_tensile_strength

62. Chiellini E, Corti, A, D'Antone S, Baciu R. Oxo-biodegradable carbon backbone polymers–Oxidative degradation of polyethylene under accelerated test conditions. Polym Degrad Stab 2006; 91(11): 2739–47.

63. Kumanayaka TO, Parthasarathy R, Jollands M. Accelerating effect of montmorillonite on oxidative degradation of polyethylene nanocomposites. Polym Degrad Stab 2010; 95: 672–6.

64. Corti A, Muniyasamy S, Vitali M, Imam SH, Chiellini E. Oxidation and biodegradation of polyethylene films containing pro-oxidant additives: Synergistic effects of sunlight exposure, thermal aging and fungal biodegradation. Polym Degrad Stab 2010; 95:1106–14.

65. http://www.cabot-corp.com/wcm/download/en-us/mb/MFI.pdf

66. Standard test methods for water vapour transmission of materials, ASTM E96/E96M–10.

APPENDIX

Paper 1:

"Polyethylene/octa-(ethyl octadeca-*10,13* dienoamide) silsesquioxane and the adhesion strength to paperboard"

International Journal of Adhesion and Adhesives (2012) 38: p. 117–124

International Journal of Adhesion & Adhesives 38 (2012) 117–124

Contents lists available at SciVerse ScienceDirect

International Journal of Adhesion & Adhesives

journal homepage: www.elsevier.com/locate/ijadhadh

Polyethylene/octa-(ethyl octadeca-10,13 dienoamide) silsesquioxane blends and the adhesion strength to paperboard

Tuan-Anh Nguyen [a,*], Ferdinand Männle [b], Øyvind Weiby Gregersen [a]

[a] Department of Chemical Engineering, Norwegian University of Science and Technology, N-7491 Trondheim, Norway
[b] SINTEF Materials and Chemistry, N0314 Oslo, Norway

ARTICLE INFO

Article history:
Accepted 3 May 2012
Available online 14 May 2012

Keywords:
Adhesion by mechanical interlocking
Infrared spectra
Interfaces
Fracture mechanics

ABSTRACT

Octa-(ethyl octadeca-10,13 dienoamide) silsesquioxane or bio-POSS was used in the fabrication of polyethylene (PE)/bio-POSS blends by melt mixing. These PE/bio-POSS blends were applied to paperboard by compression moulding coating. The *T*-peel test was used to determine the adhesion of the blends to paperboard. A FTIR-ATR spectroscopic study was performed to identify the interfacial interaction between PE/bio-POSS blends and paperboard. The *T*-peel test showed that the adhesion of PE to paperboard was enhanced when there was less than 10 wt% of bio-POSS in the blends. The best adhesions were achieved at 5 wt% and 3 wt% bio-POSS, coated at 200 °C/20 °C and 300 °C/20 °C, respectively. The increase in adhesion strength was attributed to the contribution of mechanical interlocks and probable interfacial interaction between amide groups of bio-POSS and hydroxyl groups of paperboard, as specified by FTIR-ATR. Bio-POSS content above 10 wt% led to a decrease in adhesion between PE/bio-POSS blends and paperboard because the melt flows and mechanical properties of the blends were dramatically decreased.

1. Introduction

The most widely used plastic, polyethylene (PE) is often used in laminated packaging products, *e.g.* PE-coated paperboard. A requirement for this product is good adhesion between PE and paperboard. The adhesion depends on the characteristics of the paperboard (surface roughness and porosity), PE (melt flow rate, meting point, wettability and thickness), and the coating conditions (temperature, pressure and rate of coating). It is also affected by surface chemical factors and the intermolecular forces across interface [1]. Adhesion properties may be enhanced by treating paperboard and PE before coating. Improvement in adhesion properties by surface treatment of paperboard was successfully obtained by Kemppi [1], Fredholm and Westfelt [2]. Our work has only focused on the chemical modification of the PE-containing coating layer to improve the adhesion between coating and paperboard.

Polyethylene (PE) has low surface free energy (31 mJ/m^2) and low wettability [1]. When it is coated on the paperboard, PE shows low adhesion. In order to improve the adhesion properties, it is necessary to modify the PE prior to coating. Modifying PE was performed by treating the surface (surface treatment of PE) [3,4]. In those works, the oxygen-containing polar groups such as C=O, OH, COOH are introduced to PE surface, leading to an increase in surface polarity of PE without influencing on the properties of PE. When coated on the paperboard, the interfacial attraction force is increased, thereby improving the adhesion. Besides, the properties of PE can be modified by using additives or reinforcing agents.

Inorganic/organic hybrid polymers based on polyhedral oligomeric silsesquioxanes (POSS) have been much studied in the recent years. POSS is a class of silicon compounds with an empirical formula $R(SiO_{1.5})_n$ having an inorganic core cage and organic groups attached at the vertex, with a size of 1–3 nm. The organic groups allow POSS to be easily incorporated into polymers either by copolymerisation, or physical mixing, whereupon POSS/polymer blends having significantly improved properties such as mechanical properties, thermal stability, surface hardening, and rheological properties will be made [5–9]. Recently, a considerable study on the fabrication of polymer/POSS with improved properties by using a mixing method has been published [10–16]. There is a lack of work on applying polymer/POSS to paperboard as well as determination of adhesion between the layers in such laminates.

Polymer materials fully or partly based on renewable resources are a topic of great interest. The use of such materials can significantly contribute to a sustainable development. Octa-(ethyl octadeca-10,13 dienoamide) silsesquioxane is a POSS compound derived from a natural unsaturated fatty acid (octadeca-10,13

Abbreviations: PE, Polyethylene; POSS, Polyhedral oligomeric silsesquioxanes; Bio-POSS, Octa-(ethyl octadeca-10,13 dienoamide) silsesquioxane; CTMP, Chemithermomechanical pulping; MFI, Melt flow index; FTIR, Fourier transform infrared spectroscopy; SEM, Scanning electron microscopy; DSC, Differential scanning calorimetry; IaI, IaII, Peak intensity of amide I, II; Tm, Melting temperature

* Correspondence to: Synthesis and Properties, SINTEF Materials and Chemistry, Forskningsveien 1, N0314, Oslo, Norway. Tel.: +47 40 30 86 60.
E-mail address: tuananh210281@gmail.com (T.-A. Nguyen).

0143-7496/$ - see front matter © 2012 Elsevier Ltd. All rights reserved.
http://dx.doi.org/10.1016/j.ijadhadh.2012.05.002

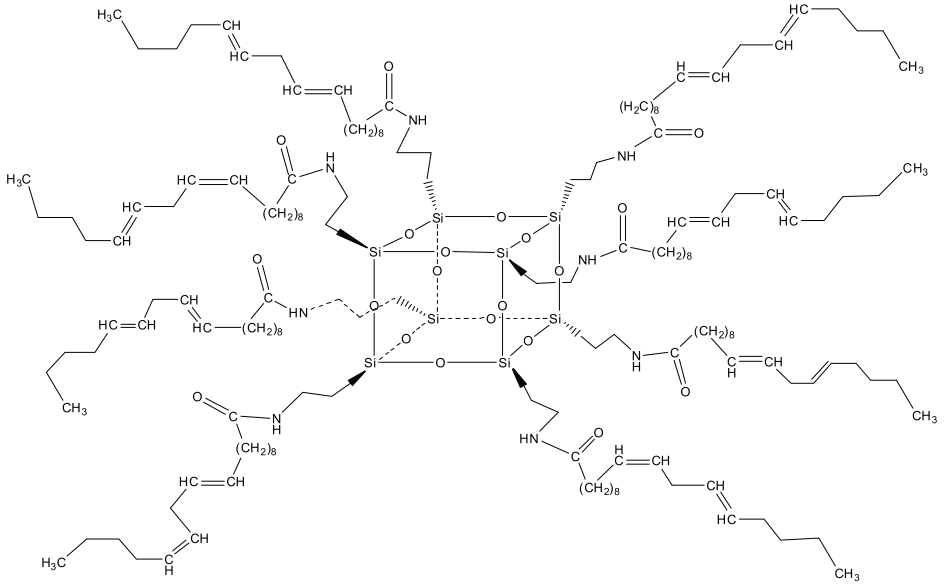

Fig. 1. Typical structure of octa-(ethyl octadeca-10,13 dienoamide) silsesquioxane (bio-POSS).

dienoic acid). This POSS compound is therefore a biological and renewable material, and called bio-POSS. The molecule of bio-POSS is typically composed of a Si_8O_{12} cubic cage and eight (ethyl octadeca-10,13 dienoamide) groups peripherally attached at eight Si vertexes, as can be seen in Fig. 1. The core cage is inorganic, giving thermal stability, while the peripheral organic groups allow bio-POSS to be incorporated into organic polymers to form POSS/polymer blends. Among the methods for fabricating polymer blends, melt mixing is efficient, cheap and simple to scale up to industrial level. Furthermore, fabricating blends by mixing will consume less time in comparison with copolymerisation that requires more time to develop new polymerisation routes. The properties of polymer/bio-POSS blends can be easily tailored by combining polymer and bio-POSS components and varying the blend composition.

The aim of this work is to investigate the effects of bio-POSS on the adhesion of polyethylene (PE) to paperboard. Various PE/bio-POSS blends have been fabricated by melt mixing in a micro-extruder. After that, the resultant blends are applied on the paperboard by compression moulding coating. The adhesion between polyethylene/bio-POSS blends and paperboard is evaluated by the *T*-peel test. The melting temperature of PE/bio-POSS blends is determined by differential scanning calorimetry (DSC). To observe the morphology of PE/bio-POSS blends, the samples are examined using scanning electron microscopy (SEM). Fourier transform infrared attenuated total reflection (FTIR-ATR) spectroscopy is used to identify the surface characteristics of the blends and paperboard.

2. Materials and methods

2.1. Materials

Polyethylene (PE) was purchased from Ineos Polyolefins and Polymers Europe, with melting point of 120 °C and the melt flow index (MFI) of 0.5 g/10 min (190 °C/2.16 kg). Norsilika8002 is a yellowish viscous liquid which was supplied by Jotun AS, Norway, containing octa-(ethyl octadeca-10,13 dienoamide) silsesquioxane (bio-POSS) dissolved in a hydrocarbon solvent, with a solid content of 40–44%. Paperboard was provided by Korsnäs AB, Sweden.

2.1.1. Paperboard

The paperboard is a much used fibre-based material for packaging due to its good stiffness, its low production cost, its lightness, its good and multiple printing opportunities and its recyclability. The paperboard has two different sides (uncoated and coated side) with different colours (brown and white), respectively. It is composed of four different layers:

(i) the bottom layer is unbleached kraft pulp of a pine and spruce softwood mix,
(ii) the middle layer is unbleached kraft pulp and chemithermo-mechanical pulping (CTMP),
(iii) the dense layer is bleached kraft pulp and
(iv) the top layer is coated by white pigments and binders (the pre-coated side).

Fig. 2 shows scanning electron microscope (SEM) images of paperboard: (a) shows the uncoated side (brown colour) and (b) shows the cross-section of the paperboard which illustrates four different layers (i, ii, iii and iv). As can be observed, the uncoated side of paperboard is very rough, containing large fibres. The rough surface of the uncoated side of paperboard is very advantageous for polymer coating mechanical adhesion.

2.2. Sample preparation

Before blending, bio-POSS was dried at 150 °C in vacuum in order to remove the hydrocarbon solvent completely. After that, the blends were prepared by melt mixing PE and dried bio-POSS at various compositions in a twin screw 15cc micro-extruder DSM

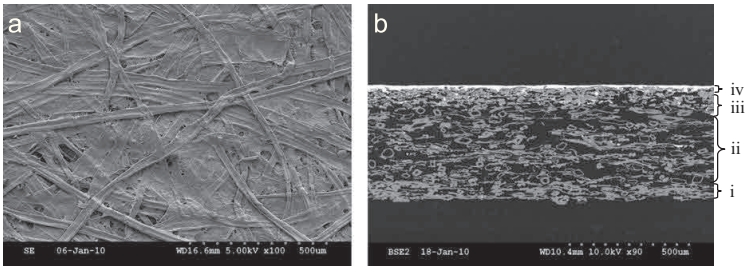

Fig. 2. SEM images of paperboard: (a) Uncoated side; (b) cross-section. (For interpretation of the references to color in this figure, the reader is referred to the web version of this article.)

MIDI2000. The extrusion temperature was kept at 180 °C from hopper to die section of micro-extruder, the operating screw speed was controlled at 50 rpm/min and total extrusion time was 5 min. The blend products were cut into pellets, 2 mm in length.

Blend films with a thickness of around 0.1 mm were obtained by compression moulding the pellets on hydraulic compressor Fontijne TH200. The temperature of top/bottom plate of hydraulic compressor was 180 °C/180 °C, the pressure was 10 MPa, and the total time was 5 min. Then, the blend films were applied on the uncoated side of paperboard by compression moulding coating, at 10 MPa and temperature of 200 °C/20 °C and 300 °C/20 °C, respectively for the two series.

2.3. Characterisation

2.3.1. Scanning electron microscopy (SEM)

The morphologies of PE/bio-POSS blends were examined by a scanning electron microscopy (SEM) instrument JEOL JSM-5900LV. The microscope was operated at 15 kV and in low vacuum mode of 20 Pa. The specimens were prepared by cutting the blend films and washed up using 100% ethanol. All samples were directly analysed without coating the surface.

2.3.2. FTIR-ATR

Fourier transform infrared attenuated total reflection (FTIR-ATR) was used for analysis of surfaces of samples. The sample was placed onto the universal diamond ATR top-plate (diamond/ZnSe) and a pressure was applied to the sample area. The scan range was in the medium infrared region from 4000 to 650 cm^{-1} at a resolution of 4 cm^{-1}, a scan number of 4. The spectra were reported as unit of transmission (%*T*). The analyses were carried out on a on a Perkin Elmer FTIR device (Spectrum One) at room temperature.

2.3.3. Melt flow index

The influence of bio-POSS content on melt flow of polyethylene (PE) was monitored by the melt flow index (MFI) method on a melt flow apparatus, Davenport 3/80. The blends were fully loaded into a cylinder of MFI device and then melted at temperature of 190 °C. Pre-heated time and extrudate time were set at 5 and 10 min. MFI was expressed as the mass of the blends per 10 min extruded through the die of 2.09 mm in diameter and 8 mm in length, under the standard weight of 2.16 kg

$$\mathrm{MFI} = \frac{\text{Average extrudate weight}}{\text{Time}} \ (\mathrm{g/10min})$$

2.3.4. Mechanical properties

The mechanical properties of PE/bio-POSS blend film were determined by tensile testing according to ISO 527-1 on the device Zwich-Z250. Test specimens were cut from the blend film with "dumbbell" shape. At least 5 specimens of each blend film were prepared for tensile test. The test was run at the speed of 500 mm/min and room temperature.

2.3.5. Differential scanning calorimetry (DSC)

DSC analysis of PE/bio-POSS blends was done using a differential scanning calorimeter Perkin Elmer DSC 8500 in nitrogen flow. The samples (2.0 – 3.0 mg) placed in a DSC pan. The samples were heated from 20 °C to 150 °C at a rate of 10 °C/min.

2.3.6. Adhesion testing

Adhesion was determined by *T*-peel testing on the testing device Zwich-Z250. At least five *T*-type specimens (200 mm in length and 15 mm in width) were prepared for each sample by using Thwing-Albert's JDC-15 mm-10 in. sample cutter. The polymer coating was peeled at the speed of 30 mm/min. and over a length of 150 mm.

The adhesion value was determined as Adhesion = peel force/width (N/m)

The adhesion strength of the sample was calculated as the average of five adhesion values that corresponded to five specimens.

2.3.7. Optical microscopy

The fracture surface (both sides) of de-bonded joints after *T*-peel testing were observed by using optical microscopy Leica M420. The photos of the fracture surface were taken using a colour high resolution camera Basler A110FC. The fracture surfaces were selected from the sample after *T*-peel test.

3. Results and discussion

3.1. Morphologic analysis

Morphological analysis of PE/bio-POSS blends was performed by a SEM method, and the result is shown in Fig. 3.

There are bio-POSS aggregates (10–20 μm) formed in the PE matrix, indicating that the dispersion of bio-POSS into PE is at micro-scale. The number of bio-POSS aggregates is increased with increasing bio-POSS content in the blends while their sizes become smaller. In fact, at below 10 wt%, there are only few bio-POSS aggregates gathering at a certain position within the PE matrix. At above 10 wt% content, bio-POSS aggregates are distributed everywhere within the blends. There are not any bio-POSS aggregates with diameter larger than 20 μm, reflecting the relatively equal distribution of bio-POSS aggregates within PE. At above 10 wt%, bio-POSS is significantly present on the surface of the blends.

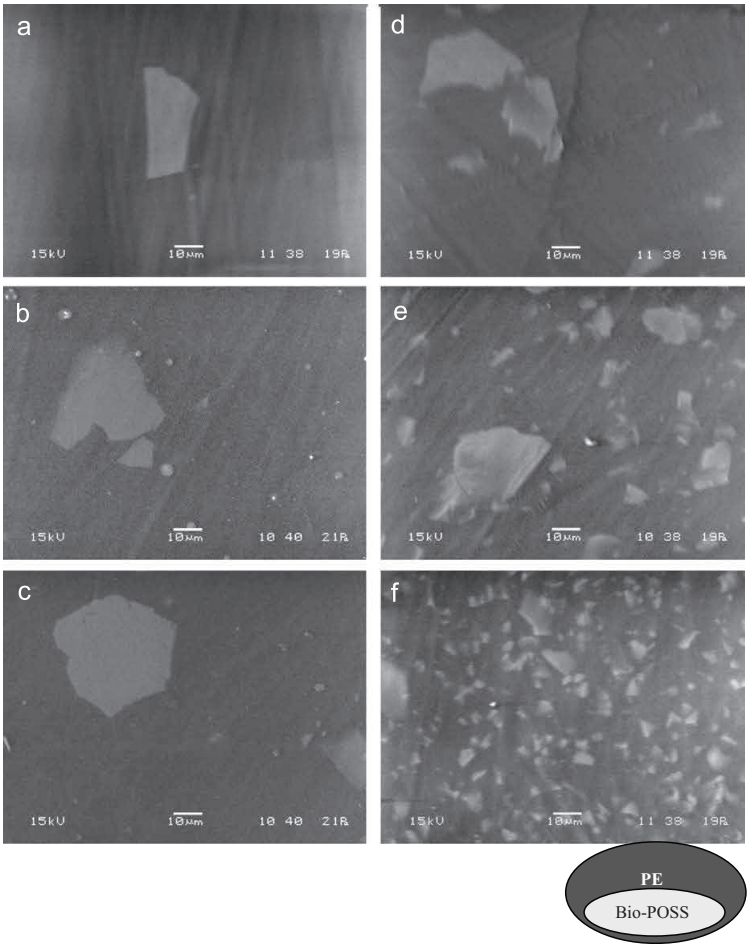

Fig. 3. SEM micrographs of PE/bio-POSS blends at bio-POSS content: (a) 1 wt%, (b) 3 wt%, (c) 5 wt%, (d) 10 wt%, (e) 20 wt%, (f) 40 wt%.

3.2. FTIR-ATR spectra

The FTIR-ATR is a useful technique for determining the surface of the material. In this study, the FTIR-ATR was used for identifying the surface characteristics of pure materials and the blends. Fig. 4 shows FTIR-ATR spectrum of PE, bio-POSS, and PE/bio-POSS blends, and Table 1 is the interpretation of FTIR-ATR spectra where the absorption band frequencies are listed.

As illustrated in Fig. 4, pure PE exhibits two absorption peaks in the range 2950–2800 cm^{-1} (CH_2 stretching), 1460 cm^{-1} (CH_2 scissoring), 719 cm^{-1} (CH_2 rocking). The spectral bands of PE are similar to the results in the study of Chandra, Rustgi [17], and Raj *et al.* [18].

Bio-POSS shows the main peaks as follows: the absorption peaks at 3300 cm^{-1} and 3084 cm^{-1} assigned to the hydrogen-bonded N–H stretching (N–H…O=C); two bands appear at 1713 cm^{-1} and 1644 cm^{-1} are assigned to amide I (carbonyl C=O) and amide II (mixed vibration of N–H bending and C–N stretching), respectively. Normally, the intensity of amide I is stronger than that of amide II. The small shoulder band at 1772 cm^{-1} is ascribed as the free C=O stretching vibration. The double bond C=C stretching vibration is found at 1543 cm^{-1}. Two strong and broad bands at 1119 cm^{-1} and 1028 cm^{-1} exhibit Si–O–Si stretching of the cubic Si_8O_{12} structure. The interpretation of the FTIR-ATR spectrum of bio-POSS was consulted the study of Rao [19].

The FTIR-ATR spectra of PE/bio-POSS blends show an absorption band of N–H stretching near 3300 cm^{-1}, two strong bands of C=O stretching vibration and mixture of C–N stretching/N–H bending near 1713 cm^{-1} and 1644 cm^{-1}, two strong and broad bands of Si–O–Si stretching of silsesquioxane cage in the range 1130–1020 cm^{-1}, as illustrated in Fig. 4. Especially, the free C=O is also present in the spectrum of the resultant blends as a shoulder band. Peak intensities of Si–O–Si stretching are increased with increasing bio-POSS content in the blends. It demonstrates that the features of PE and bio-POSS components were fully introduced to the surface of PE/bio-POSS blends.

3.3. Melt flow property

The melt flow index (MFI) method is generally used to assess the average molecular mass of a polymer and is reversed to the melt viscosity. The higher a MFI, the more polymers flow. Knowing the MFI of a polymer is helpful for controlling its

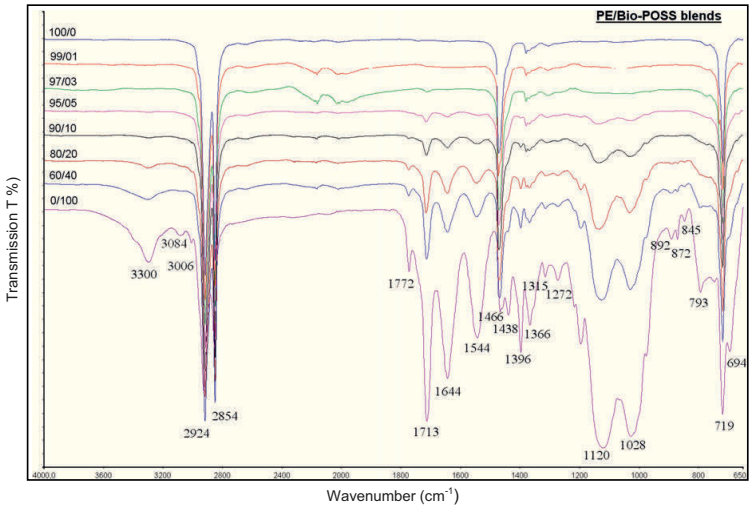

Fig. 4. FTIR-ATR spectra of PE/bio-POSS blends with various bio-POSS loadings.

Table 1
Interpretation of FTIR-ATR [19].

Bio-POSS (cm^{-1})	PE (cm^{-1})	Interpretation
3300, 3084	–	Hydrogen bonded N–H stretching
3006	–	C–H in=CH– stretching
2924, 2854	–	CH_2 stretching
	2916, 2849	CH_2 stretching
1772	–	Free C=O stretching
1713	–	Hydrogen bonded C=O stretching (Amide I)
1644	–	C=O stretching and N–H bending (Amide II)
1544	–	C=C stretching
1471	–	CH_2 bending (scissoring)
1466, 1438	–	CH_2 bending (scissoring)
1396, 1366	–	C–H in=CH– bending (in-plane)
1379	–	CH_2 wagging
1315	–	CH_2 wagging
1272	–	C–N stretching and N–H bending (Amide III)
1120, 1028	–	Si–O–Si stretching
892, 845	–	C–H in =CH– bending (out-of-plane)
872	–	Si–C stretching
793	–	CH_2 in Si–CH_2– rocking
719	–	CH_2 rocking
718	–	CH_2 rocking
694	–	N–H out-of-plane (Amide V)

processing. In this work, the melt flow property of PE/bio-POSS blends was measured and the results are shown in Fig. 5. The MFI completely decreased with increasing bio-POSS content. The higher the bio-POSS content, the lower the MFI. The differences between the MFI values of the blends at 3, 5 and 10 wt% bio-POSS are inconsiderable. The MFI's reduction is significant at above 10 wt% bio-POSS loading (more than 50% reduction). It reflects that the melt viscosity of PE/bio-POSS blends is increased and the melt flow property of PE/bio-POSS blends is decreased with increasing bio-POSS content in the blend.

3.4. Mechanical property

The elastic modulus (E_t), yield strength (σ_Y), strength at break (σ_B) and elongation at break (ε_B) obtained from tensile tests on PE/bio-POSS blend films are reported in Table 2. The mechanical properties of PE/bio-POSS are decreased with increasing bio-POSS content.

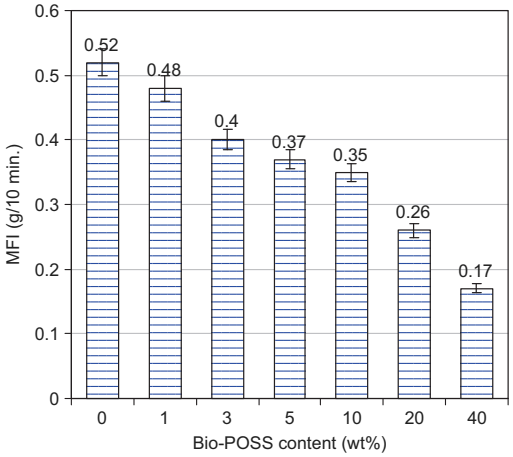

Fig. 5. Melt flow index of PE/bio-POSS blends.

Addition of bio-POSS to PE has little effect on elastic modulus and yield strength. However, strength at break of the blends at low bio-POSS content is moderately decreased, about 44% reduction at 3% bio-POSS loading, and elongation at break is slightly lowered (12% reduction). When bio-POSS content is 5 wt%, the reduction in strength at break of the blend films is approx. 50%, while the decrease in elongation at break is moderate (30%). At above 10 wt% bio-POSS loading, elongation at break of the blends is dramatically decreased. The blend of 40 wt% bio-POSS has extremely poor mechanical properties.

The overall decrease of the mechanical properties for PE/bio-POSS as compared with PE is probably related to the presence of micron size bio-POSS aggregates which behave as weakening points during blend deformation.

3.5. Adhesion of PE/bio-POSS blends to paperboard

The adhesions of PE, PE/bio-POSS blends to paperboard are shown in Fig. 6.(a) shows the adhesion properties of the samples

prepared at 200 °C/20 °C and (b) shows that at 300 °C/20 °C. Generally, in both cases, the adhesion strength of PE/bio-POSS blends on the paperboard is increased with increasing the content of bio-POSS up to 10 wt%. Whereas, loading above 10 wt% bio-POSS leads to a decrease in the adhesion of PE/bio-POSS blends to paperboard in comparison with that of PE-coated paperboard. The standard deviation is relatively small for all our samples (below 50 N/m). It reflects that the strength of adhesion of the blends to paperboard is equally distributed. Among the samples prepared at 200 °C/20 °C, the sample at 5 wt% bio-POSS shows the highest adhesion strength, and among the samples prepared at 300 °C/20 °C, the adhesion strength of PE/3 wt% bio-POSS to paperboard is greatest.

From Fig. 6, the adhesion of the samples prepared at 300 °C/20 °C is approx. 25% higher than for the sample prepared at 200 °C/20 °C. It is a consequence of the high temperature reducing the melt viscosity of the blends, thereby increasing the penetration of the blends into paperboard to form mechanical interlocks at the interface, hence enhancing the adhesion. The effect of coating composition on adhesion strength is relatively similar at both coating temperatures.

Table 2
Mechanical properties of PE/bio-POSS blend films.

PE/bio-POSS	Et (MPa)	σ_Y (MPa)	σ_B (MPa)	ε_B (%)
100/0	278	12.8	24.5	823.4
99/01	245	11.8	12.3	733.5
97/03	272	11.8	13.5	719.2
95/05	282	12.8	12.6	570.9
90/10	229	11.6	10.2	22.4
80/20	240	11.8	11.3	19.9
60/40	218	–	1.8	0.3

3.6. Failure of adhesive joint

During *T*-peel test, the blend films and paperboard are separated from the adhesive joint. Fibres of paperboard are torn and attached to the blend films after separation. This phenomenon is called "fibre-tear effect". It is impossible to avoid completely this phenomenon when *T*-peel test is running [1]. In our work, the fibre-tear effect occurred on all *T*-peeling specimens. To fully understand the failure of adhesive joint, it is necessary to examine the fracture surfaces of de-bonded joint after peeling.

Fig. 7a illustrates the specimens of PE/bio-POSS blends coated paperboard after peeling, and (b) shows the photo taken from the typical fracture surface (blend side) after peeling the sample of PE/3 wt% bio-POSS blend coated paperboard by using an optical microscope. It can be observed that the blend film and paperboard were apparently delaminated after peeling (Fig. 7a). There are only few fibres of paperboard (yellowish colour) clinging onto the blend film, and the blend films were not deformed after separation. The fracture surface of the blend side is quite rough with the trace of paperboard surface, as can be seen in Fig. 7b. In this case, the failure of adhesive joint is apparently located at interface between the blend films and the paperboard (apparently interfacial failure).

In our *T*-peel testing, the final adhesion was the average of five adhesion values of five corresponding specimens with apparently interfacial failure. Thus, the final adhesion value is neither

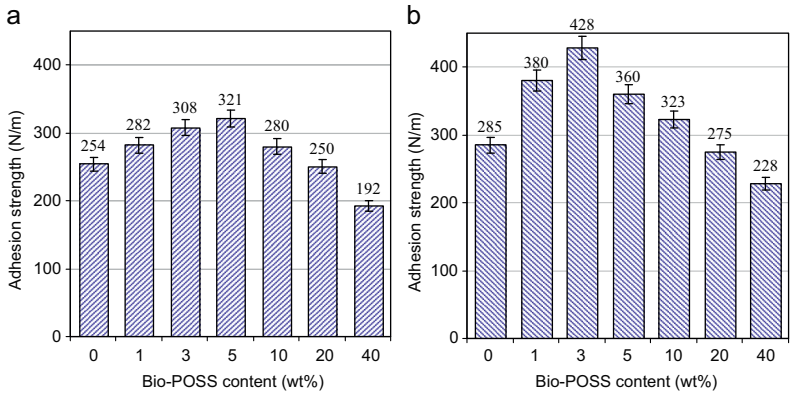

Fig. 6. Adhesion strength of PE/bio-POSS blends to paperboard when coated at (a) 200 °C/20 °C, and (b) 300 °C/20 °C.

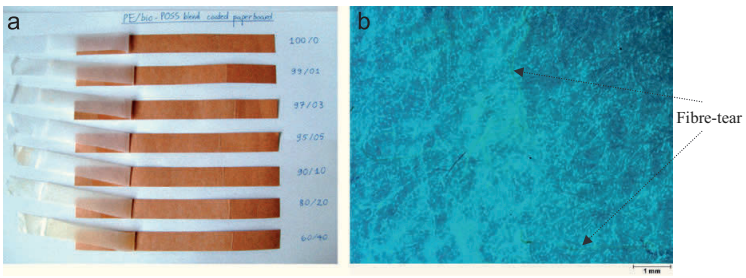

Fig. 7. Sample of PE/bio-POSS blends coated paperboard after peeling (a), and typical fracture surface of blend side with fibre-tear effect (b). (For interpretation of the references to color in this figure, the reader is referred to the web version of this article.)

cohesion strength of paperboard nor cohesion strength of the blend film. It is the strength of adhesion between PE/bio-POSS blends and paperboard.

3.7. Adhesion mechanisms

When a polymer is coated on paperboard, polymer spreads and wets the surface before its penetration into the paperboard. The spreading and wetting properties could play an important role in the distribution of the polymer on the paperboard. The paperboard surface is rough and the molten polymer can flow into the depressions on its surface. Mechanical interlocking mechanism may contribute to the adhesion strength between the polymer and paperboard [1]. In this work, the blends fabricated at different bio-POSS contents have the melting temperature (T_m) of same order as pure PE (123 ± 0.5 °C), as the result of DSC analysis. Moreover, the melt flow properties of the blends are decreased with increasing bio-POSS content, as examined by the MFI method. According to the *T*-peel test results, the adhesion strength between polyethylene and paperboard was improved by additional bio-POSS at below 10 wt%. A slight reduction in melt flows of the blends at below 10 wt% bio-POSS loadings demonstrates that the enhancement in adhesion strength to paperboard was not primarily caused by mechanical interlocking. In order to better understanding the adhesion mechanism, the surfaces of PE/bio-POSS blends, paperboard and the blend films after coating are spectroscopically studied.

FTIR-ATR analyses of the blend films before coating and the surfaces of the blends after coating (including top surface–side contact with mould, and failure surface–side contact with paperboard, see Fig. 8) were carried out. Fig. 9 shows the ATR spectra in the region of 1900–1500 cm^{-1} of the blend films before coating (a), of the fracture surfaces that have an interfacial failure (b), and of the blend top surfaces (c). As can be observed, the spectra of the fracture surfaces (Fig. 9b) are pronouncedly different from those before coating (a). Actually, if comparing the intensity ratio I_{aI}/I_{aII} between amide I (near 1713 cm^{-1}) and amide II (near 1645 cm^{-1}), is always higher than 1 in case of the blends before coating (Fig. 9a). On the blend fracture surface (Fig. 9b), such ratio varies on bio-POSS concentration: $I_{aI}/I_{aII} < 1$ (1,3,5 wt%), $I_{aI}/I_{aII} > 1$ (10,20,40 wt%). The variation of I_{aI}/I_{aII} does not reflect an increase of bio-POSS amount in the blends because if so, I_{aI}/I_{aII} ratio must be higher than 1. Meanwhile, the spectra of the blend top surfaces are relatively similar to those of before coating (Fig. 9a): intensity of amide I is always higher than that of amide II. Consequently, the ATR spectra of two sides (9b, 9c) of the blend films are different, since one side has a contact with paperboard. It can be suggested that there is an interaction occurring between the blend films and paperboard.

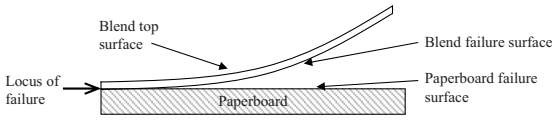

Fig. 8. A schematic of failure surface of PE/bio-POSS blends coated paperboard after peeling.

Fig. 4 illustrates the presence of amide group on the surface of PE/bio-POSS blend film, and Fig. 10 shows hydroxyl group on the surface of reference paperboard (near 3332 cm^{-1}). When the blends are coated on paperboard, it can be suggested that there is an interaction occurring between amide group of the blend films and OH of paperboard: PE/bio-POSS blends–NHC=O…HO–paperboard. The suggested interaction could lead to a change in both spectrum of amide group and OH group. In fact, the band shapes of amide groups of the blend fracture surface (spectrum 99/01, 97/03, 95/05 in Fig. 9b) were altered as discussed above, whilst the band shape of OH was less influenced, as unsmooth curve of OH band in the spectrum a, b and c in Fig. 10. Thus, the suggested interaction was probable.

However, the band shapes of OH group (spectrum d, e, and f in Fig. 10) are relatively similar to that of OH in the reference paperboard. In the spectra 90/10, 80/20, 60/40 (Fig. 9b), band intensity of amide I is still bigger than that of amide II. Here, the interaction between amide of the blends and OH of paperboard might be inconsiderable to alter amide and hydroxyl bands. As examined by tensile testing and MFI, additional bio-POSS above 10 wt% lead to a dramatic decrease in the mechanical and the melt flow properties of PE/bio-POSS blends. The dramatic decrease in melt flow properties indicates that the mechanical interlocks at interface between the blends and paperboard was

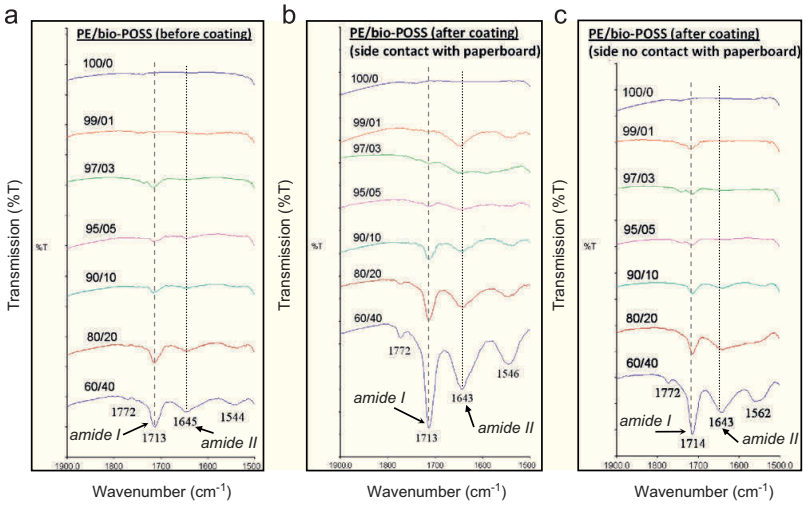

Fig. 9. FTIR-ATR spectra of PE/bio-POSS blends in the region 1900–1500 cm^{-1}: (a) before coating, and after coating: (b) side contact with paperboard, (c) side contact with mould.

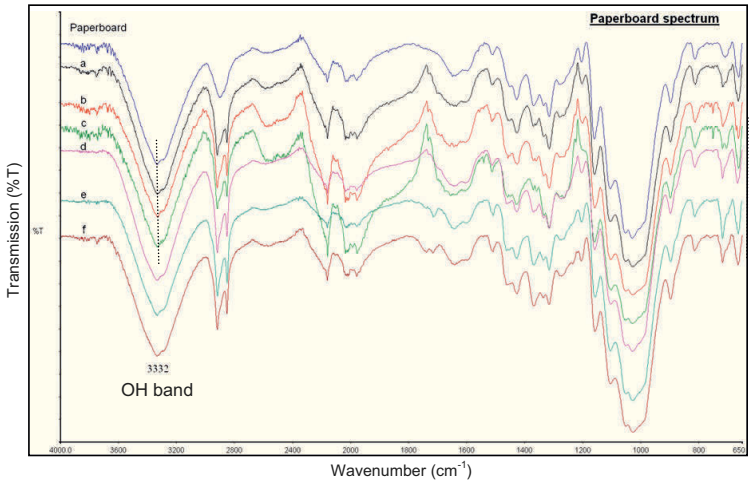

Fig. 10. FTIR-ATR spectrum of reference paperboard and of the paperboard failure surfaces after peeling blend films of bio-POSS content: (a): 1 wt%; (b): 3 wt%; (c): 5 wt%; (d): 10 wt%; (e): 20 wt%; (f): 40 wt%.

significantly decreased, thereby reducing the adhesion. Moreover, the dramatic reduction in mechanical properties of the blends could be explained as a consequence of a lubricant effect that caused by high bio-POSS loadings [20]. Such lubricant effect lowers the adhesion of bio-POSS/PE blends to paperboard, especially at high bio-POSS loadings due to much bio-POSS aggregates on the blend surface.

4. Conclusions

Polyethylene/octa-(ethyl octadeca-10,13 dienoamide) silsesquioxane (PE/bio-POSS) blends at different compositions were well fabricated by the melt mixing method, and then successfully coated on the uncoated side of paperboard by compression moulding coating. The adhesion of PE/bio-POSS blends to paperboard has been improved by low content of bio-POSS (below 10 wt%), where a remarkable enhancement in adhesion is achieved at 5 wt% bio-POSS when coated at 200 °C/20 °C, and at 3 wt% bio-POSS when coated at 300 °C/20 °C. Adhesion property of the blend coated paperboard prepared at 300 °C/20 °C is higher than that at 200 °C/20 °C. The probable reason for the adhesion improvement is mechanical interlocking, and interfacial interaction occurring between amide groups of bio-POSS with hydroxyl groups of paperboard, as identified by FTIR-ATR spectroscopy. The blends made of above 10 wt% bio-POSS results in a significant reduction in adhesion strength to paperboard because the mechanical and melt flow properties of the blends were dramatically decreased at high bio-POSS loadings.

Acknowledgements

This study has been financially supported by the Research Council of Norway and the industrial partners Dynea AS, Elopak AS, Forestia AS, Korsnäs AB, Peterson AS, and Södra AB in the KMB project (sustain-Barrier 182619).

References

[1] Kemppi A. Studies on the adhesion between paper and low density polyethylene. Laboratory of Paper Chemistry. Abo: Abo Akademi University; 1997. p. 7–39.
[2] Fredholm B, Westfelt L. New sizing chemicals for improved adhesion in polyethylene extrusion coating of sized paper. Svensk papperstidning 1979;7:202–6.
[3] Westerlind B, Larsson A, Rigdahl M. Determination of the degree of adhesion in plasma-treated polyethylene/paper laminates. Int J Adhes Adhes 1987;7(3):141–6.
[4] Kaplan SL, Rose PW. Plasma surface treatment of plastics to enhance adhesion. Int J Adhes Adhes 1991;11(2):109–13.
[5] Schwab JJ, Lichtenhan JD. Polyhedral oligomeric silsesquioxane (POSS)-based polymers. Appl Organomet Chem 1998;12:707–13.
[6] Li GZ, Wang LC, Ni H, Pittman CU. Polyhedral oligomeric silsesquioxane (POSS) polymers and copolymers: a review. J Inorg Organomet Polym 2001;11(3):123–54.
[7] Pan G. Polyhedral oligomeric silsesquioxane (POSS). In: Mark JE, editor. Physical properties of polymers handbook, 6. Springer; 2007. p. 577–84 [chapter 34].
[8] Wu J, Mather PT. POSS polymers-physical properties and biomaterials applications. J Macromol Sci: Part C: Polym Rev 2009;49:26–30.
[9] Markovic E, Constantopolous K, Matisons JG. Polyhedral oligomeric silsesquioxanes: from early and strategic development through to materials application. Application of polyhedral ologomeric silsesquioxane. In: Hartmann-Thompson C (editor). Advances in Silicon Science 2011; vol. 3: p. 1–46. [chapter 1].
[10] Fina A, Tabuani D, Frache A, Camino G. Polypropylene-polyhedral oligomeric silsesquioxanes (POSS) nanocomposites. Polym 2005;46:7855–66.
[11] Fina A, Tabuani D, Frache A, Camino G. Polypropylene-polysilsesquioxane blends. Eur Polym J 2010;46:14–23.
[12] Joshi M, Butola BS, Simon G, Kukaleva N. Rheological and viscoelastic behavior of HDPE/octamethyl-POSS nanocomposites. Macromolecules 2006;39:1839–49.
[13] Joshi M, Butola BS. Isothermal crystallization of HDPE/octamethyl polyhedral oligomeric silsesquioxane nanocomposites: role of POSS as a nanofiller. J Appl Polym Sci 2007;105:978–85.
[14] Zhou Z, Zhang Y, Zhang Y, Yin N. Rheological behavior of polypropylene/octavinyl polyhedral oligomeric silsesquioxane composites. J Polym Sci Part B: Polym Phys 2008;46:526–33.
[15] Misra R, Fu BX, Morgan SE. Surface energetics, dispersion and nanotribomechanical behavior of POSS/PP hybrid nanocomposites. J Polym Sci Part B: Polym Phys 2007;45:2441–55.
[16] Sánchez-Soto M, Schiraldi DA, Illescas S. Study of the morphology and properties of melt-mixed polycarbonate–POSS nanocomposites. Eur Polym J 2009;45:341–52.
[17] Chandra R, Rustgi R. Biodegradation of maleated linear low-density polyethylene and starch blends. Polym Degrad Stab 1997;56(2):185–202.
[18] Raj B, Sankar KU, Siddaramaiah. Low density polyethylene/starch blend films for food packaging applications. Adv Polym Technol 2004;23:32–45.
[19] Rao CNR. Chemical applications of infrared spectroscopy. New York and London: Academic Press; 1963 p. 125–263.
[20] DeArmitt C Polyhedral oligomeric silsesquioxanes in plastics. application of polyhedral ologomeric silsesquioxanes. In: Hartmann-Thompson C (editor). Advances in Silicon Science 2011; vol. 3: p. 209–228 [chapter 5].

Paper 2:

"Effects of hydrophobic polyhedral oligomeric silsesquioxanes coating on water vapour barrier and water resistance properties of paperboard"

Paper has been accepted for publication in the Journal of Sol-Gel Science and Technology (JSST), DOI: 10.1007/s10971-013-3208-1.

Effects of Hydrophobic Polyhedral Oligomeric Silsesquioxane Coating on Water Vapour Barrier and Water Resistance Properties of Paperboard

TUAN-ANH NGUYEN* AND ØYVIND WEIBY GREGERSEN

Department of Chemical Engineering, Norwegian University of Science and Technology (NTNU), N-7491 Trondheim, Norway

FERDINAND MÄNNLE* AND PHILIPPE BRACHET

SINTEF Materials and Chemistry, N 0314 Oslo, Norway

* Corresponding author:

- Tuan-Anh Nguyen

Tel.: (+47) 40 30 86 60

E-mail Address: tuananh210281@gmail.com

- Ferdinand Männle

Tel.: (+47) 98 28 24 91

E-mail Address: Ferdinand.Maennle@sintef.no

Postal Address: Synthesis and Properties, SINTEF Materials and Chemistry, Forskningsveien 1, N0314, Oslo, Norway

Abbreviations:

Bio-POSS	:	Octa-(ethyl erucamide) silsesquioxane
CTMP	:	Chemithermomechanical pulp
ATR-FTIR	:	Attenuated Total Reflection Fourier Transform Infrared spectroscopy
^{1}H NMR	:	Proton nuclear magnetic resonance spectroscopy

Abstract. The substitution of fossil based packaging materials with materials from renewable sources is a topic of current interest. Polyhedral oligomeric silsesquioxanes with fatty acid moieties can have a renewable content of more than 90% and are therefore called bio-POSS. In this study the bio-POSS octa-(ethyl erucamide) silsesquioxane was coated on a paperboard substrate as a liquid coating. The water resistance and the water vapour barrier properties of the paperboard were improved. Samples on which the bio-POSS coating layer was dried at 80^{o}C had a slightly higher water resistance and water vapour barrier than samples dried at room temperature. UV treatment of the coating layer had little effect. Solid state ^{1}H-NMR of UV treated coatings showed no reaction of double bonds of bio-POSS in the coating layer. Multiple coating considerably enhanced the water resistance and water vapour barrier properties of the paperboard, due to an increase in the coating thickness and a reduction in number of pores on top coated surfaces.

Key words: POSS, renewable materials, water resistance, water vapour barrier property.

1. Introduction

Paperboard is a cellulose based material which has been widely used in packaging due to its advantages such as low cost, lightweight, good stiffness, easy processing, renewability and recyclability. Paperboard or cellulosic material has a porous structure with a highly hydrophilic nature. This is its disadvantage, because paperboard easily absorbs moisture from environment, particularly when stored at high relative humidity conditions or when in contact with foods, leading to a reduction in the mechanical properties and strength of the paperboard, causing a degradation of packages during storage and distribution [1,2]. Therefore, it is necessary to improve water barrier properties of paperboard. In liquid packaging industry, an excellent water barrier property is achieved when laminating the paperboard with a thin layer of thermoplastics film (polyethylene PE, polypropylene PP), paraffin or aluminium. Thermoplastics are fossil based materials which are limited, and aluminium makes recycling of the paper more difficult. Recently, many studies has reported that water barrier properties of paperboard can be significantly improved by coating application with biodegradable polymers such as whey protein isolate (WPI)/cellulose-based films, polylactic acid (PLA), polycaprolactone (PCL) [3-6]. Coating solutions were prepared from mixtures of biopolymers, then applying on the surface of paperboard or combining with another biopolymer coated layer. Coated paperboards were characterized by water vapour transmission rate (WVTR). The WVTR of biopolymeric coated paperboard decreased by about 78%, reflecting an improvement in water barrier properties [5].

It has earlier been shown that inorganic/organic hybrid polymers based on organosilica are good barrier materials for water vapour, oxygen and flavours [7]. Hybrid polymers are often synthesized by sol-gel process and coated on films of conventional organic polymers. However, the use of inorganic/organic hybrid polymers to coat natural polymer materials like paperboard has not been previously tried. Recently, there has been much interest in inorganic-organic hybrid materials based on several types of polyhedral oligomeric silsesquioxanes (POSS). POSS is a special type of silica compound having a chemical formula $R(SiO_{1.5})_n$, (n is silicon atoms, n = 8, 10, 12; R is H or organic groups), with a molecular structure composed of an inorganic core cage and organic groups R peripherally attached at each Si atom [8,9]. POSS compounds have been successfully applied in thermoplastics [10-13], thermosets [14-16], and coatings [17-20].

Solvent-based coating systems are widely recognized in the field of coatings because of their outstanding chemical and wear resistant properties, toughness and performance properties.

This type of coating creates smooth finishes that have superior abrasion resistance [21]. The combination of solvent-based coating systems with POSS is feasible because POSS compounds are commonly synthesized by a sol-gel method [7-9]. Furthermore, the hydrophobicity of the peripheral organic groups of the POSS compound may make the coated material equally water repellent as the POSS compound.

UV curing is a technology of instant curing in which ultraviolet (UV) light is applied to resins such as coatings, adhesives, marking ink and photo-resists, etc., in order to cause photopolymerization reaction. UV curing can achieve the coating faster (usually takes few seconds), and therefore at a lower total cost than many other coating processes. Other advantages of UV-curing are saving space, reducing waste, and low-temperature treatment. Furthermore, UV cure coatings are considered environmentally friendly because most of the solvents that are necessary in other coating chemistries and processes are not needed in UV cure coatings [22].

In this work, we use a hydrophobic POSS compound to coat on paperboard. Our POSS has a molecular structure composed of an inorganic silica core and eight ethyl erucamide groups peripherally surrounding the core cage, with a typical structure as shown in Fig. 1. This POSS compound is actually a derivative of unsaturated fatty acid (erucic acid) with bio-based content of 91.6% (according to ASTM D6888). Therefore, it is a renewable and biodegradable material, and called bio-POSS. The double bonds in the peripheral organic groups of bio-POSS may enable its crosslink by exposing under UV light. Such crosslinking formation may lead to the improved mechanical properties of bio-POSS [23]. We assume that improved water and water vapour barrier properties of the paperboard will be obtained when bio-POSS coating layer is dried or UV-cured.

The objective of this work was to investigate the effect of bio-POSS on the water resistance and water vapour barrier properties of paperboard. Bio-POSS was applied on paperboard by solvent based coating using a rod coater. After that, the bio-POSS coated paperboard was dried at 80^{o}C in a circulation oven or exposed to UV light. Attenuated Total Reflection Fourier Transform Infrared (ATR-FTIR) spectroscopy was applied to investigate the surface coverage. Nuclear magnetic resonance (NMR) spectroscopy was used to identify the variation in the bio-POSS coating layer during drying and UV treatment. The penetration of the bio-POSS into the paperboard was investigated to better understand the water penetration mechanism.

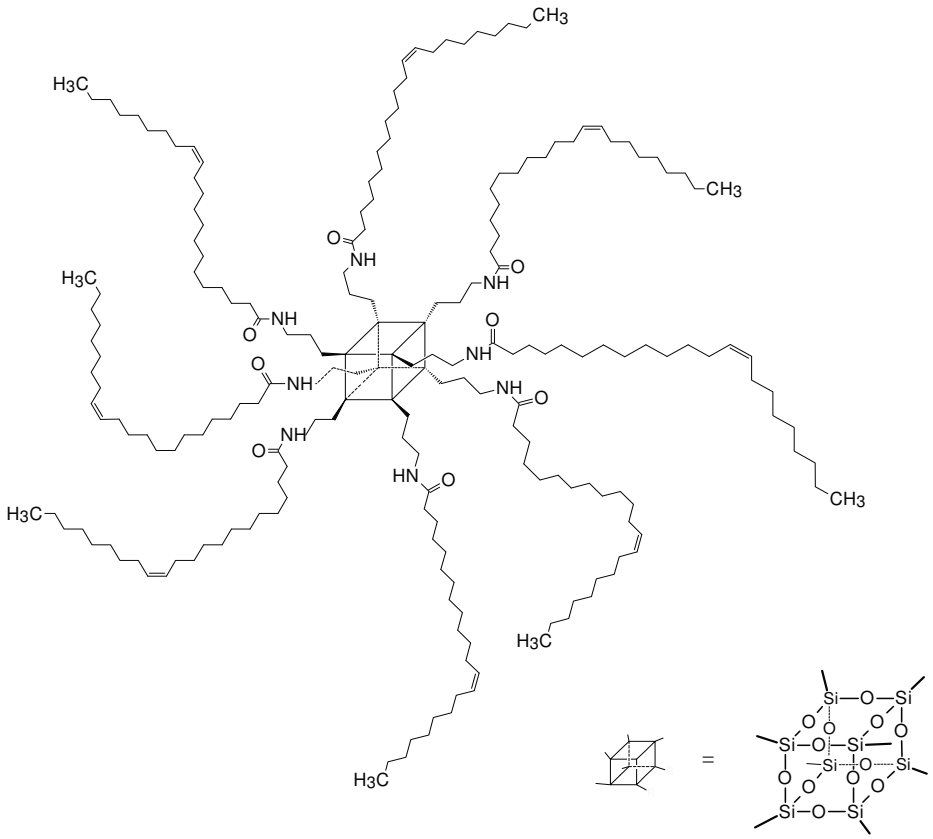

Figure 1. Typical structure of octa-(ethyl erucamide) silsesquioxane (bio–POSS)

2. Experimental

2.1. Materials

Bio-POSS was synthesized in our laboratory by a two-step procedure [24]. In the first step ethylamine silane was converted to ethylamine POSS by a sol-gel process, using 2-butoxy ethanol solvent. In the second step, the organic groups of ethylamine POSS were modified by a fatty acid (erucic acid). The solvent was thereafter removed by vacuum drying.

Single coated three ply paperboard was supplied by Korsnäs AB, Sweden.

2.1.1. Paperboard

The paperboard has two sides with different colour: an uncoated side (brown) and a pre-coated side (white) (Fig. 2a); 2b shows a scanning electron microscopy (SEM) image of the uncoated side of the paperboard; 2c is the cross-section of the paperboard which illustrates four different layers:

(i) the bottom layer is unbleached kraft pulp of a pine and spruce softwood mix;
(ii) the middle layer is unbleached kraft pulp and chemithermomechanical pulp (CTMP);
(iii) the dense layer is bleached kraft pulp;
(iv) the top layer is coated by white pigments and binders (the pre-coated side).

The uncoated side of paperboard is very rough, containing large fibres. There are many pinholes and depressions on the uncoated side of the paperboard. Furthermore, paperboard has a porous structure. Therefore, the absorption of water and moisture into paperboard is facilitated.

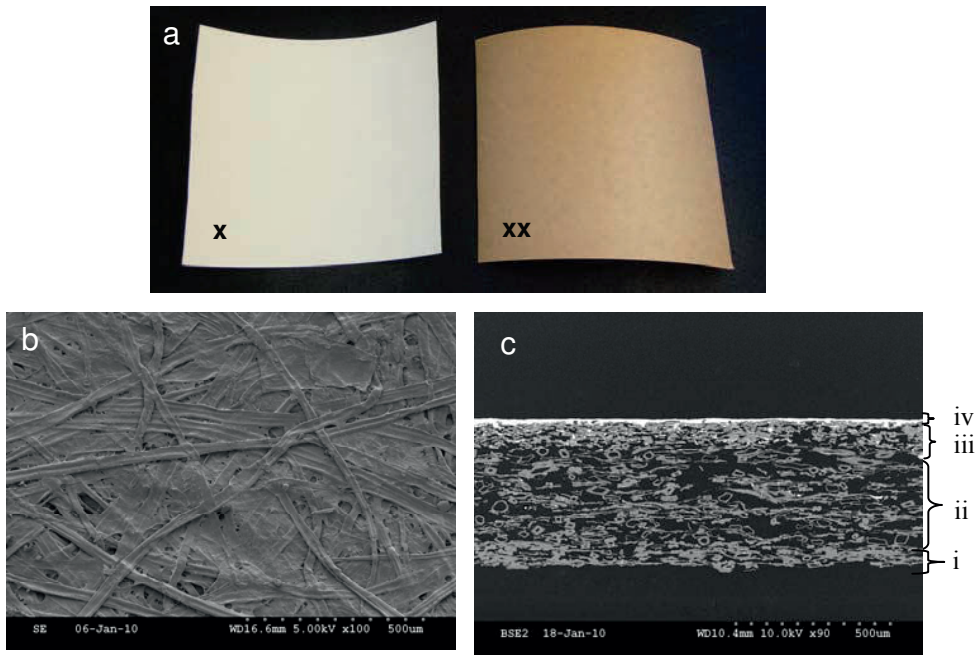

Figure 2. (a) Two sides of paperboard: (x) pre-coated side and (xx) uncoated side;

(b) SEM images of uncoated side of the paperboard, (c) Cross-section

2.2. Sample Preparation and Characterization

2.2.1. Preparation of Coating

The coating solution consisting of bio-POSS dissolved into toluene (40 wt% solid content) was prepared by using a microwave synthesizer Biotage Initiator 2.0. The paperboard was mounted on a flat steel plate by fastening the edges of paperboard to inhibit wrinkling of paperboard during the coating process. The coating solution was coated on the paperboard (single, double and triple coated) using a TQC Baker film applicator (VF2146, 60mm in width, 30μm in gap). Figure 3a illustrates the preparation of coating.

The coated paperboards were then dried at room temperature for 24hrs, and at 80^{o}C for one hour in a circulation oven (Termaks 4057), and treated for 99 seconds in a UV-light treating system Dymax 1200-EC focused beam (power output range 395W, typical initial output intensity at UV-A of 365 nm: 400mW/cm^{2}).

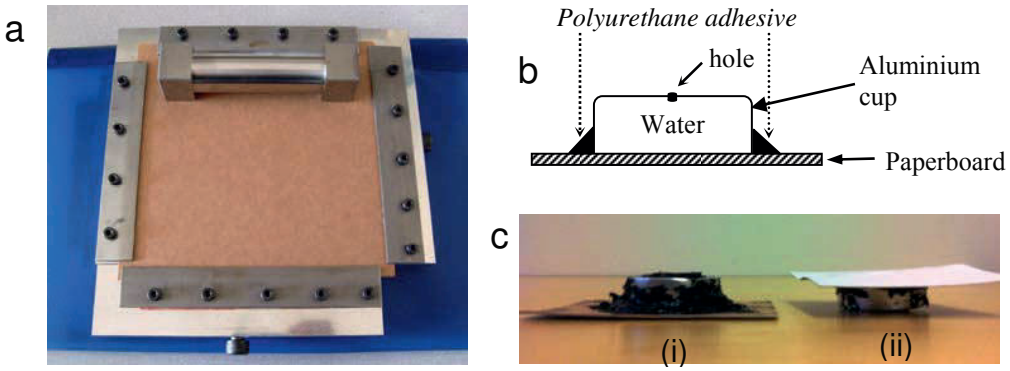

***Figure* 3.** a) TQC Baker film applicator and flat steel plate;
b) Sample preparation: A schematic drawing of the specimen test for water permeability and water vapour permeability;
(c) Specimen arrangement in climate chamber: (i) for water barrier test; (ii) for water vapour barrier test

2.2.2. Fourier Transform Infrared Attenuated Total Reflection (ATR-FTIR) Spectroscopy

Fourier transform infrared attenuated total reflection (ATR-FTIR) was used for analyzing the top surface of coated paperboards. The sample was placed onto the Universal diamond ATR top-plate (Diamond/ZnSe) and a pressure was applied to the sample area. The scan range was in the medium infrared region from 4000 to 650 cm^{-1} at a resolution of 4 cm^{-1}, and a scan number

of 4. The resultant spectra were reported as transmission (%T). The analyses were carried out on a on a PerkinElmer FTIR device (Spectrum One) at room temperature.

2.2.3. Optical Microscopy

The surface and cross-section of bio-POSS coated paperboard was observed by using an optical microscope Leica M420 and photos were taken by a digital microscope colour camera Image Leica DFC295. The thickness of the POSS layer was estimated from the cross-section using the Leica Application Suite LAS 4.1.0 software.

2.2.4. Pinholes

The top surface of the coated layer was examined using an aqueous indicator solution of crystal violet ($C_{25}H_{30}ClN_3$, 5 wt%). 5 ml violet solution was sprayed on top surface of the coated paperboard, and then wiped by a blotting-paper. The obtained surface was observed using an optical microscope and surface images were taken.

2.2.5. Water Barrier and Water Vapour Barrier Test

Water vapour and water permeability of paperboard was monitored by using the cup method [25]. The specimens for two tests were similar. An aluminium cup (38.0 mm in inner diameter and 12.0 cm in depth with an exposure coating area of 1133.54 mm^2) was mounted on the coated paperboard and sealed by polyurethane adhesive. A small hole was carved in the top of the cup to fill distilled water in. After fully filling distilled water into the cup (about 10-11g), the hole was tightly sealed by polyurethane adhesive. Figure 3b describes clearly the sample preparation. At least three specimens were prepared for each test. The specimens were then placed in a climate chamber (KB 8400 F, 400 litres, Termaks AS), set at 50 % of relative humidity (RH) and 23^oC. A fan was used to keep uniform conditions for all test specimens. The arrangement of specimens for each test is illustrated in Fig. 3c: (i) for the water barrier test: the water stays in direct contact with the paperboard, (ii) for the water vapour barrier test, liquid water stay in the bottom of the tray and only water vapour is in contact with the paperboard. The weight of each specimen was measured at 24h intervals for 30 days.

A reference sample was made by substituting the paperboard by using a board from milk carton of Tina AS, Norway.

2.2.6. Calculation of Water and Water Vapour Transmission Rate

The water transmission rate is calculated as:

$$WTR = (W_1 - W_2)/tA \text{ , (g/m}^2 \text{ day) (Eq. 1),}$$

where W_1 and W_2 are the weights of the specimens before and after water permeability test (g) during the time period t (days), and A is test area (m^2).

According to the ASTM E96/E96M-10 [24], calculation of the WVTR is expressed as follows:

$$WVTR = G/tA \text{ (g/m}^2\text{day) (Eq. 2)}$$

where WVTR is rate of water vapour transmission, G is weight change in grams for the time period t (days); A is test area, m^2.

The water vapour permeability (WVP, gm/m^2dayPa) was calculated as:

$$WVP = \frac{WVTR.L}{\Delta p} = \frac{WVTR.L}{S.(R_1 - R_2)} \text{ (Eq. 3) [24],}$$

where WVTR is the measured water vapour transmission rate (g/m^2day) through the paperboard, L is the mean thickness (m) of the paperboard and Δp is vapour pressure difference across two sides of the paperboard, S is saturation vapour pressure at test temperature and calculated as $S = \exp(20.836 - 5132/T)$, where T is Kelvin temperature; R_1 and R_2 is relative humidity inside and outside the test cup [26].

2.2.7. Proton Nuclear Magnetic Resonance (^{1}H NMR) Spectroscopy

Proton nuclear magnetic resonance (^{1}H NMR) spectroscopy was performed on an instrument Bruker Avance III spectrometer in solid state and high resolution liquid state configuration including Ultra Shield Plus 500MHz WB magnet. The spectrometer is equipped with a triple resonance 3.2 mm CP-MAS probe head (H/X/Y).

3. Results and Discussion

3.1. Bio-POSS Coated Layer

ATR-FTIR is a useful technique for determining the surface characteristics of materials. In our study, the top surface of bio-POSS coated paperboard was characterized by the ATR-FTIR. The result is shown in Fig. 4. The main peaks of paperboard surface (see Fig. 4a): the absorption peaks at 3332 cm^{-1} is assigned to hydroxyl (OH) stretching, 2919 and 2851 cm^{-1}: CH_2 stretching, 1644 and 1594 cm^{-1}: water associated with cellulose, 1160 and 1104 cm^{-1}: C–O–C asymmetric stretching, 1051 and 1027 cm^{-1}: C–O stretching [27]. The intensity of OH peak is strong, reflecting a high hydrophilicity of paperboard surface.

The main peaks of bio-POSS are: the absorption peaks at 3665 cm^{-1}, 3290 cm^{-1} and 3082 cm^{-1} are assigned to the free and hydrogen bonded N–H stretching (N–H…O=C); two bands appear at 1643 cm^{-1} and 1547 cm^{-1} are assigned to amide I (carbonyl C=O) and amide II (mixed vibration of N–H bending and C–N stretching), respectively. The intensity of amide I is stronger than that of amide II. The small shoulder band at 1736 cm^{-1} is ascribed as the free C=O stretching vibration. A small peak at 1492 cm^{-1} is attributed to the double bond C=C stretching vibration because the absorption peak of the double bond normally appears behind the amide band. Two strong and broad bands at 1114 cm^{-1} and 1027 cm^{-1} exhibit Si–O–Si stretching vibration, reflecting a cubic Si_8O_{12} structure. The interpretation of the ATR-FTIR spectrum of bio-POSS was consulted the study of Rao [28]. If comparing ATR-FTIR spectrum of uncoated paperboard (Fig 4a) and bio-POSS coated one (Fig. 4b), it can easily see that the bio-POSS layer completely covers the paper surface.

3.2. Coating Layer Thickness

After coating, a bio-POSS layer was formed on the paperboard. The inherently rough surface of the paperboard was covered by a yellowish layer, as illustrated in Fig 5 (a, b). The top surface of the bio-POSS layer was relatively smooth and glossy. The thickness of the coated paperboard was increased with bio-POSS coating.

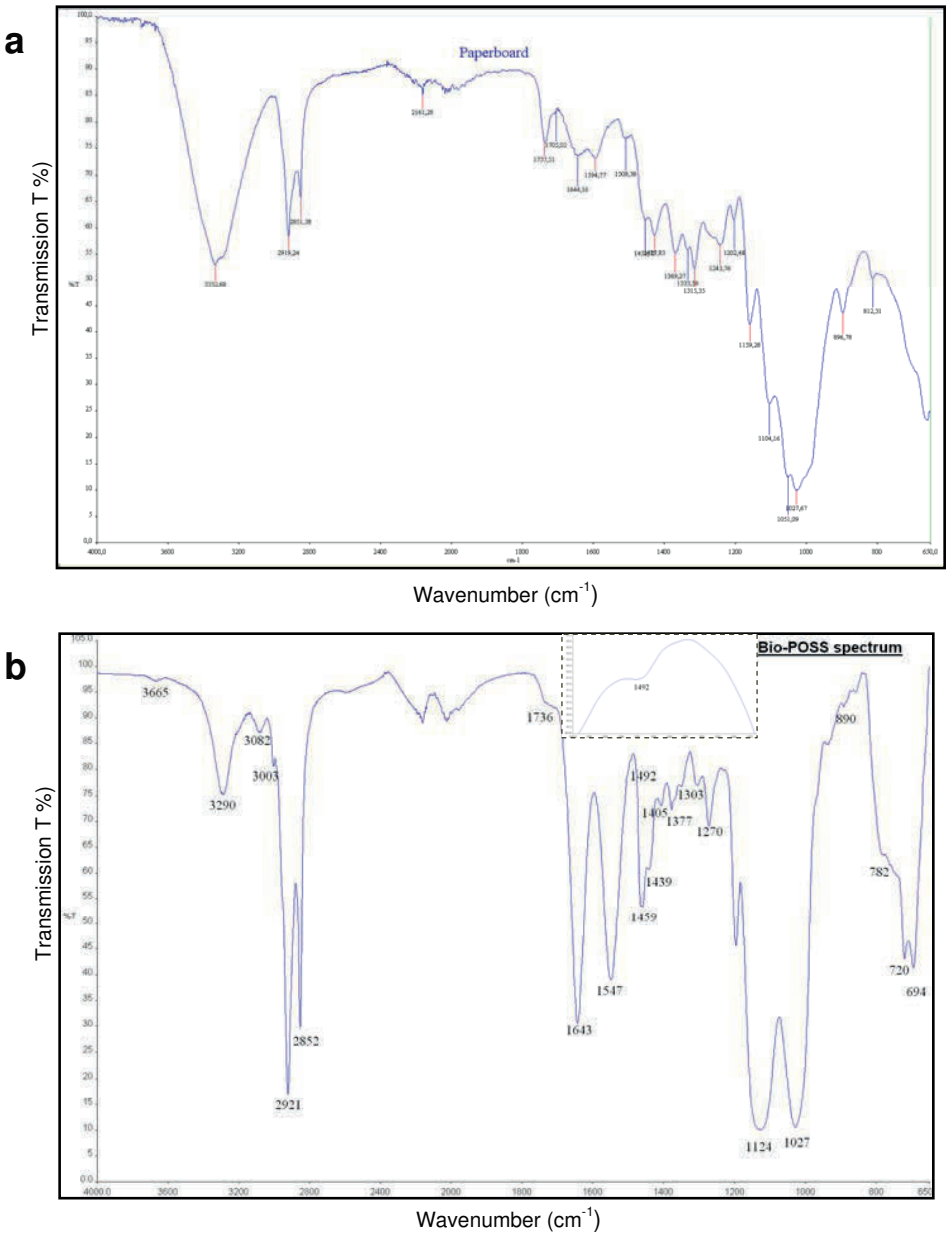

Figure 4. FTIR spectrum of (a) uncoated paperboard; (b) bio-POSS coated paperboard

In order to measure the coating layer thickness, the cross-section of bio-POSS coated paperboard was observed using an optical microscope, and resulted in Fig. 5 (c, d). In the cross-section of the paperboard (Fig. 5c), a pre-coating layer (white colour) and a cellulosic layer (yellow colour) can be seen. The top surface of the cellulosic layer is very rough, and causes a large standard deviation of the estimated thickness (Table 1). The thickness of bio-POSS single-

coated paperboard is slightly smaller than that of the paperboard. It may be explained by a compression of the paperboard by the TQC Baker film applicator during the coating process, resulting in permanent compression of the porous structure of the paperboard. The bio-POSS coating layer (brown colour) can be seen in Fig. 5d. The roughness of the top coated surface was progressively reduced and resulted in reduced standard deviations in the estimated thickness. In fact, bio-POSS coating decreased the standard deviations of the measured thickness by 80%. This may be due to the fact that the depression areas on the paperboard surface are filled with coating material, resulting in a smoother surface.

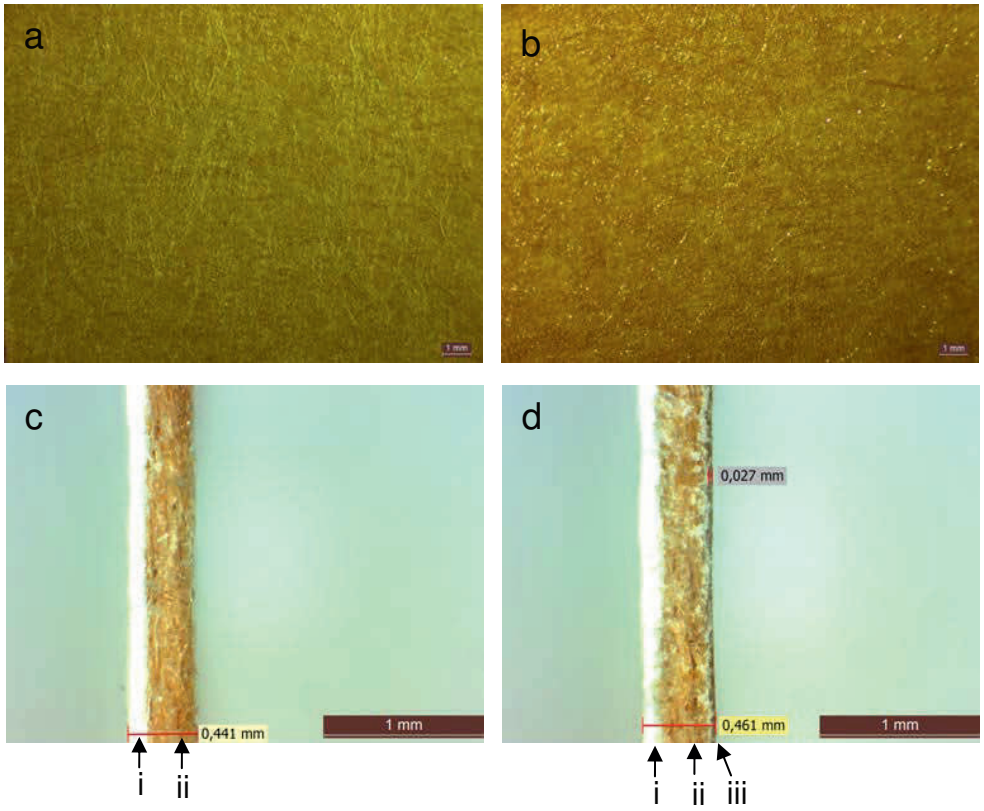

Figure 5. Surface of a) uncoated paperboard, and b) bio-POSS single coated paperboard Cross-section of (c) uncoated paperboard, and (d) bio-POSS triple coated paperboard. i-Pre-coating layer; ii-Cellulosic layer; iii-Bio-POSS coating layer

The estimated thickness of the bio-POSS coating layers are: 10.7 µm (single coating), 19.3 µm (double coating) and 27.7 µm (triple coating). The coating layer thickness was influenced by the solids content of the coating solution. In this work, the solids content of bio-POSS solution was constantly kept at 40 wt%, so that the thickness of bio-POSS coated layer was relatively equal.

Table 1. Thickness of bio-POSS coated paperboard.

Sample	Total (μm)	bio-POSS layer (μm)
Paperboard (pb)	441.6±7.2	0
I-coated pb	438.0±1.7	10.7±1.2
II-coated pb	448.6±1.3	19.3±0.6
III-coated pb	458.7±1.5	27.7±1.5

3.3. Pinholes Test

Pinhole, incomplete coverage, is a common disadvantage for solvent based coating, especially at low coat weight. The pinholes are usually created by the escaping of any volatiles (solvent, air or moisture) which are entrapped within the coated layer after the coating process. Pinholes extend entirely through the coating layer, leading to a reduction in some properties of the coating layer such as gas and water barrier. In our work, an aqueous solution of crystal violet was used to qualitatively measure the defects and pinholes of the paperboard and the top coated layer. The result is shown in Fig 6.

It is easily observed that violet colour entirely covered the uncoated area of the paperboard after the pinhole test (image u). This reflects a hydrophilic nature and a porous structure of the paperboard. Furthermore, the rough surface of the paperboard is advantageous for penetration of aqueous indicator solution. The pinholes were dramatically decreased by coating bio-POSS on the paperboard since the number of violet traces remained on the coated area was remarkably reduced (image I-a). In this case, the thin bio-POSS layer does not completely cover the paperboard. Violet traces were further decreased when the coating layer was dried at high temperature (image I-b) or exposed to UV light (image I-c). It is interesting to recognise that no pinholes were found in the multiple coated paperboard samples.

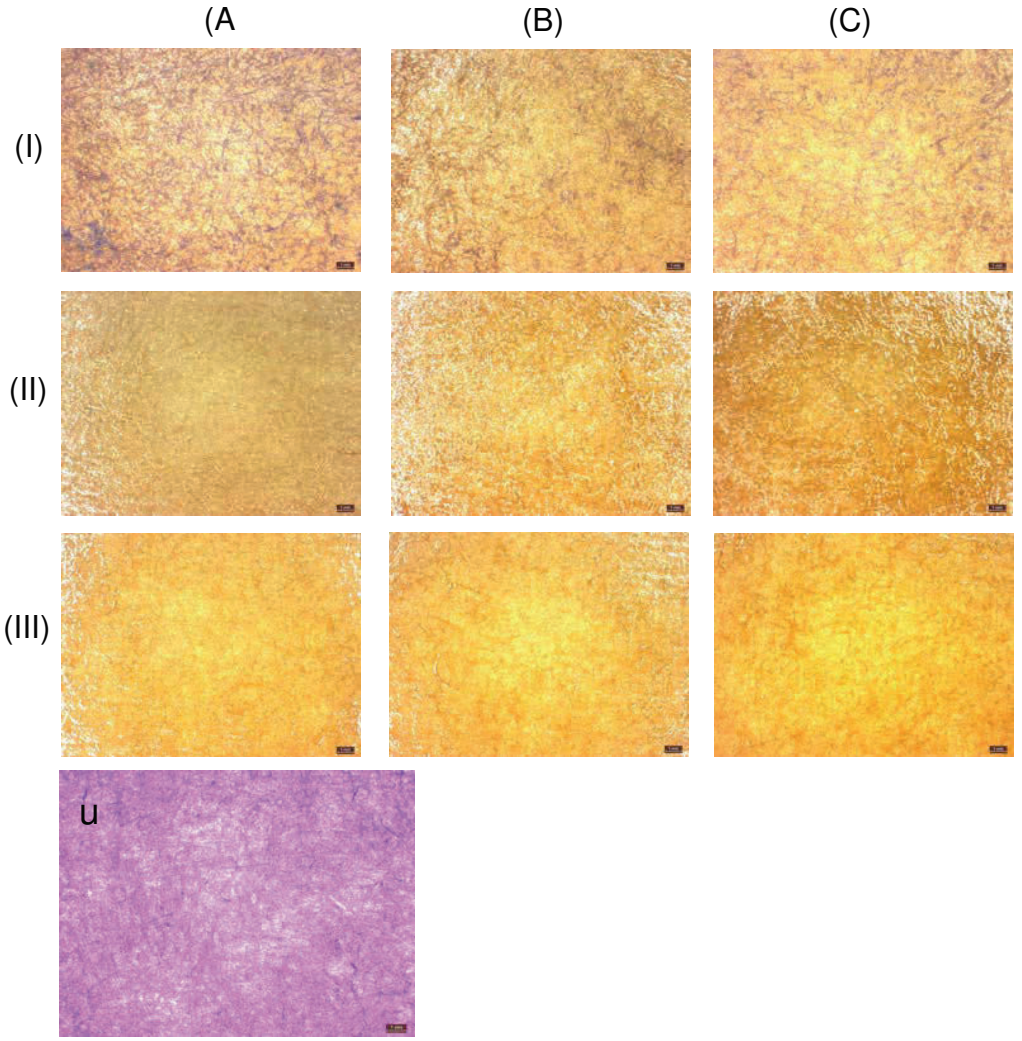

Figure 6. Surface of bio-POSS coated paperboard after pinhole test with crystal violet solution:
(I) Bio-POSS single coated; (II) Double coated; (III) Triple coated
(A) dried at 23^{o}C, (B) dried at 80^{o}C, (C) UV-treated ; (u) uncoated paperboard;

3.4. Water Permeability Test

The water resistance property was investigated through the water permeability test and the result is shown in Fig. 7. Linear regression analysis was performed to estimate the rate of water transmission (WTR) and water vapour transmission (WVTR) through the paperboard. The results are shown in Table 2.

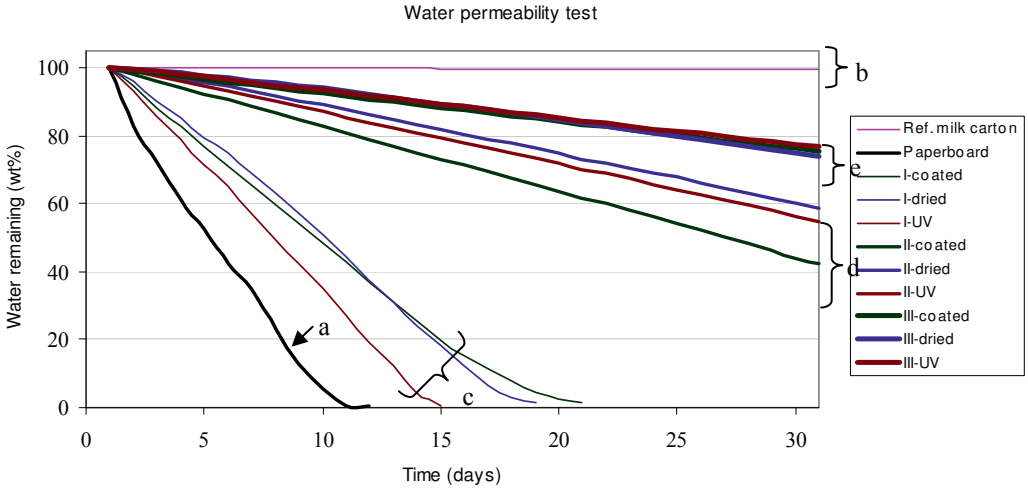

Fig. 7. Water permeability of bio-POSS coated paperboard: a) Un-coated paperboard; b) Reference sample; c) Single coated (I—); d) Double coated (II─); e) Triple coated (III▬)

As can be seen in Fig. 7, the total amount of water inside the test cup of reference sample is unchanged after 30 days, indicating an excellent seal-ability of polyurethane adhesive as well as a good water barrier of the reference substrate. Whereas, the uncoated paperboard has a high WTR (999 g/m^{2}day). The WTR was reduced when a bio-POSS layer was applied on the paperboard surface. At the coating layer thickness of about 10.7 μm, an improvement in the water barrier was obtained: WTR was reduced to 579 g/m^{2}day. Further improvement was achieved by drying the coated samples at high temperature: WTR = 506 g/m^{2}day. However, UV-treatment of the coated sample did not reduce the WTR (595 g/m^{2}day).

When the coating thickness was increased by multiple coating, the water permeability of coated paperboard was significantly reduced, as the water permeability curve moved towards the curves of reference substrate. The WTR dropped from 579 g/m^{2}day (single coating) to 194 g/m^{2}day (double coating), and to 83 g/m^{2}day (triple coating). The thicker the coating layer thickness, the better the water resistance property.

As aforementioned, the paperboard is composed of cellulosic fibres and has a porous structure. Water is soluble in the amorphous parts of cellulose fibres, and therefore will both diffuse through the solid phase (cellulose) as well as in gas phase in pore network, resulting in a high WTR of the paperboard. When the paperboard was coated with bio-POSS, water transport was obstructed by the coated layer. However, there are still a number of pores on the top

surface of the single coated layer (as investigated by the pinhole test). Furthermore, amide groups of bio-POSS give water certain solubility in the coating layer. Therefore, water transport can take place by pore diffusion and diffusion of dissolved water in the solid phase. The enhancement of water resistance property with increasing the coating layer thickness reflects that there are fewer pores in the coating layer after multiple coating. The standard deviation of the WTR of the paperboard was very high due to its porous structure. It is reduced when bio-POSS was coated on the paperboard, particularly with multiple coating. As the result, bio-POSS layer efficiently prevented water transport and controlled the WTR at a steady state. The effect of heat drying and UV treatment on WTR is similar to those in single coating.

Table 2. Water transmission rate (WTR) and water vapour transmission rate (WVTR) of bio-POSS coated paperboard

Substrate	WTR (g/m^2day)	WVTR (g/m^2day)
Paperboard	999±333	1011± 447
Single coating (I—)		
I-coated	579±88	477±129
I-dried	506±133	209±28
I-UV-treated	595±193	450±78
Double coating (II—)		
II-coated	194±18	229±19
II-dried	142±23	128±16
II-UV-treated	152 ±17	163±18
Triple coating (III—)		
III-coated	83±8	105±11
III-dried	74±15	80±21
III-UV treated	71±12	72±12

3.5. Water Vapour Permeability Test

Water vapour permeability (WVP) of the bio-POSS coated paperboard is shown in Fig. 8. From the diagram, the total amount of water in the reference sample hardly changed during 30 days, indicating an excellent water vapour barrier property of the reference substrate. The paperboard itself has a high WVTR of 1011 g/m^2day. This high WVTR is caused by a highly porous structure of the paperboard. In the diagram, the WVP curve of the uncoated paperboard is the steepest curve. Bio-POSS coating reduced the WVP of the paperboard to 477 g/m^2day for a single coating, indicating a moderate water vapour barrier property of bio-POSS layer. Similarly to the water permeability, drying the coated layer improves the water vapour barrier

to 209 g/m^{2}day. However, UV-treatment of the coated layer hardly influenced on the water vapour barrier properties of the paperboard compared to untreated bio-POSS coated one.

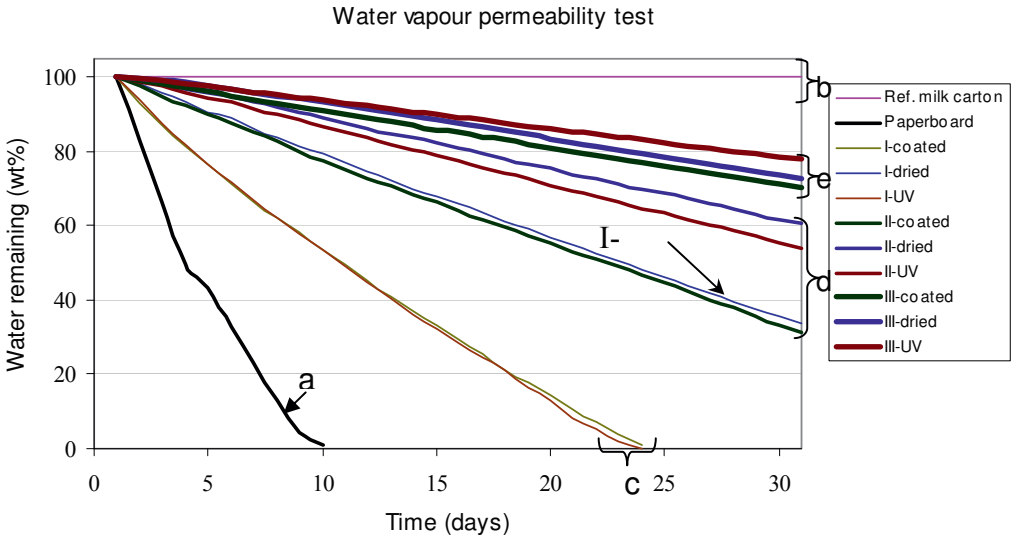

Figure 8. Water vapour permeability of bio-POSS coated paperboard:
a) Un-coated paperboard; b) Reference sample;
c) Single coated (I—); d) Double coated (II─); e) Triple coated (III━)

Similar to water barrier, the water vapour barrier property of the paperboard was enhanced with multiple coating. Thus, the WVP curves corresponding with each coating move towards those of the reference substrate. The WVTR of double coated and triple coated samples was 229 and 105 g/m^{2}day, respectively.

The porous structure of the uncoated paperboard causes its low water vapour barrier property, as high WVTR. The standard deviation of WVTR of the paperboard was high due to its inhomogeneous porous structure. The standard deviation was decreased when bio-POSS was coated on the paperboard, especially by multiple coating. The reduction in the WVTR's standard deviation indicates a more homogeneous structure of the coated paperboard.

The water vapour permeability (WVP_{total}) of bio-POSS coated paperboard was calculated by using equation (Eq. 3). When the paperboard (pb) was not coated, the water vapour permeability coefficient of the paperboard (WVP_{pb}) equals WVP_{total} (318.8 g µm/m^{2}dayPa).

In this work, the water vapour barrier property of the paperboard was improved by bio-POSS coating. In order to determine the water vapour barrier property of each coating layer, the equation of gas permeability of multi-layered film with n layers was used [29]:

$$\frac{l_{total}}{WVP_{total}} = \sum_{i=1}^{n} \frac{l_i}{WVP_i} \quad \text{(Eq. 4)}$$

where l_{total} is the total thickness of bio-POSS coated paperboard, l_i and WVP_i are the thickness and water vapour permeability of the coating layer i, respectively. In our work, the coated paperboard consists of the paperboard substrate and bio-POSS coated layer. Eq. 4 becomes:

$$\frac{l_{total}}{WVP_{total}} = \frac{l_{pb}}{WVP_{pb}} + \frac{l_{coat}}{WVP_{coat}} \quad \text{(Eq.5)}$$

Table 3 lists the thickness and WVP_{coat} of bio-POSS coating layer calculated by Eq. (4).

From the result in Table 3, it can be seen that bio-POSS coating is effective in increasing the water vapour barrier property of the paperboard. The WVP_{coat} was decreased with increasing the coating thickness, indicating that multiple coating closes macroscopic pores as was also seen by the pinhole test.

Table 3. Water vapour permeability of bio-POSS coated paperboard

Layer	WVP_{total} (g μm/m^{2}dayPa)	Thickness (μm)			WVP_{coat} (gμm/m^{2}dayPa)
		Total	pb	coating layer	
Paperboard (pb)	318.8	441.6	441.6	0	0
Bio-POSS I	149.1	438.0	427.3	10.7	6.7
Bio-POSS II	73.5	448.6	429.3	19.3	4.1
Bio-POSS III	34.4	458.7	431	27.7	2.3

3.6. Effect of Post Treatment on The bio-POSS Coating Layer

The water resistance and the water vapour barrier properties of the coated paperboard were further enhanced when bio-POSS coated paperboard was post-treated by drying at high temperature or UV-treatment (as shown in Table 2, Fig. 7 and 8). It was therefore necessary to

examine the effects of post-treatment on the bio-POSS coating layer. Solid state proton nuclear magnetic resonance (^{1}H NMR) spectroscopy was performed on three bio-POSS thin films: (RT): dried at room temperature, (DRY80): dried at 80^{o}C, and (UV): treated by UV light. Figure 9 shows the result of solid state ^{1}H NMR.

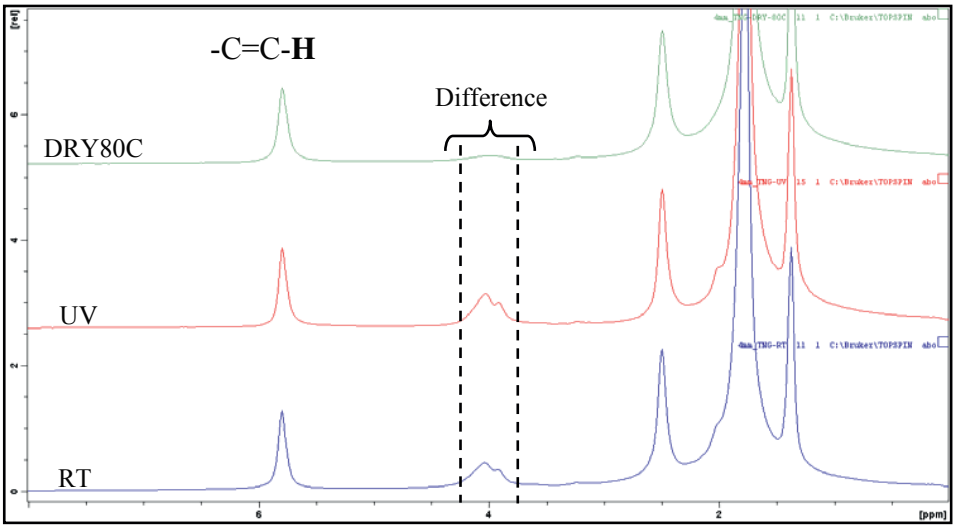

Figure 9. Solid state ^{1}H NMR spectrum of bio-POSS layer:
(RT): dry at room temperature; (DRY80C): dried at 80^{o}C; (UV): UV-treated

As can be seen, solid state ^{1}HNMR spectra of 3 samples seem identically except for the signal around 4 ppm. There are two peaks (3.9 and 4.0 ppm) at this signal. The sample DRY80C shows smallest peaks, whereas the sample RT and UV show larger ones. Perhaps such peaks may be from some liquid-rest.

Figure 10 shows ^{1}H NMR solid state spectrum of sample DRY80C and sample DRY80C/$CDCl_3$ (powder of DRY-80C was shacked with $CDCl_3$ and then $CDCl_3$ was quickly removed). Interestingly, the signal near 4 ppm disappeared in the solid state spectrum of the sample DRY80C/$CDCl_3$. It strongly reflects that the peaks near 4 ppm are from the liquid-rest. The disappearance of such peak was due to the dissolution of the liquid-rest into $CDCl_3$. High resolution liquid ^{1}H-NMR (in $CDCl_3$) was also carried out and the result is shown in Fig. 11. As can be seen, the spectra of 3 samples look similarly. However, the signal in the region 3.4 – 3.8 ppm of the sample DRY80C was weakest. This signal includes multiplicity peaks: a triplet at 3.5 ppm, and a quartet of triplets in the region 3.6-3.8 ppm. Such multiplicity peaks are from 2-butoxyethanol. The liquid-rest is therefore identified.

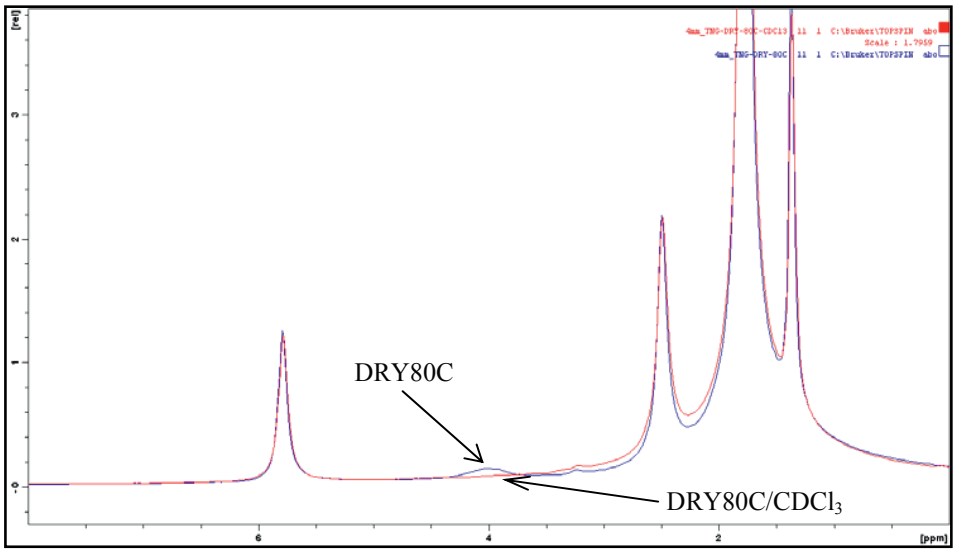

Figure 10. Comparing ^{1}H NMR -solid state spectrum of DRY-80C and DRY-80C/$CDCl_3$

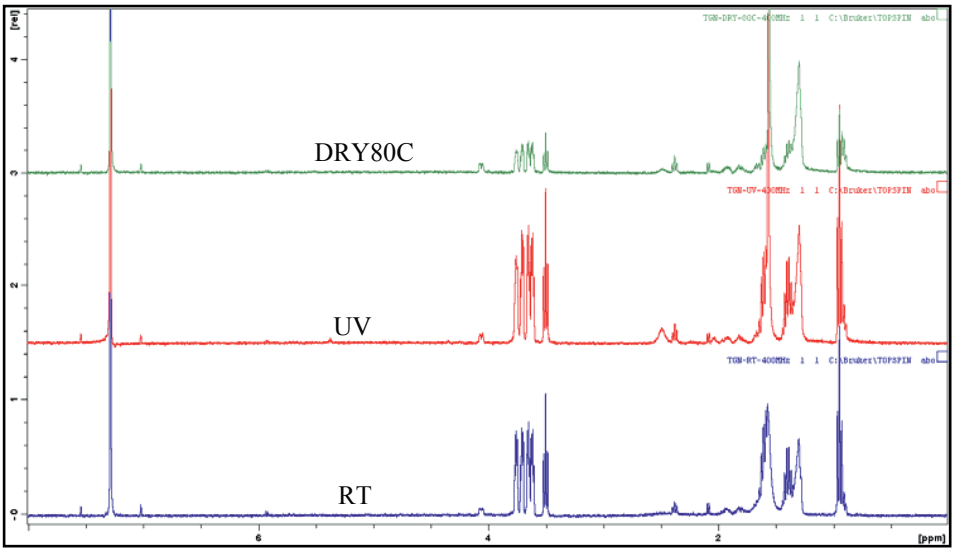

Figure 11. High resolution liquid ^{1}H NMR spectra (in $CDCl_3$ of bio-POSS layer: (RT): dry at room temperature; (DRY80): dried at 80^{o}C; (UV): UV-treated

In Figure 9, the peak at 5.8 ppm was attributed to hydrogen (H) attached to double bond (C=C) that was similar in the spectra of 3 samples. It indicates that the double bond did not alter during heat drying and UV treatment of the bio-POSS coating layer. The crosslinking reaction between unsaturated organic groups of bio-POSS did not occur. There is not any peak

in the region 7-8 ppm for 3 spectra, reflecting that no toluene remains within the coating layer after the coating process.

Consequently, the bio-POSS coating layer contains less 2-butoxy ethanol when it was dried at 80^{o}C, in comparing with those dried at room temperature and exposed to UV light. The dried bio-POSS coating layer became more rigid and had a better structure, thereby further improving the water resistance and water vapour barrier properties of the paperboard.

4. Conclusion

Water resistance and water vapour barrier properties of the paperboards were successfully improved by bio-POSS coatings. This was due to the pores and the depression areas of the cellulose structure of the paperboard were filled with coating materials, as examined by the pinhole test. Consequently, bio-POSS layer was formed on the paperboard and obstructed the water transport through pore diffusion. The inherent hydrophilic surface of paperboard was hydrophobized and somewhat exposure water-repellent. The water resistance and water vapour barrier properties could be further improved by heat drying but UV-treatment had little effect. This was due to the influence of high temperature on the spreading and penetration of bio-POSS into depressions areas of the cellulose structure of the paperboard, resulting in a larger coverage of coating material on the paperboard surface. A crosslinking reaction between the double bond of bio-POSS's organic groups could not be found using solid state ^{1}H-NMR of the UV-treated coating layer. Multiple coating significantly enhanced the water and water vapour barrier properties of the paperboard.

Acknowledgements

The authors thank the Research Council of Norway and the industrial partners Dynea AS, Elopak AS, Forestia AS, Korsnäs AB, Peterson AS, and Södra AB in the KMB project (sustain-Barrier 182619) for financial support.

References

[1] J.W. Rhim, J.H Lee, S.I. Hong, LWT- Food Sci. Technol. **39**, 806, (2006).

[2] T. Suchada, J. Tunyarut, S. Ampron, R. Pornchai, B. Dheerawan, Jnl. Metal. Mater. Minerals **18(2)**, 153, (2008).

[3] S. Butkinaree, T. Jinkarn, R. Yoksan, Jnl. Me. Mater. Min. 18, 219-222, (2008).

[4] T. Archaviboonyobul, T. Jinkarn, S. Sane, S. Chariyachotilert, S. Kongcharoenkiat. Packaging Technol. Sci. DOI: 10.1002/pts.2034

[5] J. Han, S. Salmieri, T.C. Le, M. Lacroix, J. Agric. Food Chem. 58 (5), 3125–3131, (2010).

[6] http://www.iscst.org/pages/ISCSTConf/ISCST2012/Posters/10%20Recalde.pdf

[7] S. Amberg-Schwab, M. Hoffmann, H. Bader, M. Gessler, Jnl. Sol-Gel Sci. Technol. 13, 141, (1998).

[8] J.J. Schwab, J.D. Lichtenhan. Polyhedral oligomeric silsesquioxane (POSS)-based polymers. Appl. Organometal. Chem. 12, 707, (1998).

[9] E. Markovic, K. Constantopolous, J.G. Matisons, Application of Polyhedral Oligomeric Silsesquioxanes: Chap. 1. C. Hartmann-Thompson (ed.) Advances in Silicon Science **3**, 5, (2011).

[10] A. Fina, D. Tabuani, A. Frache, G. Camino, Polymer **46**, 7855–7866, (2005).

[11] M. Sánchez-Soto, D.A. Schiraldi, S. Illescas, Euro. Polym. Jnl. **45**, 341, (2009).

[12] S.K. Lim, E.P. Hong, H. Choi, I.J. Chin, Jnl. Industrial Eng. Chem. **16**, 189, (2010).

[13] S. Bourbigot, T. Turf, S. Bellayer, S. Duquesne, Polym. Degrad. Stab. **94**, 1230, (2009).

[14] Z. Zhang, A. Gu, G. Liang, P. Ren, J. Xie, X. Wang, Polym. Degrad. Stab. **92**, 1986, (2007).

[15] C. Ramírez , M. Rico, A. Torres, L. Barral, J. López, B. Montero, Euro. Polym. Jnl. **44**, 3035, (2008).

[16] L. Matějka, P. Murias, J. Pleštil, Euro. Polym. Jnl. **48**, 260, (2012).

[17] G. Mirchandani, G. Waghoo, R. Parmar, S. Haseebuddin, S.K. Ghosh, Prog. Organ. Coat. **65(4)**, 444, (2009).

[18] I. Jerman, M. Koželj, B. Orel, Solar Energy Materials and Solar Cells **94**, 232, (2010).

[19] E. Amerio, M. Sangermano, G. Colucci, G. Malucelli, M. Messori, R. Taurino, P. Fabbri, Macromol. Mater. Eng. **293**, 700, (2008).

[20] F. Männle, T.R. Tofteberg, M. Skaugen, H. Bu, T. Peters, Pascal D.C. Dietzel, M. Pilz, J. Nanopart. Res. **13**, 4691, (2011).

[21] http://www.pbmdf.com/Liquid-Coatings

[22] http://www.senlights.com/gijyuu/uvcure/UVcuring.html

[23] G. Tillet, B. Boutevin, B. Ameduri, Progress in Polymer Science **36**, 192, (2011).

[24] http://www.sintef.no/Projectweb/FunzioNano/Synthesis-of-FunzioNano-/

[25] Standard test methods for water vapour transmission of materials, ASTM E96/E96M-10.

[26] http://en.wikipedia.org/wiki/Vapour_pressure_of_water

[27] http://www.ipst.gatech.edu/faculty/ragauskas_art/technical_reviews/FT-IR.pdf

[28] C.N.R. Rao. Chemical Applications of Infrared Spectroscopy. Academic Press, New York and London, 125, (1963).

[29] J.Crank. The mathematics of diffusion. 2nd ed. Oxford: Clarendon Press 266, (1975).

Paper 3:

"Effects of a pro-oxidant additive on the adhesion of polyethylene/amino-functionalized POSS compounds to paperboard"

Submitted to Journal of Applied Polymer Science, Ref. APP-2013-07-2568.

Effects of a pro-oxidant additive on the adhesion of polyethylene/amino-functionalized POSS to paperboard

Tuan-Anh Nguyen [a,*], Øyvind Weiby Gregersen [a], Ferdinand Männle [b,*]

[a] *Department of Chemical Engineering, Norwegian University of Science and Technology, N-7491 Trondheim, Norway*

[b] Synthesis and Properties, *SINTEF Materials and Chemistry, N 0314 Oslo, Norway*

* Corresponding author:

- Ferdinand Männle

  Tel.: (+47) 98 28 24 91

  E-mail Address: Ferdinand.Maennle@sintef.no

  Postal Address: Synthesis and Properties, SINTEF Materials and Chemistry, Forskningsveien 1, N0314, Oslo, Norway
- Tuan-Anh Nguyen

  Tel.: (+47) 40 30 86 60

  E-mail Address: tuananh210281@gmail.com

Keyword

Polyethylene, pro-oxidant, amino-POSS, adhesion strength, carbonyl index, thermal ageing

Abbreviations:

Amino-POSS : [3-(11-aminoundecanoyl) amino) propane-1-] silsesquioxane

ATR-FTIR : Attenuated Total Reflectance Fourier transform infrared spectroscopy

CI : Carbonyl index

$FeSt_3$: Ferric stearate

MFI : Melt flow index

PE : Polyethylene

Highlight

- Ferric stearate improved the adhesion of PE films to paperboard
- The PE films were not brittle despite of oxidation
- Adhesion strength was improved by an oxidation of PE chains

ABSTRACT

Mixtures of ferric stearate ($FeSt_3$) and [(3-(11-aminoundecanoyl) amino) propane-1-] silsesquioxane (amino-POSS) were introduced into polyethylene (PE). The PE/amino-POSS/ $FeSt_3$ compounds were converted to thin film and exposed to thermal ageing at 70°C in a circulation oven. Carbonyl groups were formed on the film surfaces and characterized as carbonyl index (CI) by ATR-FTIR. The result indicated that PE was oxidized by the presence of $FeSt_3$. The melt flow index (MFI) test showed that the melt flows of the compounds increased due to an oxidation and a chain scission. Tensile testing of the film samples showed no significant decrease in the tensile strength and moderate changes in elongation at break when compared to reference polyethylene films containing no $FeSt_3$.

The PE/amino-POSS/ $FeSt_3$ compounds were compression moulded to paperboard. The adhesion of non-aged films to paperboard decreased with increasing amino-POSS content. This is in good aggrement with an earlier reported lubricant effect of high amounts of POSS in PE. Thermal ageing of PE/amino-POSS/$FeSt_3$ films prior to coating however led to an increase in the adhesion. Adhesion was increased by 30% when a film containing 99% PE, 0.5 wt% amino-POSS and 0.5 wt% $FeSt_3$ was thermally aged 6 days prior to compression moulding. The physical interlocking and interaction between C=O of the compounds and OH of paperboard may explain the adhesion improvement. The films were not brittle after thermal ageing which make their use in industrial packaging feasible.

INTRODUCTION

Polyethylene (PE) coated paperboard has been widely applied for packaging foods, beverages and pharmaceuticals because of its low cost, lightweight, non-toxicity, excellent water barrier, good mechanical properties and processability. Adhesion strength between PE and paperboard is an important property of this packaging material [1]. The adhesion was improved by introducing the polar groups such as CO and OH on the surface of PE prior laminating with paperboard [2,3]. A pro-oxidant additive (such as stearate salt of iron, cobalt and manganese) may be added to PE to improve its biodegradability [4-8]. Non-sterically hindered aliphatic amines are known to act as decomposer of hydroperoxides which is the rate limiting step in the oxidation of polyethylene. A combination of iron (III) stearate and stearylamin has shown considerably faster degradation of polypropylene than iron (III) stearate alone. Aliphatic amines can therefore act as accelerators in combination with pro-oxidants [9-11]. Many studies have reported that the oxidation of the PE films containing pro-oxidant additive prevalently produces carbonyl (C=O) on its surface [6, 12-18]. The presence of carbonyl group on PE film surface can lead to an increase in its surface polarity. When such film is laminated with paperboard, the adhesion can be improved due to an increase in the interfacial attractive force [19-21].

Polyhedral oligomeric silsesquioxane (POSS) is an inorganic-organic hybrid compound with a general formula $(RSiO_{1.5})_n$, where R is an organic group, n is number of silicon atoms (n = 8, 10, 12), and a special molecular structure which is composed of an inorganic core cage and the functional organic group surrounding the core cage. The organic groups allow POSS compounds to be easily incorporated into organic polymers [22,23]. POSS has recently been used in thermoplastics and improve several properties of the materials [24-32]. In our previous work, small amounts of bio-POSS octa-(ethyl octadeca *10,13* dienoamide silsesquioxanes) was added to polyethylene (PE) and laminated with paperboard. The adhesion property of this packaging material was successfully improved [33]. Due to the general advantage of using pro-oxidant additives, we wanted to investigate if the incorporation of pro-oxidant additive into POSS/PE films could create an improved surface polarity. If this is the case, improved adhesion will be achieved when the plastic is laminated with paper board.

POSS compound [(3-(11-aminoundecanoyl) amino) propane-1-] silsesquioxane, with a typical structure shown in Fig. 1, was used in this work. This compound was composed of an inorganic silica core and the functional group was a derivative of 11-aminoundecanoic acid. Such POSS compound was called amino-POSS. The objective of this study is to incorporate the

pro-oxidant additive ferric stearate and amino-POSS into PE and examine the effect on the adhesion strength of PE films to paperboard. Amino-POSS is supposed to act as accelerator together with the pro-oxidant.

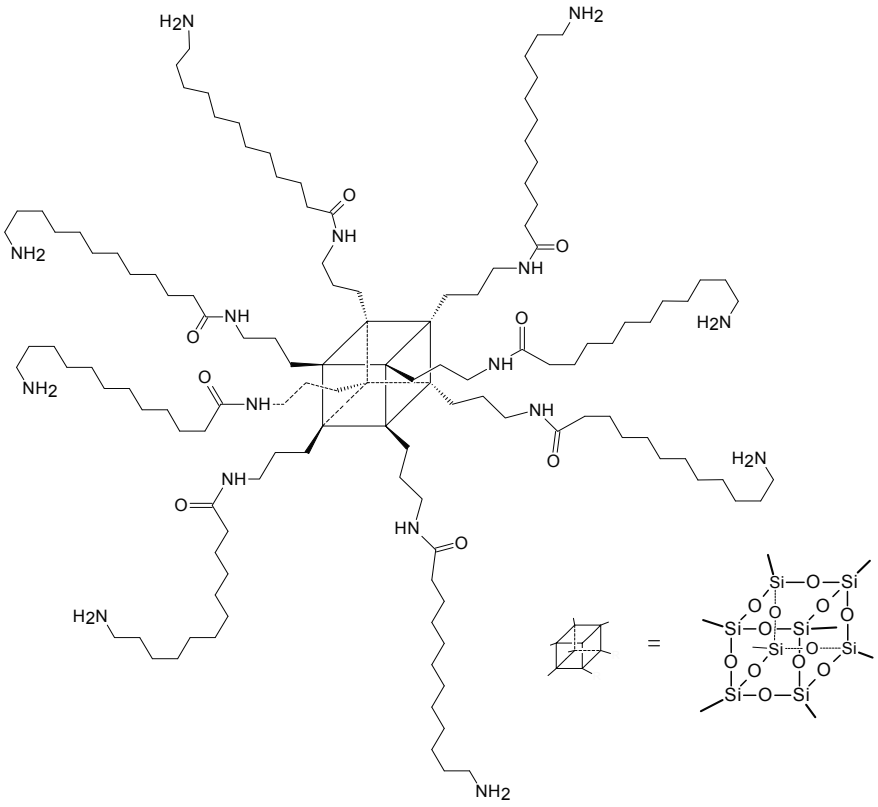

Fig. 1. Typical structure of [3-(11-aminoundecanoyl amino) propane-1-] silsesquioxane (amino-POSS)

EXPERIMENTAL

Materials

Polyethylene (PE) was provided from Normatch AS, Norway, with melting point of 120^{o}C and the melt flow index (MFI) of 20 g/10 min (190^{o}C/ 2.16 kg). The pro-oxidant additive was a masterbatch of ferric stearate ($FeSt_3$) in polyethylene with an iron content of 0.4% which was provided by Nor-X Industry AS, Norway. Paperboard was provided by Korsnäs AB, Sweden.

POSS compound

The POSS compound [(3-(11-aminoundecanoyl) amino) propane-1-] silsesquioxane or amino-POSS, was previously synthesized by in our laboratory by a two-step procedure [34]. In

the first step 3-aminopropyltriethoxy silane was converted to amino functionalized POSS by a sol-gel process. In the second step the amine groups were further modified by an amino acid (11-aminoundecanoic acid).

Paperboard

The paperboard has two sides with different colour: Fig. 2a shows an uncoated side (brown) and a pre-coated side (white), Fig. 2b shows a scanning electron microscopy (SEM) image of the uncoated side of the paperboard, and Fig. 2c is the cross-section of the paperboard which illustrates four different layers:

(i) the bottom layer is unbleached kraft pulp of a pine and spruce softwood mix;
(ii) the middle layer is unbleached kraft pulp and chemithermomechanical pulp (CTMP);
(iii) the dense layer is bleached kraft pulp;
(iv) the top layer is coated by white pigments and binders (the pre-coated side).

The uncoated side of paperboard is very rough, containing large fibres. There are many pinholes and depressions on the uncoated side of the paperboard. As can be observed, the uncoated side of paperboard is very rough, containing large fibres. The rough surface of the uncoated side of paperboard is advantageous for mechanical adhesion of the polymer coating.

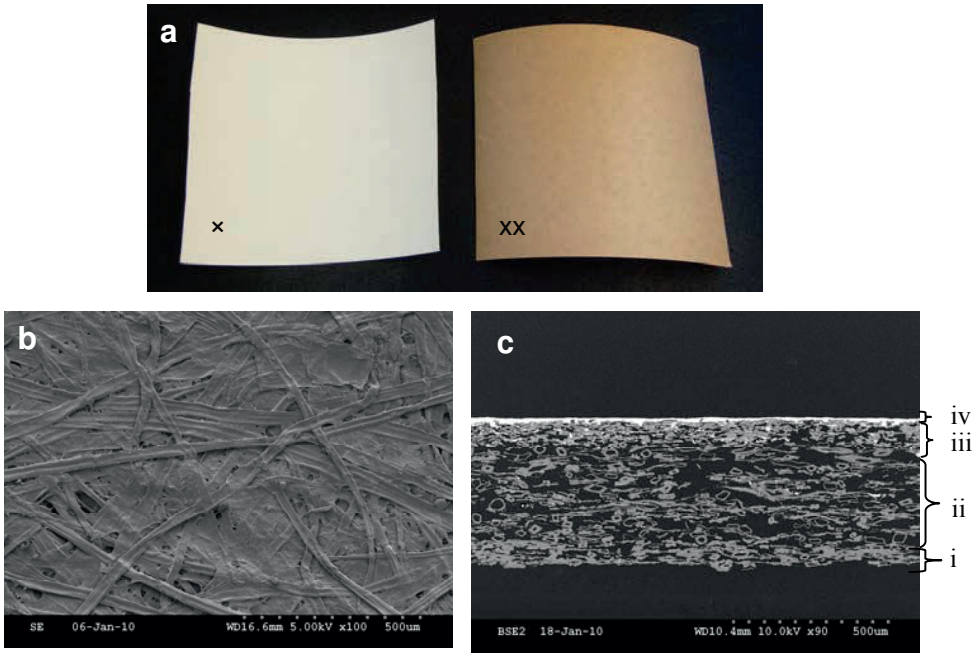

Fig. 2. (a) Two sides of paperboard: x) pre-coated side and (xx) uncoated side;
(b) SEM images of uncoated side of the paperboard, (c) Cross-section

Sample preparation

Preparation of PE and PE/amino-POSS/$FeSt_3$ film

The pro-oxidant masterbatch of PE containing 10 wt% of ferric stearate ($FeSt_3$) was called masterbatch A and used as received.

Amino-POSS was dried at 120°C to fully remove solvent (2-butoxy ethanol). Masterbatch B including 90 wt% PE powder and 10 wt% dried amino-POSS was prepared in a twin screw 15cc micro extruder (DSM MIDI2000). After that, the mixture of PE, masterbatch A and masterbatch B was blended by melt mixing in different ratios (see Table 1) in which the content of $FeSt_3$ was constantly kept at 0.5 wt% for all samples. The extrusion temperature of two processes was constantly kept at 180°C from hopper to die section of micro-extruder, the operating screw speed was controlled at 50 rpm/min and the resident time distribution profile was 5 min. The compound product was cut into pellets.

Table 1
Compositions of PE/amino-POSS/$FeSt_3$/ compounds.

Sample code	PE (pellet)	mb A	mb B	Composition		
	wt%	wt%	wt%	PE	$FeSt_3$	amino-POSS
PE	100	0	0	100	0	0
90505	90	5	5	99	0.5	0.5
85510	85	5	10	98.5	0.5	1
80515	80	5	15	98	0.5	1.5

Thin films of PE and the compounds were prepared by compression moulding pure PE powder and PE/amino-POSS/$FeSt_3$ pellets on a hydraulic compressor (Fontijne TH200), respectively. The film thickness was 0.1 mm. The temperature of both the top and bottom plates of the hydraulic compressor was 180°C, the pressure was 10 MPa, and the pressing time was 5 minutes.

Thermal ageing of the film

The PE/amino-POSS/$FeSt_3$ films were thermally exposed at 70°C for 3 or 6 days in an air circulation oven (Termaks 4057).

Coating the paperboard

The films and the aged films were coated on paperboard by compression moulding coating on a hydraulic compressor (Fontijne TH200). The coating conditions were kept constant at the pressure of 10 MPa and the temperature of the top/bottom plate of 200^{o}C/20^{o}C. The coating process was complete after cooling down two plates of the compressor to the room temperature by opening cold water system. The coating time was 3 minutes.

Characterization

ATR-FTIR and carbonyl index (C.I.)

Attenuated Total Reflection Furrier Transform Infrared (ATR- FTIR) was performed in a PerkinElmer FTIR device (Spectrum One) at room temperature in the wave number range 650-4000 cm^{-1}, at a resolution of 4 cm^{-1}, and scan number of 4. The result spectrum was reported as absorbance unit (a.u).

Results from ATR-FTIR analysis were used to determine the carbonyl index (C.I.). C.I. is a measurement of the amount of carbonyl compounds formed during the thermal oxidation and is calculated as the ratio of the absorbance (A) of carbonyl peak in the region 1700–1780cm^{-1} and the CH_2 scissoring peak at 1464 cm^{-1} [15-17]:

$$C.I = \frac{A_{1700-1780 cm^{-1}}}{A_{1464\, cm^{-1}}} \quad \text{(Eq. 1)}$$

Adhesion measurement

A T-peel test was performed on a tensile tester (Zwich-Z250) to determine the adhesion of our samples. At least five *T*-type specimens (200 mm in length and 15 mm in width) were prepared for each sample by using Thwing-Albert's JDC-15 mm-10 in. sample cutter. The polymer coating was peeled at the speed of 30 mm/min. and over a length of 150 mm.

The adhesion value was determined as: $\text{adhesion} = \text{peel force/width}$ (N/m) (Eq. 2)

The adhesion strength of the sample was calculated as the average of five adhesion values from five different specimens.

Melt flow index

The effect of amino-POSS content on melt flow of polyethylene (PE) was monitored by melt flow index (MFI) method on a melt flow apparatus, Davenport 3/80. The materials were fully loaded into a cylinder of the MFI device and then melted at temperature of 190^{o}C. Pre-

heating time and extrudate time were set at 5 and 10 minutes. MFI was expressed as the mass of the material per 10 minutes extruded through the die of 2.09 mm in diameter and 8mm in length, under the standard weight of 2.16 kg:

$$MFI = \frac{Average\ extrudate\ weight}{Time} \text{ (g/10 min.) (Eq. 3)}$$

Mechanical properties

The mechanical properties of the film were determined by tensile testing according to ISO 527-1 on the device Zwich-Z250. Test specimens were cut from the film with "dumbbell" shape. At least 5 specimens of each film were prepared for tensile testing. The test was run at the speed of 50 mm/min and room temperature.

RESULTS AND DISCUSSION

ATR-FTIR studies

PE/amino-POSS/$FeSt_3$

The ATR-FTIR is a useful technique for characterizing the surface of the material. In this work, the ATR-FTIR analyses were performed on pure materials (PE, amino-POSS, and $FeSt_3$/PE masterbatch), PE/amino-POSS/$FeSt_3$ compounds and the result are shown in Fig. 3. The study of Rao was used for the interpretation of our ATR-FTIR spectra [35].

The main peaks of PE are 2920 cm^{-1} and 2851 cm^{-1} (CH_2 stretching), 1471 cm^{-1} and 1430 cm^{-1} (CH_2 bending), 720 cm^{-1} (CH_2 rocking). The main peaks of amino-POSS are: the absorption peaks at 3287 cm^{-1} and 3074 cm^{-1} are assigned to the hydrogen-bonded N–H stretching (N–H…O=C); two bands appear at 1640 cm^{-1} and 1548 cm^{-1} are assigned to amide I (carbonyl C=O) and amide II (mixed vibration involving N–H in-plane bending and C–N stretching), respectively. Normally, the intensity of amide I is stronger than that of amide II. A band at 1271 cm^{-1} is amide III (mixed vibration of C–N stretching and N-H bending). Two strong and broad bands at 1119 cm^{-1} and 1028 cm^{-1} exhibit Si–O–Si stretching of the cubic Si_8O_{12} structure. The spectrum of masterbatch $FeSt_3$/PE shows two strong peaks near 2920 and 2851 cm^{-1} (CH_2 stretching), a strong and sharp peak at 1700 cm^{-1} (carbonyl C=O of ester group), 1471 cm^{-1} (CH_2 bending), 1430 cm^{-1} (stretching vibration of C–O group). The band characteristic to the symmetric stretching vibration of the group COO appears at 1355 cm^{-1}. The band from 1298 cm^{-1} can be assigned to the C–COO vibrations. The interpretation of ATR-

FTIR spectrum of $FeSt_3$/PE is similar to that in other studies concerning the spectrum of carboxylate group [36,37].

As can be observed in Fig. 3, the main characteristics of PE, amino-POSS and $FeSt_3$ were introduced into the spectra of the compounds 90505, 85510, and 80515.

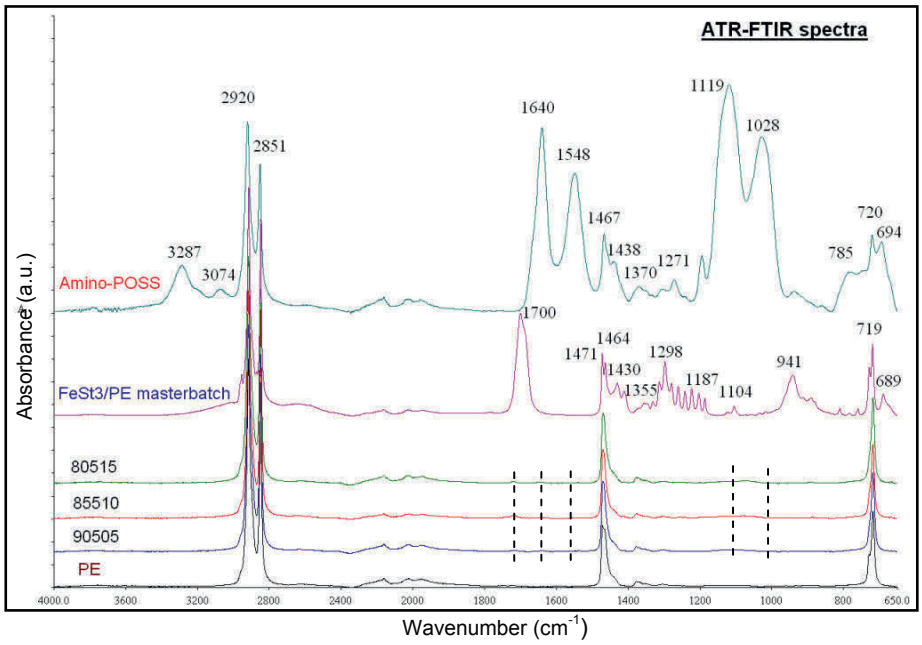

Fig. 3. FTIR spectra of PE/amino-POSS/$FeSt_3$ compounds

Thermal ageing

The thermally aged films were characterized by ATR-FTIR and the result is shown in Fig. 4. All spectra of the aged film exhibit the absorption band in the region 1700–1780cm^{-1} which is assigned to carbonyl (C=O) groups, as determined by the overlapping bands corresponding to ester (1737 cm^{-1}), ketone (1715 and 1717 cm^{-1}). These bands are evidence for the formation of different oxidized products similar to those found in other studies involving the oxidation of PE [12, 15-17]. If comparing the intensity of carbonyl peak of the film after thermal ageing to that before ageing (as reference peak), an increase with increasing the ageing time can be seen.

The oxidation level of PE/amino-POSS/$FeSt_3$ can be evaluated by the carbonyl index (CI). Fig. 5 shows the CI of PE and PE/amino-POSS/$FeSt_3$ film before and after thermal ageing. In general, the CI is increased with increasing the ageing time. The increase in CI of the pure PE film was negligible. The CI of the film containing pro-oxidant was higher than that of the PE

film, emphasizing the degrading effect of $FeSt_3$. In fact, there was slight increase in the CI of the aged film 85510, 80515 whereas the CI of the film 90505 was substantially increased with increasing the ageing time. It strongly reflects that the oxidation level of the compound was limited when amino-POSS content is increased.

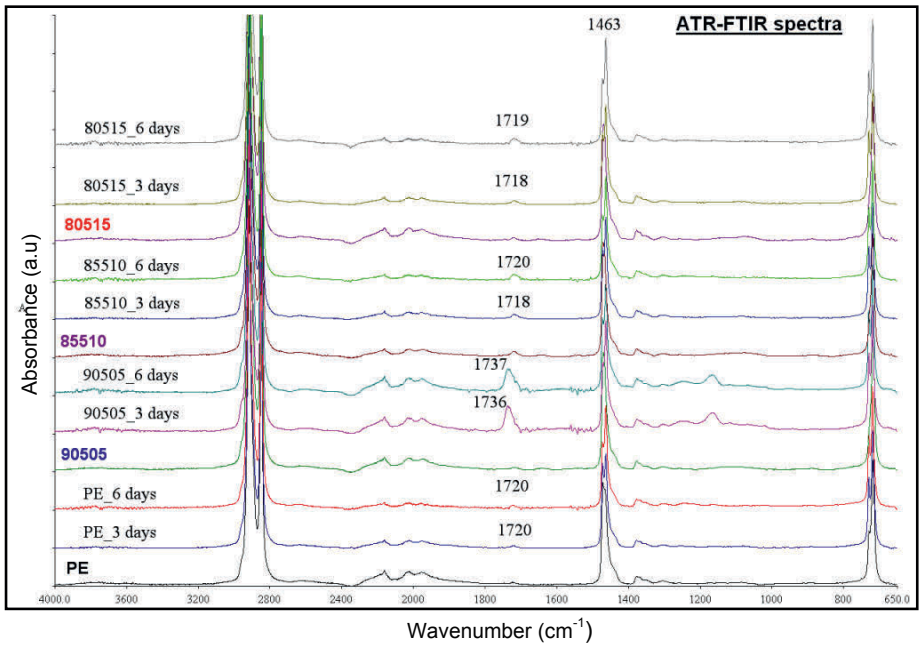

Fig. 4. ATR-FTIR spectra of the compounds before and after thermal ageing

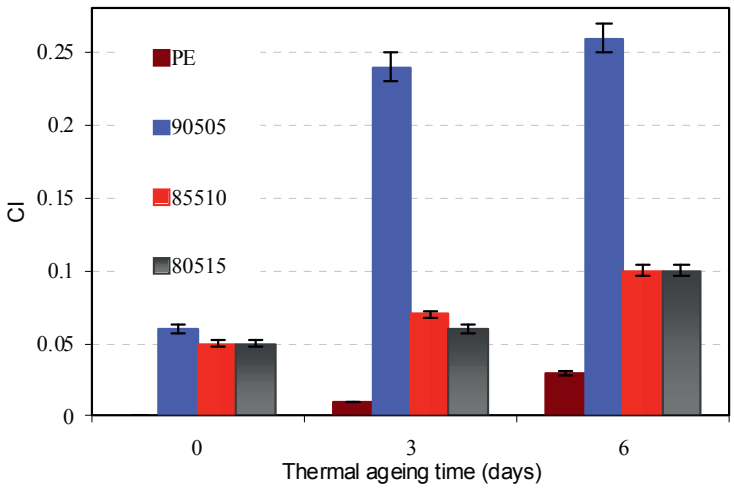

Fig. 5. Carbonyl index (CI) of PE and PE/amino-POSS/$FeSt_3$ film

Melt flow index (MFI)

The melt flow index is an inverse measure of the melt viscosity. The higher a MFI, the more easily the polymer flows under the test conditions. Knowing the MFI of a certain polymer is vital for controlling its processing [38]. The melt flow properties of our PE/amino-POSS/$FeSt_3$ compounds were determined by MFI testing and are shown in Fig. 6.

Neat PE showed a decrease in the MFI after thermal ageing. It suggests that some cross-linking have formed by oxidative degradation of PE during thermal ageing [39,40]. The MFI of the PE/amino-POSS/$FeSt_3$ compounds were decreased with increasing amino-POSS content. However, after thermal ageing in air circulation oven, the MFI of the compounds containing pro-oxidant additive were increased with increasing the ageing time. In fact, the increase in the MFI of the compounds was negligible after 3 days but was considerable after 6 days of air oven ageing. The compound 90505 after being thermally aged for 6 days exhibited the highest MFI value. It indicates that the presence of pro-oxidant leads to a chain scission of PE during thermal ageing and thus cause an increase in the melt indices [39]. The MFI of the aged compounds were also decreased with increasing amino-POSS content. As determined above, the CI of the sample 90505 was much higher than that of 85510 and 80515. It indicates that the PE chain scission might be hindered by increasing amino-POSS content.

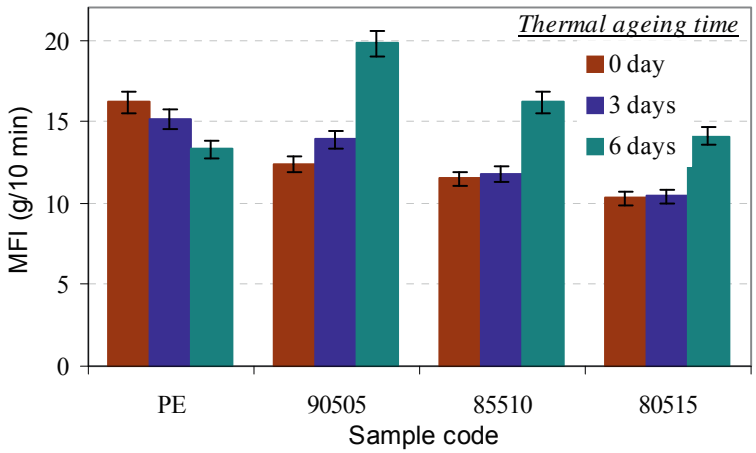

Fig. 6. Melt flow index of PE and PE/amino-POSS/$FeSt_3$ compounds after thermal ageing

Mechanical properties

The mechanical properties of PE and PE/amino-POSS/$FeSt_3$ films were determined by tensile testing. Fig. 7 illustrates the effect of thermal exposure on the tensile yield strength (σ_Y)

and elongation at break (ε_B) of films, respectively. It can be recognized that σ_Y of PE/amino-POSS/$FeSt_3$ films were slightly decreased with increasing amino-POSS content (Fig. a), while ε_B was moderately decreased (Fig. b). The decrease in σ_Y and ε_B might be due to the presence of amino-POSS aggregates within the PE/amino-POSS/$FeSt_3$ compounds [33]

When the films were thermally aged, their mechanical properties were decreased with the ageing time. The tensile strength of PE and PE/amino-POSS/$FeSt_3$ films was moderately decreased after 3 days thermal ageing, but hardly changed afterwards. The elongation at break of pure PE film dropped to 261% and 128% from an initial figure of 265% after 3 and 6 days of thermal ageing, respectively. However, the effect of thermal exposure on the ε_B of the films was small. ε_B of all the aged films was more than 50% after thermal ageing.

As identified above, thermal ageing of PE/amino-POSS/$FeSt_3$ films led to a formation of carbonyl groups. Increasing the ageing time produced an increase in the intensity of carbonyl peak, as determined by the CI. It indicates that the polymer chains were cleaved to give a rise in carbonyl groups. Due to the cleavage of polymeric chains, also ε_B decreased as the ageing time was increased. The elongation at break was the most suitable parameter to quantify the degradation. The result of mechanical properties demonstrates that the film was degraded by thermal oxidation.

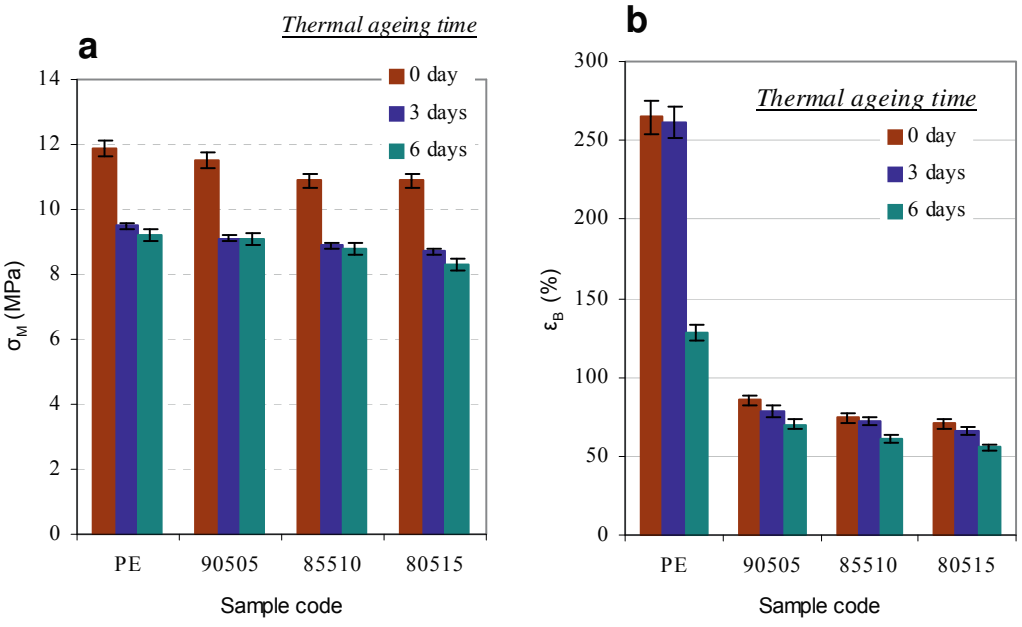

Fig. 7. Effect of thermal ageing on the tensile yield strength (a), and elongation at break (b) of PE/amino-POSS/$FeSt_3$ films

The incorporation of amino-POSS into the compounds led to a larger reduction on σ_Y and ε_B of the films (Fig. 6b). Furthermore, the presence of amino-POSS reduced the oxidation level of the compounds, as the CI reduced when increasing amino-POSS content in the compounds (Fig. 4). It reflects that amino-POSS has an influence on the effectiveness of the pro-oxidant $FeSt_3$.

Adhesion

Adhesions of PE and PE/amino-POSS/$FeSt_3$ compounds to paperboard are summarized in Fig. 8. As can be seen, the adhesion was decreased with increasing amino-POSS content. Such phenomenon is relatively similar to the reduction in the adhesion of PE/bio-POSS octaethyl octadecamide silsesquioxane blends to paperboard when increasing bio-POSS content, as reported in our previous work. It strongly reflects a lubricant effect of POSS compound [33]. The standard deviation of the adhesion test is relatively small for all our samples (below 50 N/m).

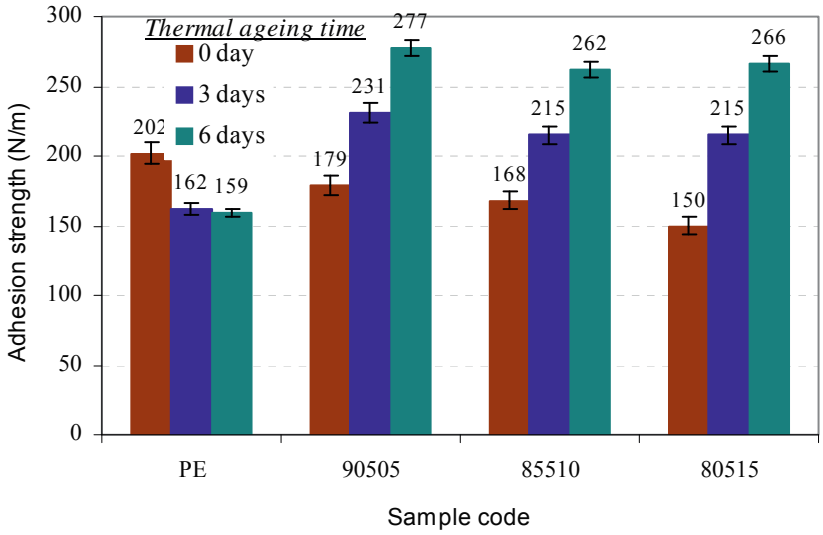

Fig. 8. Adhesion strength of PE/amino-POSS/$FeSt_3$ blends to paperboard

When the film was thermally treated in a circulation oven, its adhesion to paperboard was altered. The adhesion strength of the aged PE to the paperboard was decreased. It was probably due to a reduction in the melt flow property of the aged PE, as determined by the MFI testing. Whereas, when PE/amino-POSS/$FeSt_3$ compounds were thermally treated prior to coating, the adhesion to the paperboard increased with increasing the ageing time. Remarkably, the adhesion was improved approx. 30% by thermal treating the compound 90505 before coating on

paperboard. The MFI test shows that the flowability of the compounds increased with increasing the ageing time. In this case, physical interlocking could cause an enhancement in the adhesion of the compounds to paperboard.

As identified by ATR-FTIR, there was carbonyl group formed on the surface of the PE/amino-POSS/$FeSt_3$ films. When PE/amino-POSS/$FeSt_3$ films was coated on paperboard, the interaction between C=O groups and hydroxyl group (OH) of the paperboard could occur to form hydrogen bond at the interface. In our previous work, the formation of such interfacial hydrogen bonding interaction was confirmed by ATR-FTIR analysis of the fracture surface of the polymer containing layer and the paperboard surface. The intensity of amide (I, II) peak was altered and C=O peak intensity was weakened after interaction [33]. The formation of interfacial hydrogen bonding interaction can lead to an enhancement in the adhesion of PE/amino-POSS/$FeSt_3$ films to paperboard.

CONCLUSIONS

The pro-oxidant additive ferric stearate and amino-POSS were introduced into PE by using a melt mixing method. The effect on the adhesion strength of the resulting PE films to paperboard has been examined. Amino-POSS is supposed to act as accelerator together with the pro-oxidant. The oxidative degradation and melt flow properties of the PE were obviously affected. Small amounts of amino-POSS resulted in a fast increase of the carbonyl index showing a fast oxidation. Increasing amino-POSS content did not accelerate but de-accelerate the oxidation. This behaviour shows that the amount of amine-POSS has to be low and should be optimized in order make a fast oxidation feasible. The mechanical properties (tensile yield strength and elongation at break) of PE/amino-POSS/$FeSt_3$ films decreased, but the films still remained flexible. When PE/amino-POSS/$FeSt_3$ films were compression moulding coated on paperboard, the adhesion strength decreased with increasing amino-POSS content. The adhesion was however increased when such films were treated at 70^{o}C prior to coating. The adhesion improvement was probably due to the interaction between OH groups of paperboard and C=O groups of PE/amino-POSS/$FeSt_3$ compounds. The physical interlocking due to reduced melt viscosity could be considered as a reason for adhesion improvement. Processing of coated paperboard in state-of-the-art packaging machines should be feasible.

Acknowledgements

This study has been financially supported by the Research Council of Norway and the industrial partners Dynea AS, Elopak AS, Forestia AS, Peterson Linerboard AS, Korsnäs AB, and Södra Cell AB in the KMB project (SustainBarrier 182619). The authors are grateful for the materials received from Normatch AS and Nor-X Industry AS, (Norway), and Korsnäs AB (Sweden).

References

[1] Kemppi, A.; Laboratory of Paper Chemistry. Åbo Akademi University. Åbo, 1997, 39.
[2] Westerlind, B.; Larsson, A; Rigdahl, M. Int Jnl Adhesion Adhesives 1987, 7(3), 141.
[3] Kaplan, S.L.; Rose, P.W. Int Jnl Adhesion Adhesives 1991, 11(2), 109.
[4] http://en.wikipedia.org/wiki/Oxo_Biodegradable
[5] Scott, G. Polym Degrad Stab 1990, 29, 135.
[6] Roy, P.K.; Surekha, P.; Raman, R.; Rajagopal, C. Polym Degrad Stab 2009, 94(7), 1033.
[7] Männle, F.; Rødseth, K.R.; Kleppe, E.A.; Hauge, R.; Tanem, B.S. US Patent Application Publication US 2009/0226749 A1, p1.
[8] Männle, F.; Jørgensen, J.; Tanem, B.S. Int Jnl Polym Sci 2012, doi:10.1155/2012/297923.
[9] Männle, F.; Rødseth, K.R; Kleppe, E.A.; Hauge, R.; Tanem, B.S. WO2007123413 2007; 22.
[10] Salem, I.A.. J Molec Cat 1993, 80(1), 11-19.
[11] Eyler, G.N.; Canizo, A.I.; Alvarez, E.E. Afinidad 2007, 64(530), 538.
12] Tidjani, A. Polym Degrad Stab, 2000, 68(3), 465.
[13] Chiellini, E.; Corti, A.; Swift, G. Polym Degrad Stab 2003; 81, 341.
[14] Koutny, M.; Sancelme, M.; Dabin, C.; Pichon, N.; Delort, A.M.; Lemaire, J. Polym Degrad Stab 2006, 9, 1495.
[15] Chiellini, E.; Corti, A.; D'Antone, S.; Baciu, R. Polym Degrad Stab 2006, 91(11), 2739.
[16] Kumanayaka, T.O.; Parthasarathy, R.; Jollands, M. Polym Degrad Stab 2010, 95, 672.
[17] Corti, A.; Muniyasamy, S.; Vitali, M.; Imam, S.H.; Chiellini, E. Polym Degrad Stab 2010, 95, 1106.
[18] Yashchuk, O.; Portillo, F.S.; Hermida, E.B. Procedia Materials Science 2012, 1, 439.
[19] Briggs, D.; Brewis, D.M.; Konieczko, M.B. Jnl Mater Sci 1979, 14, 1344.
[20] Junnila, J.; Savolainen, A.; Forsberg, D. Polymers, Laminations and Coatings Conference, Orlando 1989. Tappi Press 1989, 353.
[21] Savolainen, A.; Kuusipalo, J. Tappi Extrusion Coating Short Course, Düsseldorf 1991. Tappi Press 1991, 897.
[22] Li, G.Z.; Wang, L.C.; Ni, H.; Pittman, C.U. Jnl Inorg Organomet Polym 2001, 11(3), 123.
[23] Markovic, E.; Constantopolous, K.; Matisons, J.G. Advances in Silicon Science 2011, 3, 40.
[24] Fina, A.; Tabuani, D.; Frache, A.; Camino, G. Polym 2005; 46, 7855.
[25] Fina, A.; Tabuani, D.; Frache, A.; Camino, G. Euro Polym Jnl 2010, 46: 14.
[26] Joshi, M.; Butola, B.S.; Simon, G.; Kukaleva, N. Macromol 2006, 39, 1839.
[27] Joshi, M.; Butola, B.S. Jnl Appl Polym Sci 2007, 105, 978.
[28] Zhou, Z.; Zhang, Y.; Zhang, Y.; Yin, N. J Polym Sci Part B: Polym Phys 2008, 46, 526.
[29] Misra, R.; Fu, B.X.; Morgan, S.E. Jnl Polym Sci, part B: Polym Phys 2007, 45, 2441.
[30] Sánchez-Soto, M.; Schiraldi, D.A.; Illescas, S. Euro Polym Jnl 2009, 45, 341.

[31] Bourbigot, S.; Turf, T.; Bellayer, S.; Duquesne, S. Polym Degrad Stab, 2009, 94, 1230.
[32] Lim, S,K.; Hong, E.P.; Choi, H.; Chin, I.J. Jour Indus Eng Chem 2010, 16, 189.
[33] Nguyen, T-A.; Männle, F.; Gregersen, Ø.W. International Journal of Adhesion & Adhesives 2012, 38: 117. http://dx.doi.org/10.1016/j.ijadhadh.2012.05.002,
[34] http://www.sintef.no/Projectweb/FunzioNano/Synthesis-of-FunzioNano-/
[35] Rao, C.N.R. Chemical Applications of Infrared Spectroscopy. Academic Press, New York and London 1963, 125–263.
[36] Abrahamson, H.B.; Lukaski, H.C. Jnl Inorg Biochem 1994, 54, 115.
[37] Barbu, M.; Stoia, M.; Stefanescu, O.; Stefanescu, M. Chem. Bull. Politechnica Univ. Timisoara 2010, 55(69), 182.
[38] http://www.cabot-corp.com/wcm/download/en-us/mb/MFI.pdf
[39] Zweifel, H. Plastic Additives Handbook. 5th ed. Hanser Publisher, 2001, 8–9.
[40] Eyenga, I.I.; Fockr, W.W.; Prinsloo, L.C.; Tolmay, A.T. Macromol. Symp. 2002, 178,139.